Towards a high resolution view of infrared line formation

Martin Montelius

Lund Observatory
Lund University

2021-EXA172

Degree project of 60 higher education credits (for a degree of Master)
May 2021

Supervisors: Nils Ryde and Henrik Jönsson

Lund Observatory
Box 43
SE-221 00 Lund
Sweden

Abstract

Observing in the infrared has many benefits, such as seeing through the interstellar dust in the galaxy, easier use of adaptive optics, and better flux ratios for direct observations of exoplanets. Before the infrared spectral range can be utilised for highly accurate stellar spectroscopy there is a need for a better understanding of both stellar modelling and the atomic physics that go into forming spectral lines. In this thesis I aim to evaluate to what extent abundances derived from infrared spectra agree with optical values, and which aspects of the line formation cause eventual discrepancies. The aspects investigated in this study are: macroturbulence determination; astrophysical linestrengths; NLTE corrections; and hyperfine structure splitting of atomic energy levels.

For this purpose I have analysed H band (1.49 to 1.80 μm) spectra of 34 K giants, taken with the spectrometer IGRINS. The elemental abundances derived from these infrared spectra are benchmarked against results from high resolution optical spectra of the same stars. This study uses stellar parameters derived from the same optical spectra, as techniques for determining them from infrared spectra are still being developed.

My results for the elemental abundances of C, Na, Mg, Ca, Ti, V, Cr, Co, Ni, Cu and Ce show good agreement with the optical values. Significant differences are seen in the abundances of Al, Si, Mn and Nd. I have also measured the abundances of P, S, K and Zn, elements which lack optical benchmark values. No measurements have been possible for Ge and Rb.

Different factors affecting the analysis have been studied in more detail. I show that the method used for determining macroturbulence is an important factor in abundance determination, especially for stars with supersolar metallicity. The lack of accurate measurements of spectral linestrength is addressed in the thesis by my astrophysical measurements of the quantity, using a method developed in the thesis that accounts for the relative strengths of fine and hyperfine structure lines. For elements with NLTE corrections from Amarsi et al. (2020) I show how these corrections improve the agreement between optical and infrared results. For elements with data on the hyperfine structure splitting of the energy levels, I have assessed the impact of including the additional transitions, showing the importance of doing so.

Populärvetenskaplig beskrivning

Först smör, sedan sylt
-visdomsord

Astronomernas främsta verktyg har alltid varit ljus. I många tusen år har vi observerat ljuset från stjärnorna med blotta ögat och noterat deras positioner på himlavalvet. Ett av de största genombrotten i astronomi var upptäckten att när ljuset bryts ner i ett spektrum med ett prisma eller ett gitter, och alla färger syns separat, syns det mörka linjer i spektrumet. Varje grundämne har sitt egna karakteristiska mönster av så kallade spektrallinjer, lite som ett fingeravtryck. Det finns många användningsområden för de här linjerna: genom att mäta vilken våglängd på ljuset de blockerar kan man mäta hur snabbt stjärnan rör sig i förhållande till oss; och genom att studera formen och storleken på linjerna kan vi mäta vad stjärnorna innehåller.

Mitt arbete handlar om att studera spektrallinjer i infrarött ljus istället för synligt ljus som brukar användas. Det primära målet är att utvärdera vilka grundämnens halter som kan mätas från infraröda spektra med samma noggrannhet som vi kan mäta dem från spektra i synligt ljus. Historiskt har det varit svårt att bygga precisa detektorer för infrarött ljus, på grund av det har många aspekter av vad som behövs för att göra en noggrann analys inte testats ordentligt. Det saknas både labbmätningar av olika atomers spektrallinjer likväl tekniker för hur man ska tolka observationer på bästa sätt. Trots bristen på data är det ändå angeläget att använda infrarött ljus då det har många fördelar, bland annat kan man se igenom stoftmolnen som skymmer mycket av vår galax, Vintergatan, (från synligt ljus) och utforska dess centrum. Det är även optimalt för att observera atmosfärer hos exoplaneter.

I framtiden hoppas vi att stora kartläggningar kan använda infrarött ljus för att observera miljontals stjärnor från alla olika hörn i Vintergatan. Mycket kan förändras hos en stjärna från att den föds tills den dör, den kan migrera från mitten av galaxen till utkanterna; nära möten med tyngre stjärnor kan slunga ut den från galaxen. Men en sak är i stort sett oförändrad: halterna av olika grundämnen i stjärnans atmosfär. När man analyserar en stjärnas spektrallinjer öppnar man ett fönster tillbaka i tiden till när stjärnan bildades. Genom att öppna så många sådana fönster som möjligt kan vi se hur alla de olika delarna av Vintergatan har utvecklats genom tiden, ända sedan galaxen bildades. Förhållandet mellan olika grundämnen kan säga mycket om vilken typ av stjärnor som fanns då och om hur grundämnena bildades.

I min uppsats presenterar jag mätningar av: kol, natrium, magnesium, aluminium, kisel, fosfor, svavel, kalium, kalcium, titan, vanadium, krom, mangan, kobolt, nickel, koppar, zink, cerium och neodymium. Jag utvärderar även en teknik för att mäta styrkan på spektrallinjer; hur den så kallade hyperfinstrukturen hos atomernas energinivåer påverkar spektrumet; hur förenklingar i teoretiska stjärnmodeller kan korrigeras; och hur man kan mäta turbulens hos gasen i stjärnatmosfärer. Resultaten visar på att det finns goda möjligheter

att använda infrarött ljus för att mäta grundämneshalter. De tekniker vi har testat har visats sig vara viktiga för att få noggranna resultat, men de behöver fortfarande förstärkas med fler noggranna labbmätningar.

Contents

List of Figures

List of Tables

Chapter 1

Introduction

Large spectroscopic surveys aiming to chemically map the galaxy need to both cover a broad range of different stellar populations, and to measure their elemental abundances accurately. Infrared spectroscopy solves the first problem, but still needs work to reach the same level of accuracy as optical analysis. This thesis seeks to determine for which elements accurate abundances determinations can be made from near infrared spectra, and which factors are important for achieving the highest levels of accuracy. Studied factors are: astrophysical linestrength measurements, macroturbulence determination, hyperfine structure splitting and Non Local Thermodynamic Equilibrium corrections.

The largest observational projects of our time, such as JWST and the ELT, are increasingly incorporating the infrared spectral range into their designs. The reasons for doing this is multifaceted, with many fields of astronomy having their own reasons for wanting observations in the infrared. Infrared light allows astronomers to observe parts of our galaxy which are hidden from visible light by dust, an important consideration for studying stars in the galactic centre. Adaptive optics, used to correct for the effects of the Earth's atmosphere in the highest resolution studies, is also more effective in the infrared (see for example, Chromey, 2010 for a theoretical description). For direct observations of exoplanets, and especially spectroscopy of exoplanet atmospheres, the higher ratio between the flux of the planet and the host star in the infrared makes the faint light from the planet easier to distinguish.

This thesis is focused on how to analyse stellar spectra in the infrared. The science case which provides the most context for such studies is galactic archaeology, the study of the history of our galaxy's formation and evolution. One of the most powerful tools for such studies is measuring the chemical abundances of stars. Stellar atmospheres preserve the elemental composition of the gas cloud they were born from, giving us a window into the conditions of the galaxy at the time of formation.

The vast majority of abundance measurements have been performed for stars in the galactic disc, where changes in the relative abundance of elements have shown us features

such as the onset of supernovae type Ia (SNe Ia) and the separation of the so-called "thin" and "thick" discs. Infrared light allows for observations of different populations, such as the dust obscured bulge and galactic centre. Searching for differences in chemical abundances between these populations and the disc will constrain on formation scenarios for these regions.

In models of the galaxy's chemical evolution, such as the one by Kobayashi et al. (2020), the evolution of the chemical elements galaxy is simulated using models of nucleosynthetic yields. In this context, each element provides an opportunity to find differences between our best knowledge of stellar physics, and the observed data.

While observing many stars across different regions of the galaxy is an important goal for galactic archaeologists, it is not the only one. Pushing down the errors in abundance measurements is just as important for distinguishing and categorising different populations (see for example, Lindegren et al., 2013). Many different factors contribute to the uncertainties in abundance analysis, many of which can not be solved by a larger telescope or a better spectrograph, even though those things do help. The reason for this is that abundances are not measured directly; what is actually measured is the shape of spectral lines. Line formation is the process in which light of different wavelengths is transported through the stellar atmosphere, forming spectral lines. The two most important factors affecting line formation besides the elemental abundance are,

- Atomic structure: the strength and energy level structure of the spectral lines
- Stellar parameters: primarily the effective temperature $T_{\rm eff}$, surface gravity $\log(g)$, metallicity [Fe/H], and microturbulence $v_{\rm mic}$.

These factors can have a larger impact on the shape of a spectral line than the abundance, meaning they have to be accurately determined to reach the highest level of precision in abundance measurements.

These two features of line formation highlight the biggest challenges for infrared spectroscopy: incomplete or inaccurate atomic data, and a lack of techniques for accurately determining stellar parameters from infrared spectra. The reason for this is a long history of lacking detector technology, with CCD's used for optical astronomy being functionally transparent for infrared light. A thorough history of the field has been written by Rieke (2009).

Atomic data are nominally determined from laboratory measurements and detailed theoretical calculations which can provide accurate values of wavelengths, linestrengths and energy level excitation values. In practice, most of the data for the lines in the near infrared are calculated with what is called a semi-empirical method, where simplified calculations are calibrated with laboratory measurements (Kurucz, 1973). While the linestrengths from laboratory and theoretical studies generally have an uncertainty on the order of 10 - 20 % (Barklem, 2016) the error in the semi-empirical calculations can be on the order of magnitude scale, see e.g. Lind et al. (2017).

The primary stellar parameters of effective temperature and surface gravity can be determined in a number of different ways. Doing so spectroscopically usually involves

using several lines of the same element, sensitive to different parameters, and requiring that the same abundance is derived from each line. To achieve a high level of precision using this method, a set of reliable lines is required, something which is currently under investigation for infrared lines (Puspure, in prep.; Forsberg, in prep.).

The purpose of this thesis is to determine for which elements highly accurate abundances can be derived from near infrared spectra, and to what degree these results match the ones from optical spectroscopy, which is considered more reliable due to being well studied. To achieve this goal I have attempted to address the issues raised above, and to create ideal circumstances for reaching the highest level of accuracy. The spectra analysed in this project comes from 34 K-giants, observed at the Lowell observatory with the high resolution spectrometer IGRINS at a high signal-to-noise ratio to reduce errors from the instrumental profile and random fluctuations to the highest possible degree. Further description of the observations is presented in chapter 3, and the method of analysis is presented in chapter 4.

To address inaccuracies in atomic data I use astrophysical linestrengths, a common technique described in section 2.2.1. I expand upon the implementation in section 4.4.1 and describe a system for handling fine and hyperfine structure splitting I developed for the thesis in appendix B. The linestrengths for approximately 850 lines not used in abundance analysis have also been measured astrophysically, a procedure mostly used by spectral surveys to reduce the impact of large errors on nearby lines or continuum levels, see Jönsson et al. (2020) and Buder et al. (2020).

The impact of including atomic data on the hyperfine splitting of energy levels is described in section 2.2.3. The process of correcting for the assumptions made when modelling stellar atmospheres is described in section 2.2.4. The stellar parameters used for the stars have been derived from high quality optical spectra by Jönsson et al. (in prep.) with a high level of accuracy and precision. The exception is macroturbulence, which is determined in this thesis by the process described in section 4.2.2.

The methods used for analysing uncertainties, errors and biases in the abundance analysis are presented in section 4.6, with the results of the bias analysis presented in section 5.1.

The main results of this thesis consist of a critical evaluation of the abundances derived from infrared spectra and the abundances derived for the same stars from high resolution optical spectra in Jönsson et al. (in prep.), and medium resolution infrared spectra analysed in Christensen (2020). The details of the different observations are described in section 3.2, with a deeper discussion of the purposes of comparing against these studies and differences in methodology between them presented in section 4.7. The results of the analysis abundance trends and comparisons are shown in section 5.2.

A conclusion describing the results of this thesis and what future work can be done to build upon its findings is presented in chapter 6.

Chapter 2

Theoretical background

In this chapter I will cover some of the theory important to my work:

- The characteristics of the near infrared spectral region, including which elements have spectral lines there
- A summary of the theory of line formation, how the strength and broadening of spectral lines are calculated, which will affect the precision and accuracy of abundances derived from the spectral lines investigated in this thesis
- A description of hyperfine structure splitting of energy levels and the impact it has on observed spectra
- The use of the Local Thermodynamic Equilibrium approximation in stellar models and how issues arising from that assumption are ameliorated.

2.1 The Near-infrared

Light is typically categorised into spectral regions based on wavelength, e.g. ultraviolet at shorter wavelengths, optical for the light we can see, and infrared for longer wavelengths. The division is primarily motivated by the differing technologies required to observe and record the light, with materials such as silicon which can form excellent detectors for optical light, being completely transparent in the infrared.

Within the field of observational astronomy, infrared light is further broken down into spectral regions by molecular absorption bands in the Earth's atmosphere, which make the wavelengths where they are present unusable. The brightness of most stars peaks in the optical wavelength range, but due to the shape of the black body radiation curve they remain bright in the near infrared up until the end of the so called K band at 2.5 μm. My work focuses on the H band, from 1.49 to 1.80 μm, as aside from the stars being brighter than in the K band, there is the additional opportunity of comparing my results to the

large APOGEE survey (Majewski et al., 2017; Jönsson et al., 2020), which operates in a reduced portion of the H band.

The wavelength of a spectral line is determined by the energy difference between the excitation states involved in the transition. The longer wavelengths in the infrared correspond to a smaller energy difference between the levels. Due to the way energies of quantum states for atoms and ions are distributed, this means that these transitions are between higher energy levels, as they are more closely packed than the lower ones. In general there are fewer lines from the upper levels, leading to there being fewer lines at longer wavelengths. The first question one must ask when investigating infrared spectroscopy is therefore, which elements have detectable spectral lines in the infrared?

2.1.1 The elements of the H band

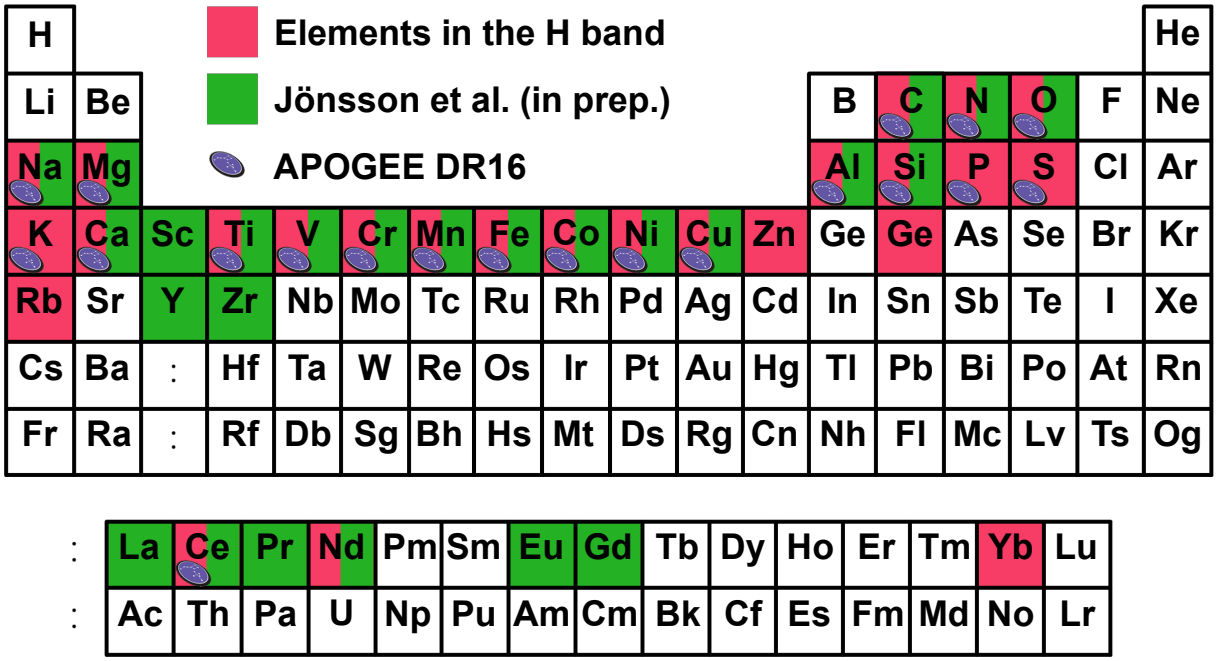

Figure 2.1: Periodic table showing the elements with known spectral lines in the H band marked in red. Nitrogen and oxygen lack atomic lines but have plentiful molecular lines in the forms of OH, CO and CN. Carbon has both atomic lines and C_2 lines in addition to previously mentioned molecules. Elements measured in Jönsson et al. (in prep.) have been marked in green, while elements in the APOGEE survey's data release 16 (Jönsson et al., 2020) have been marked with the SDSS logo.

The first step to measuring the abundance of an element from a spectral line in a stellar spectrum is to identify which element is responsible for forming the line in the first place. Accurate laboratory measurements are essential for this identification process as it is important to have a good sense of both the wavelength and the strength of a spectral line for

a correct line identification. There are 25 elements with identified spectral lines in the H band, marked in red in the periodic table in Figure 2.1. Many laboratory measurements of spectral lines do not have any data redwards of 9000 Å, because of issues with instrumentation during the 60's and 70's, when most measurements were carried out. This means that there are most likely additional elements whose spectral lines are currently unidentified which could be detected and measured if identified. Some of the elements shown in Figure 2.1 will have lines that are of insufficient quality for abundance analysis. Which lines are useful and which are not is not a constant, different types of stars will have different spectral lines visible, depending on their stellar parameters. Evaluating which elements can be measured from H band spectra is therefore something that needs to be done for each spectral class. The elements which have been successfully measured by APOGEE have been marked in Figure 2.1 with the SDSS logo.

2.2 Spectral line formation

A spectral line is observed as the contrast between the baseline of stellar emission, called the continuum, and the reduced emission caused by absorption by transitions between quantum energy levels (for an in-depth explanation see for example Rutten, 2003). Therefore the first, and very important, step to analysing the spectra of a star is to carefully normalise the spectra, establishing a continuum level from which the spectral lines deviate. Properly defining the continuum level can affect the derived abundances to a significant degree (for a detailed study of this effect see Santos-Peral et al., 2020) and should therefore be done carefully. After establishing a baseline, chemical abundances are not directly measured, but are one of many parameters which contribute to the depth and width of spectral lines. Untangling which process has led to a feature of a line can be a very difficult process, but a necessary one in order to determine elemental abundances. Without understanding the other processes that can affect the linestrength, the abundance cannot be determined with accuracy. As there is no practical possibility of modelling every particle of a star's photosphere, approximations have to be made for both computational modelling and theoretical descriptions. This section will cover the most important details of the theoretical approximations which are used to describe the work done in this thesis.

2.2.1 Linestrength

The Weak Line Approximation

When determining abundances, there is a preference for using "weak" spectral lines with a Gaussian shape, as they have a linear dependence on elemental abundance. Strong lines will be less sensitive to abundance and more sensitive to stellar parameters through the broadening processes described in section 2.2.2. For these weak lines, an approximation can be made, aptly named the Weak Line Approximation, that illustrates the principal parameters involved. In the approximation spectral lines are described by their equivalent

width, EW. This quantity represents the width of a rectangle with the height of the continuum level and the same area as the spectral line. To correct for wavelength dependent broadening effects the EW is divided by the wavelength of the line, creating the reduced EW. For a spectral line from element X the EW can be calculated as,

$$\log\left(\frac{EW}{\lambda}\right) = \log\left(A_X\right) + \log\left(gf\right) + \log\left(C\right) - \theta_{ex}\chi - \log\left(\kappa_\lambda\right) \tag{2.1}$$

$\log_{10}$ is used as the quantities involved often differ by several orders of magnitude. Most parameters are therefore given in the unitless quantity dex, signifying an order of magnitude. The parameters in the formula are:

- A_X, the abundance of element X. In the approximation the abundance is represented as the number density of atom X compared to hydrogen ${}^{N_X}/_{N_H}$.
- g and f; g is the statistical weight of the lower level in the transition, defined as $g = 2J + 1$, where J is the J quantum number; f is the oscillator strength, directly related to the Einstein transition probability A_{ij} (additional details on this relation are given in appendix B.2). In the lab f is commonly measured via A_{ij} and the branching fraction (Huber et al., 1986). The combined quantity $\log(gf)$ is often referred to as the linestrength or the gf-value by astronomers.
- C is a combination of parameters that describe the distribution of different ionisation stages, dependant on the temperature and element.
- θ_{ex} and χ; θ_{ex} corresponds to inverse temperature, written in cgs units to compliment χ which is the excitation energy of the lower level in electronvolts.
- κ_λ is the opacity of the continuum emission per unit mass at the wavelength of the transition.

Further details can be found in Gray (2005). Precisely determined stellar and atomic parameters combined with a robust model of the stellar atmosphere should solve the degeneracy between these quantities, so that the abundance of an element can be measured through the EW of a lines. Important to note is the fact that the abundance and the gf-value have equivalent impacts on the spectral line, unrelated to the star in question. This means that the uncertainty in the abundance derived from a line can never be smaller than the uncertainty in the gf-value.

Astrophysical oscillator strengths

In the near infrared region, many spectral lines lack lab measurements of their gf-values; the same issues with building infrared detectors for astronomical purposes have also made it difficult for atomic physicists to measure the properties of the line. Theoretical calculations of the gf-values are also difficult, as the higher energy levels involved in infrared lines require more complete and complex atomic models. As the techniques for observing these

lines have been developed, the demand for lab measurements has grown, but in many cases the measurements have not yet been performed. Both methods of determining gf-values can reach precisions of $10 - 20\%$ or $0.04 - 0.08$ dex, with larger errors being possible for the calculated values for weak lines and complex atoms (Barklem, 2016).

In the absence of accurate lab-measured or theoretically calculated values, the vast majority of the spectral lines in the H band have semi-empirically calculated gf-values. The semi-empirical method calculates the excitation energies of energy levels in a simplified manner and calibrates them using empirical measurements (Kurucz, 1973). After calibration, the simplified calculations are extended to energy levels that are yet to be measured. As these energy levels cannot be calibrated, a significant error is introduced. Based on these calculations, properties such as the gf-values of the transitions between these energy levels are derived. The purpose of these semi-empirical calculations is less about finding exact values for abundance analysis, and more about creating a complete library of spectral lines for calculating photospheric opacities for stellar atmosphere models. The accuracy of the gf-values is therefore markedly worse than both lab measurements and more careful theoretical calculations. A comparison between semi-empirical linestrengths from Kurucz et al. (1995) and lab measured values for Fe I lines shown in Lind et al. (2017) shows a deviation from lab results of 0.08 ± 0.29 dex (standard deviation of roughly a factor of 2) for Kurucz $\log(gf) > -2$, and a corresponding mean deviation of -0.40 ± 0.79 dex (standard deviation roughly a factor of 6) for lines with $\log(gf) < -2$. This shows that even the strongest lines have significant uncertainties in the calculations, and the weaker lines can be off by several orders of magnitude, potentially disrupting the measurement of nearby lines (see figure 5.22 for a similar analysis comparing Kurucz to my astrophysical values).

Because the accuracy of abundance analysis is directly dependent on the accuracy of the gf-values adopted, finding more accurate estimates is essential. One common way of doing this is to exploit the degeneracy between the gf-value and the abundance, turning around equation (2.1) to solve for $\log(gf)$ instead of $\log(A_X)$. The spectra from a benchmark star with well known stellar parameters, and elemental abundances accurately determined from lines with lab measured gf-values is used for this purpose, typically the Sun or Arcturus (see e.g. Smith et al., 2021). This process is called astrophysical $\log(gf)$ measurement. It incorporates all the errors associated with abundance analysis into the $\log(gf)$ value, from the stellar parameters and model atmospheres to the potential of other spectral lines influencing the measurement. To minimise the errors high resolution spectra are used, along with a spectral synthesis analysis method (see section 4.1). An advantage of using the solar spectra is that molecular lines are much weaker than in cooler stars such as Arcturus, but a drawback is that other lines of potential interest are also weaker, possibly to the point where no reliable measurement can be made. Under ideal circumstances, using very high resolution spectra for unblended lines, the accuracy of astrophysical $\log(gf)$ measurements can be comparable to lab values (Borrero et al., 2003). Lab values will still be preferable: they allow for measurements in less-than-ideal circumstances, such as when the spectral lines are blended together; for getting proper error estimates; and for evaluating inaccuracies in stellar modelling (see section 2.2.4). The process used for astrophysical $\log(gf)$ measurements in this thesis is described in section 4.4.1.

2.2.2 Line width

Sources of line broadening

Even though the transition between a particle's energy levels absorbs light of only a specific wavelength, observed spectral lines will not be laser sharp. The broadening of spectral lines has different causes, some affecting all spectral lines equally, others depend on the particle absorbing the light. A quick summary of the main types of broadening, following Rutten (2003):

- Natural broadening: The connection between an excited energy state's energy and lifetime described by the uncertainty principle will cause a tiny spread in wavelength. It is mostly important in lab conditions and the outer regions of stellar atmospheres, where other sources of broadening are less impactful. Natural broadening gives a Lorentzian profile to the line.

- Thermal broadening: The thermal motion of the particles creates a Doppler broadening effect with a Gaussian profile, the strength of the broadening depends on the temperatures in the different layers of the photosphere and the mass of the absorbing particle.

- Rotational Doppler broadening: caused by the velocity from stellar rotation. The strength of the observed broadening depends on the rotational speed v_{rot}, but also on the angle between the star's axis of rotation and the observer's line of sight i. The observed quantity is therefore $v_{rot} \sin i$, the sine taken to get the vector pointing to Earth.

- Instrumental response function: A broadening profile, commonly Gaussian, is added by the spectrograph recording the spectra, the width of the broadening profile is determined by the resolution of the spectrograph, with higher resolutions broadening the spectra less.

- Micro and macroturbulence are fudge parameters meant to represent Doppler broadening from random motion on scales smaller/larger than the photon mean free path. Both contribute to the broadening with a Gaussian profile. Microturbulence, v_{mic}, affects strong lines more than weak ones and can therefore be determined by measuring lines of different strengths. Macroturbulence, v_{mac}, affects all lines equally, making it degenerate with the effects of rotational broadening and the instrumental profile. This degeneracy makes it difficult to disentangle v_{mac} using only spectral analysis, because of this the instrumental profile, rotational broadening and stellar macroturbulence are determined collectively in this thesis and referred to as the "macroturbulence". In principle the macroturbulence can be determined from any set of lines, but unblended lines of middling strength are often chosen to lessen the impact of noise and other broadening effects. The process of determining macroturbulence is described in section 4.2.2.

- Collisional broadening: caused by interactions with other particles in the photosphere. Charged or polarised particles can broaden the spectral lines in a number of ways, usually split into different categories based on how the interaction scales with the distance between the particles. Most of the interactions give a Lorentzian profile. The importance of these effects will depend on which particles are most commonly involved in the interaction, either atomic hydrogen or electrons depending on the level of ionisation in the photosphere. For the cool stars studied in this thesis, ionisation is less prevalent and broadening by hydrogen atoms are the most important collisional broadening effect. Collisional broadening by atomic hydrogen will be discussed further below.

Collisional broadening by atomic hydrogen

As mentioned in the section above, the most important source of collisional broadening for cool stars is hydrogen atoms. Handling atomic hydrogen at the temperatures and pressures present in stellar photospheres is difficult in the lab, so theoretical approximations are the primary source of our understanding of this interaction. Because the interaction of particles with hydrogen atoms shares certain similarities with the van der Waals force known from intermolecular interactions in chemistry, the name "van der Waals broadening" is often used.

A complete description of how the different ways of estimating the van der Waals broadening work can be found in Heiter et al. (2021), the following is a short summary describing the main features of the three commonly used approximations. The approximations seek a way of estimating the full-width-half-maximum of the Lorentzian broadening profile:

- Unsöld (1955) starts with two common assumptions: long range interactions, where the distance to the hydrogen atom is larger than the valence electron radius, dominate; that the first order term in a multipole expansion of the interaction energy is cancelled out, leaving the interaction dominated by the second order term. The energy structure of the perturbed atom is assumed to be smaller than the one for hydrogen, and thus neglected. A final approximation is made by assuming the energy levels can be described by the Bohr radius of their valence electrons.

- Kurucz (1981b) follows a similar strategy to Unsöld (1955), but replaces the use of the Bohr radius of the involved excitation states with a summation over the oscillator strengths of all possible transitions.

- The Anstee–Barklem–O'Mara (ABO) approximation (Anstee et al., 1995) attempts to provide more precise values by including many of the things neglected by the Unsöld theory: intermediate range interactions; rotational energy of the atoms; and the first order term of the interaction energy. The method of calculating the interaction is also significantly different, calculating wavefunctions for each individual orbital. The result is a description of the broadening that is described by two param-

eters instead of one, σ, the cross section of the broadening, and α, which describes how σ depends on the speed of the collision with the hydrogen atom.

The approximations of Unsöld and Kurucz have been shown to yield a too small van der Waals broadening (Anstee et al., 1991). ABO values show better agreement with observations, but take a lot of resources to calculate. This is due to a combination of the complexity in the calculation itself, but also since the values have to be evaluated by comparison with stellar spectra to verify the fit. As such, most of the lines in the H band have values calculated with Kurucs's approximation. For lines considered for abundance analysis this can be a significant source of error, especially for lines used to calculate the star's macroturbulence, as an error in this parameter will impact all spectral lines. The determination of macroturbulence in this thesis is described in section 4.2.2.

2.2.3 Hyperfine structure

The energy structure of atoms is divided into related levels by perturbations from a number of different sources, enabling the formation of many additional spectral lines. The division mainly caused by the interaction between the magnetic moment of the nucleus and the magnetic field generated by the electrons is called hyperfine structure (HFS), in contrast to fine structure which is mainly caused by electron spin. Hyperfine structure is not present for all isotopes, as the magnetic moment of the nucleus is caused by an odd number of either protons or neutrons.

In most cases, the hyperfine structure is small enough that the individual hyperfine lines blend together in a stellar spectra to the point where they are no longer distinguishable. The effect of HFS on spectral lines is not uniform, it depends to a large degree on both the wavelength distance between the HFS lines and also on the relative strengths between the lines. Two examples of this is shown in Figure 2.2: for the Al I line at 16750.5 Å and the Mn I line at 15217.7 Å. In the figure the synthetic spectra of the individual hyperfine lines and their combined profile are shown and contrasted with the profile of using just a singular line without HFS. The Al lines are spread over a smaller wavelength range (0.26 Å) and largely follow a Voigt broadening profile, the most notable difference to the single line being the much weaker wings. The Mn lines are spread further (0.64 Å), showing a larger warping of the line profile. The main effect of HFS is desaturation; spreading the line out in wavelength keeps it from reaching a saturated state where it is less sensitive to changes in abundance. This effect is most notable in strong lines, where the difference in derived abundance can differ by an order of magnitude, see (Thorsbro et al., 2018), also section 5.2.13. It is not negligible for weaker lines however, where differences of 0.10 - 0.15 dex are possible, see (Booth et al., 1983; Jofré et al., 2017).

The calculation of HFS lines is not trivial and requires lab measurements of the HFS constants A and B, describing the nuclear magnetic moment and the electric quadrupole moment respectively. A compilation of HFS data has recently been made available to the Vienna Atomic Line Database (VALD) (Ryabchikova et al., 2015) by Pakhomov et al. (2019), making it possible to investigate the impact of HFS for a large number of elements.

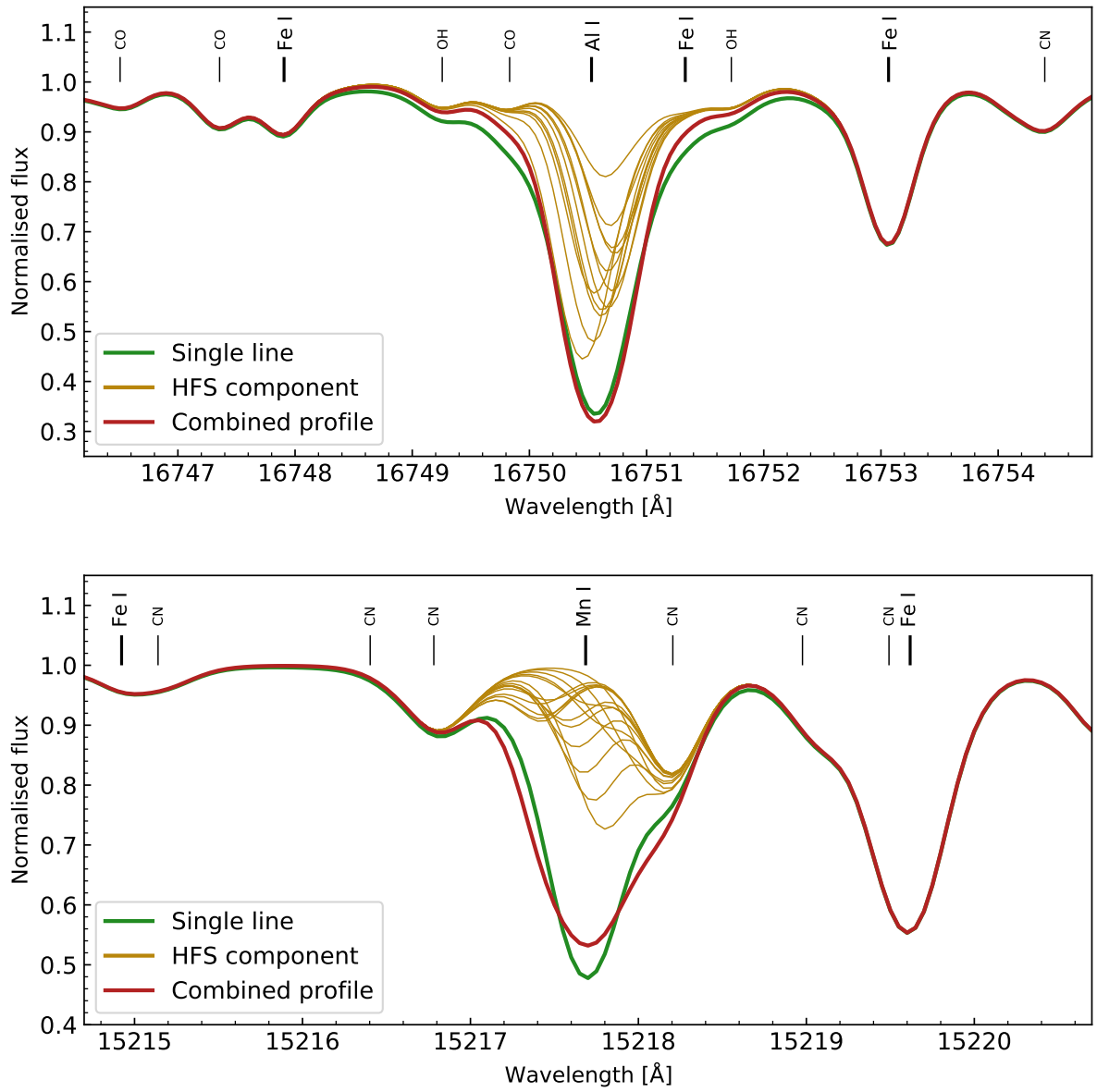

Figure 2.2: Illustration showing the hyperfine components, combined hyperfine profile and single line profile for two different lines. The stellar parameters are the same as those of μ Leo and the abundances are set to reflect the difference from abundance determination with and without HFS, see sections 5.2.4 and 5.2.13.
Top: the 12 hyperfine structure lines which together form the combined profile of the Al I spectral line at 16750.5 Å.
Bottom: the 16 hyperfine structure lines forming the combined profile of the Mn I line at 15217.7 Å.

The elements with HFS data from VALD which are measured in this thesis are: Na, Al, V, Mn, Co and Cu.

2.2.4 NLTE corrections

Most commonly used spectral synthesis codes make use of the assumption of Local Thermodynamic Equilibrium (LTE), that the temperature of any given particle in a star's photosphere is set by collisions with nearby particles. This means that even though the photosphere as a whole cannot be treated as being in thermal equilibrium, it can be assumed to hold at each depth-point in a model atmosphere. A number of approximations regarding the velocity, excitation and ionisation of particles need thermal equilibrium to hold, and a lot of computational time can therefore be saved by computing in LTE.

The major issue with calculating spectra in LTE is that the approximation neglects one of the most noticeable features of stars, radiation. Where the energy of the particles in the atmosphere are dominated by collisions, radiation effects can be negligible, while in the thinner outer layers of the atmosphere neglecting them can have major consequences. Effects caused by processes neglected in the LTE approximation are dubbed non-LTE, or NLTE, effects. A thorough description of what causes various NLTE effects and how they affect line formation can be found in Bergemann et al. (2014).

It is possible to correct for NLTE effects with pre-computed grids of NLTE departure coefficients, β. β is defined as the ratio between the number density of electrons in a given energy level in LTE, and when accounting for NLTE effects. The electron number density of a level will affect the likelihood of absorption and transitions involving that level. The departure coefficients are given for a varying set of stellar parameters and elemental abundances at different depth-points in the atmosphere. Including the departure coefficients in the analysis can affect not just the strength of the line, but also the line source function, creating deviations from the blackbody radiation curve. This thesis uses the NLTE grids presented in Amarsi et al. (2020), supplemented by the grid for Fe lines in Amarsi et al. (2016). The elements in this thesis with available grids for our type of stars are: C, Na, Mg, Al, Si, K, Ca and Mn. Not all of the lines in the H band for these elements are included in these grids, but all lines used for abundance analysis of these elements in this thesis are present.

Chapter 3

Stellar Sample

Stars of different spectral classes can have very different spectra. When analysing stellar spectra, it is therefore a good idea to restrict your sample to one spectral class. In this chapter the chosen spectral class, K giants, and the reasons for choosing it is described, along with a more detailed description of the stars and observations used. The observations in the comparison samples from Jönsson et al. (in prep.) and Christensen (2020) are also described.

3.1 K giants

As the goal of Galactic archaeology is to study the formation and evolution of our galaxy, a main criteria for choosing a spectral type to study is thus that the stars have to be capable of showing a range of ages. O stars with a lifetime of a million years make excellent probes of the current makeup of the galaxy, but there are no O stars from 10 Gyr's ago around today. Going to the opposite end of the temperature range more long lived stars can be found, with the additional benefit from the point of view of this thesis, that the stars emit a large portion of their light in the infrared. A second criteria is that the ease of analysis for the spectra must be good enough that accurate abundances can be derived for the stars.

K giants are a good candidate to meet these criteria. They are generally long lived enough that there is a wide range of ages to observe. Their temperatures are roughly in the 3900 - 5800 K range, depending on which definition is used, meaning they are bright in the infrared, while being hot enough to reduce the amount of molecular lines visible in the spectra.

Working with giants brings both advantages and disadvantages. Being much brighter than dwarfs, high signal to noise (S/N) spectra can reliably be obtained at much greater distances. This could for example allow followup studies comparing the abundance trends in this thesis with stars of the same spectral class in the distant bulge (the central concentration of stars in our galaxy). The much lower surface gravity of giants will in general

make the spectral lines stronger compared to dwarfs of the same temperature and metallicity: lines which have been proven reliable for dwarfs can therefore be saturated, while lines which were previously too weak to detect can be well suited for analysis.

Working with K giants will therefore enable me to construct a sample which in future studies can be compared to a wide range of stellar populations: from inner regions such as the dust obscured bulge and nuclear stellar cluster; outer regions like the halo and orbiting dwarf galaxies; and using the next generation of instrumentation, to even more distant targets such as the Andromeda galaxy.

3.2 Observed stars

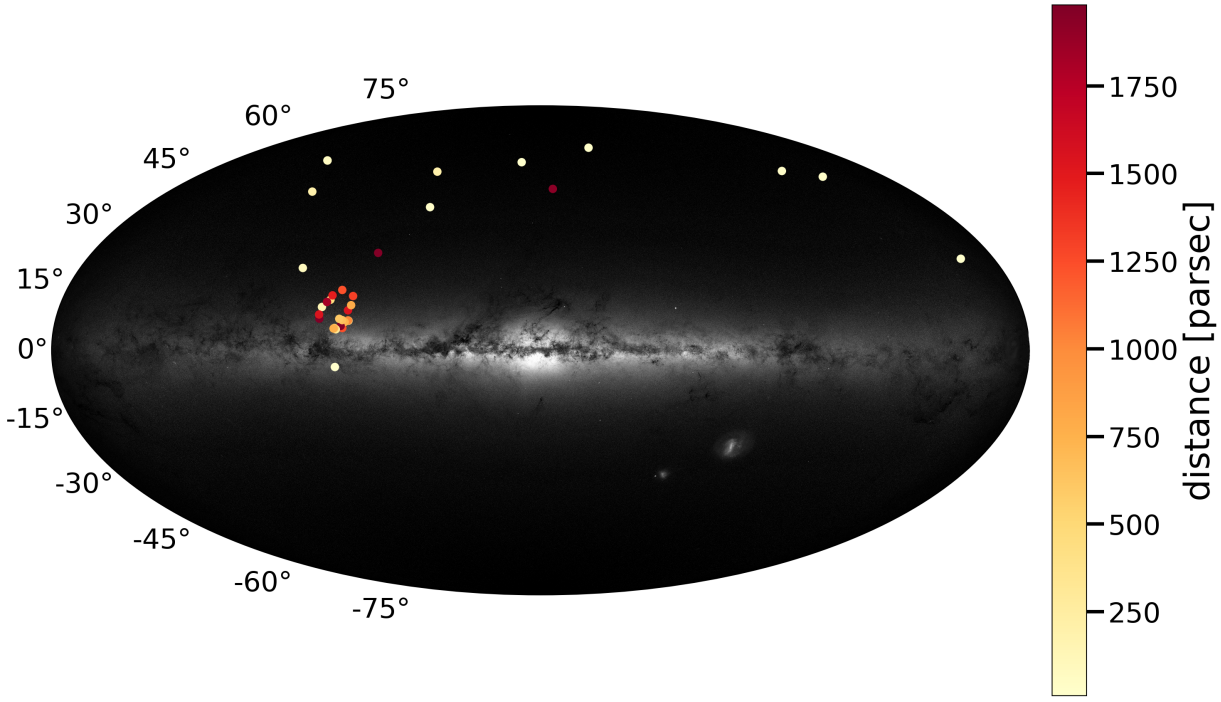

Figure 3.1: Distribution of the stellar sample in galactic coordinates against a view of the Milky Way. Plotted using `https://github.com/henrysky/milkyway_plot`.

In this work I have analysed 34 K giants, a subsample of the stars analysed in Jönsson et al. (in prep.). The stars were observed with the 4.3 meter Lowell Discovery Telescope (see Figure 3.2) in Flagstaff, Arizona, with the Immersion GRating INfrared Spectrometer, IGRINS (Park et al., 2014). The instrument observes the whole H and K bands simultaneously at a spectral resolution of $R \sim 45000$. As an example, the H band spectra of Arcturus is shown in Figure 3.4. Details on the observations can be found in table 3.1. The distribution of S/N values can be seen in Figure 3.3. The distribution of the stars in the galaxy can be seen in Figure 3.1. The main features of the distribution being the concentration

of stars in the Kepler field and the band of stars which appear to be above the galactic plane, but are in fact just nearby. The observatory is situated in the northern hemisphere, which is also reflected in the distribution of the stars. The distances shown are calculated as $d = \frac{1000[\mathrm{pc}]}{\mathrm{parallax[mas]}}$ using parallaxes from Gaia DR2 (Gaia Collaboration et al., 2018) and the Hipparcos catalogue (Perryman et al., 1997), with a min/median/max of 10/580/1980 parsec. The signal to noise ratios (S/N) for the IGRINS observations have been calculated using the code DER_SNR (Stoehr et al., 2008). There are several different ways to define S/N in spectroscopy, the one used here is a relative measure instead of an absolute one. The wavelength ranges used to compute the S/N are: 15482.6-15484.4, 15486.3-15487.6, 15547.5-15549.7, 16734.3-16735.8, 16789.0-16791.0, 16920.0-16923.0 Ångström. Figure 3.4 shows these regions marked in red.

Jönsson et al., in prep.

The optical observations in Jönsson et al. (in prep.) which are used for stellar parameters and to benchmark abundances in this thesis, are from the 2.5 m Nordic Optical Telescope (NOT), using the FIbre-fed Echelle Spectrograph (FIES). FIES covers the optical range from 3500 - 8300 Å at $R \sim 67000$. More details about the observations can be found in Forsberg (2019).

Christensen, 2020

25 of the stars have also been observed by the survey APOGEE, Apache Point Observatory Galactic Evolution Experiment. Comparisons will mainly be done to results from the manual re-analysis of APOGEE spectra by Christensen (2020), substituting APOGEE DR16 (Jönsson et al., 2020) results where needed.

Details on how the method of analysis differs for these different studies are discussed in section 4.7.

Study	This work	Jönsson	Christensen
Spectrograph	IGRINS	FIES	APOGEE
Number of stars	34 (+ Solar Spectrum)	34	25
Wavelength region	14900-18000, 19600-24600 Å	3700 - 8300 Å	15000 - 17000 Å
Resolving power	45000	67000	22500
S/N (min/median/max)	80/180/410	30/100/320	140/480/1060

Table 3.1: Observational statistics for the stellar sample in this thesis for the three different spectrographs the stars have been observed with.

Figure 3.2: The 4.3 meter Lowell Discovery Telescope, used for the observations in this thesis. Photo credit Commons (2013).

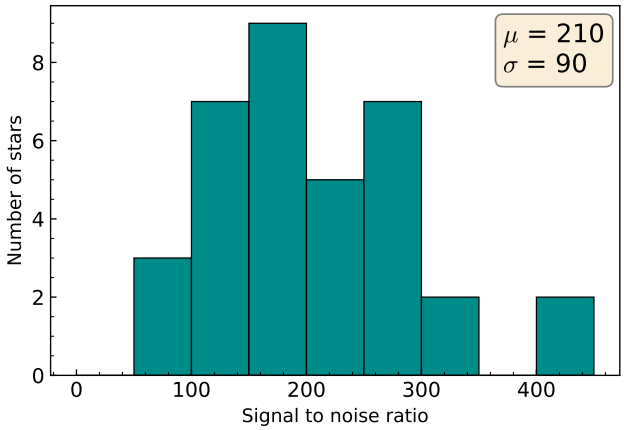

Figure 3.3: Distribution of the signal to noise ratio for the stars analysed in this thesis, calculated with DER_SNR from 6 wavelength regions within the APOGEE range. The outlier with a S/N over 400 is the solar spectra.

Figure 3.4: (Shown on next page) Observed spectra of Arcturus, α Boo, analysed in this thesis. Regions marked in red have been used to measure the signal to noise ratio.

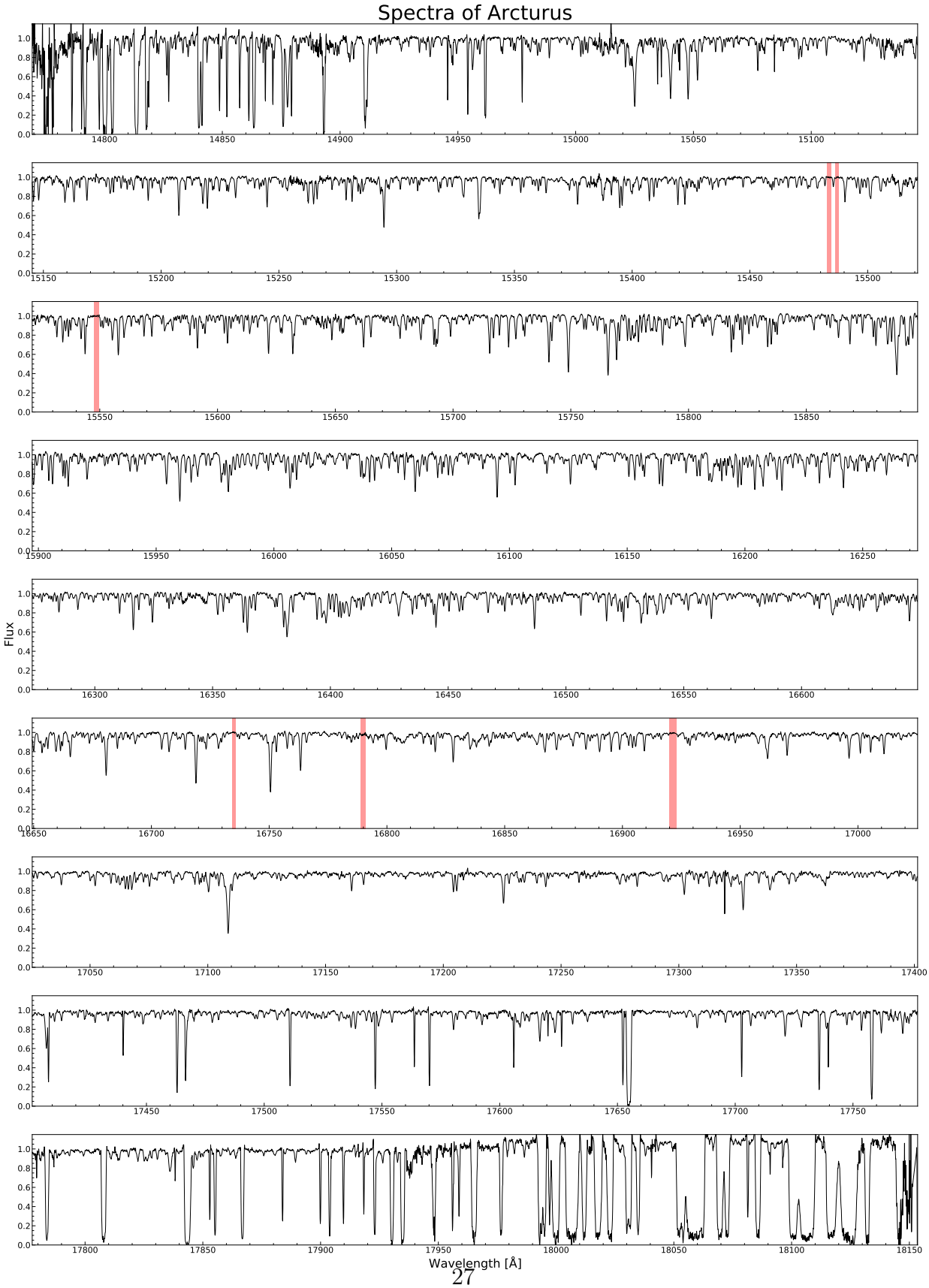
Spectra of Arcturus
Flux
Wavelength [Å]

Chapter 4

Methodology

In this chapter the method used for spectral analysis is presented, together with the required models and data:

- Spectral line synthesis: the features of the SME software
- Stellar parameters: temperature, surface gravity, metallicity, micro- and macroturbulences
- Model atmospheres: how stars are modelled
- Spectral line data: used databases and how the data has been improved and supplemented
- Uncertainties: analysis of errors in stellar parameters, instrumental errors, and parameter biases

Measuring the elemental abundances of a star from its spectral lines is a non-trivial task. There are several different methods developed to solve this, each with their own strengths and weaknesses (see e.g. Blanco-Cuaresma (2019) for a comparative study). In this thesis a spectral synthesis code called Spectroscopy Made Easy (SME) (Valenti et al., 1996; Piskunov et al., 2017) will be used. Methods based on spectral synthesis makes use of databases on the physical properties of stellar photospheres, and atomic data, to construct a synthesised spectra. Abundances or other parameters can then be tweaked to fit the synthesised spectrum to observations. Compared to other methods, such as measuring equivalent widths, the spectral synthesis method sacrifices some speed for a better handling of strong and blended lines, which are both common features of cool giants.
In this chapter the process of producing a synthesised spectrum is described, starting with how SME functions, how the stellar parameters have been determined, and a description of the model atmospheres and spectral linelists used.

4.1 Line synthesis

Spectral synthesis relies on modelling the photosphere of a star and how light would pass through it. The resulting synthesised spectrum can then be fitted to observed data by varying the parameters of the model until the synthesised spectrum matches the observations. Although it is not used in the process of spectral synthesis, the weak line approximation (see section 2.2.1) shows us some of the principal factors beyond abundances which affect the size of the spectral line. Degeneracies between these parameters stop us from determining all parameters simultaneously. Different methods have therefore been developed for determining stellar parameters first, so that the elemental abundances can be determined afterwards, one by one, with as little dependence on each other as possible. The process of determining these parameters is described in section 4.2, the model atmospheres which outline the physical conditions of the photosphere are described in section 4.3, the atomic data determining the strength and shape of the spectral lines is described in section 4.4, and the process of manually analysing the spectra is described below.
Assuming that accurate parameters and atmospheric models have been found, the process of determining abundances still needs some manual input. The first step is marking which areas are of interest for which elements, as studying the whole spectrum simultaneously would be considerably more computationally expensive. Three kinds of regions are marked, shown in Figure 4.1:

- Line masks, shown in orange: designates the area around a spectral line where it is expected to dominate the spectrum.
- Continuum masks, shown in yellow: designates areas free from spectral lines, where the spectra are close to the continuum level. For each segment the continuum level is calibrated from these regions.
- Segments: the edges enclosing line masks and continuum masks. Only the wavelength range within the segments get synthesised to save computational time.

With regions of interest carefully selected, a synthetic spectrum can be produced based on a set of given parameters. Selecting one or more parameters as "free" will then allow for their determination through χ^2 fitting. In Figure 4.2 an example of this is shown; how the Si abundance is determined for α Boo, using a spectral line at 16163 Å. Starting from a solar Si abundance, [Si/Fe] = 0, the abundance is varied, causing different line profiles; the χ^2 between the observed and the synthesised spectra within the linemask is calculated; the fit with the lowest χ^2 is assumed to correspond to the true value of the abundance.
After abundances have been determined with each line separately, I have verified the results of the χ^2 fitting by visual inspection of the goodness of fit for the synthesised spectrum and the observed spectrum; there are many effects which can disrupt a spectral line, atmospheric disturbances, molecular lines, etc., that the automatic process does not pick up on. Some issues can be fixed by adjusting the linemask to avoid ill fitting regions. The lines with the best fitting synthetic spectra get selected and final abundance determination is performed by fitting the observed spectrum to all of the selected lines simultaneously.

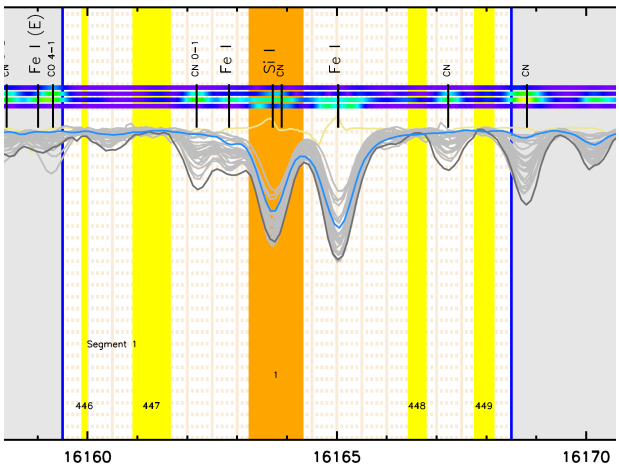

Figure 4.1: Small segment showing the spectra from all of the stars in this thesis around the Si I line at 16163.71 Å. The area marked in orange marks the spectral line of interest, while the yellow areas mark the continuum level. The grey lines are the stellar spectra, with the blue line (the Sun) and the dark grey line (metal-rich giant μ Leo) enhanced for clarity. The thin yellow line close to the continuum level shows the telluric spectra, to show where potential issues can arise from so-called telluric lines. The coloured lines above the spectra indicate that particular wavelength's sensitivity to stellar parameters.

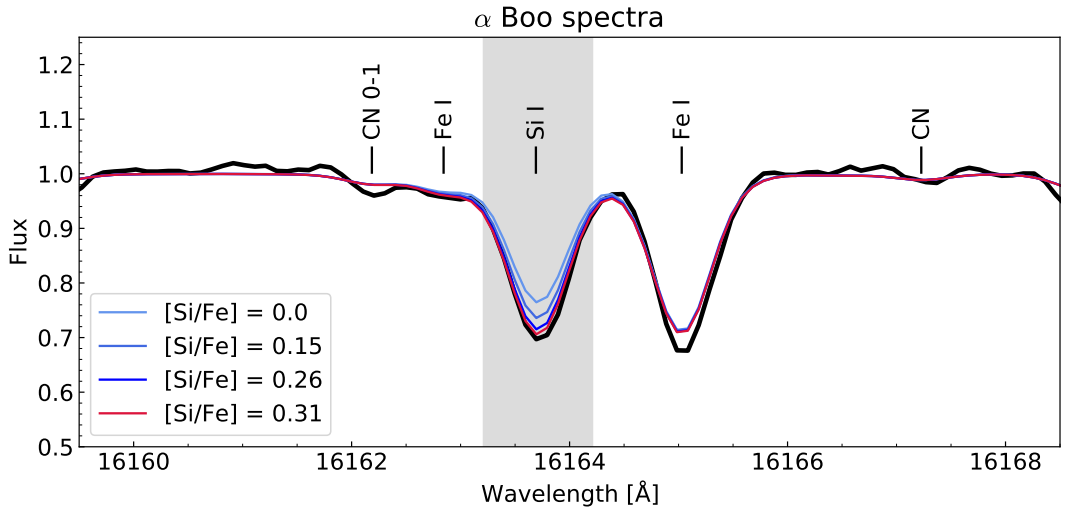

Figure 4.2: A cutout of the wavelength region shown in Figure 4.1. The black line is the observed spectra of α Boo, while the coloured lines are spectra synthesised using different Si abundances. Starting from 0.0 SME evaluates small variations around these values before changing the abundance and reevaluating the fit. The red line indicates the last evaluated abundance, for which the χ^2 between synthesised and observed spectra cannot be decreased. The grey region is the line mask where the goodness of fit is evaluated.

4.2 Stellar parameters

The physical conditions of a star's photosphere are described by a set of parameters:

- $T_{\rm eff}$: effective temperature, is a measure of surface temperature by approximating the star as a black body. Measured in Kelvins [K].
- $\log(g)$: the logarithm of the surface gravitational acceleration, $g = G\frac{M_\star}{R_\star^2}$ with units [$\mathrm{cm\,s^{-2}}$]. $\log(g)$ is measured in orders of magnitude, labelled [dex].
- Metallicity: in this thesis this refers to the Fe abundance. In other contexts this can refer to the overall content of elements heavier than helium. The Fe abundance is given as $[\mathrm{Fe/H}] = log_{10}\left(\frac{N_{Fe}}{N_H}\right)_\star - log_{10}\left(\frac{N_{Fe}}{N_H}\right)_\odot$, the logarithm of the number density of iron atoms compared to hydrogen, scaled to the solar values.
- Microturbulence, $v_{\rm mic}$: fudge parameter necessary for 1D models, describes small scale motions in the photosphere. Measured in [$\mathrm{km\,s^{-1}}$].
- Macroturbulence, $v_{\rm mac}$: large scale motions in the photosphere, in this work it includes the effects of the instrumental profile and rotational broadening, all assumed to have Gaussian profiles. Measured in [$\mathrm{km\,s^{-1}}$].

In the following subsections the process of determining these parameters is described.

4.2.1 Parameters from optical spectra in Jönsson et al. (in prep.)

Most stellar parameters have been adopted from Jönsson et al. (in prep.), with the exception of macroturbulence, the process of determining $v_{\rm mac}$ is described in section 4.2.2. The Kiel diagram in Figure 4.3 shows the distribution of parameters and how they fit with isochrones for 1 Gyr and 10 Gyr respectively. A perfect fit is not achieved to the isochrones as the stars will have a range of ages. As age determination is difficult and uncertain for giants, it will not be performed in this thesis.

$\mathbf{T}_{\rm eff}$

Effective temperatures are determined by fitting the synthetic spectra to a number of Fe I lines with different excitation energies, as level populations are affected by the temperature a large enough set of these lines will be sensitive to temperature variations. These results have been benchmarked against results obtained from angular diameter measurements (Mozurkewich et al., 2003), calculated from $L = 4\pi R^2 \sigma T_{\rm eff}^4$ providing a fundamental measurement of $T_{\rm eff}$, and found to be in good agreement.

log(g)

Surface gravities are determined by a combination of fitting Fe I/Fe II lines and fitting the wings of strong Fe I lines. The combination of neutral and ionised iron lines is sensitive to the electron pressure of the photosphere, while the wings of strong lines are sensitive to the pressure of the hydrogen atoms through the van der Waals broadening. These pressures make the lines sensitive to the surface gravity through the hydrostatic equilibrium equation. These results are benchmarked against asteroseismic measurements (Huber et al., 2014) which derive surface gravity from stellar pulsation, a fundamental measurement, and are found to show good precision and accuracy.

Metallicity

As iron lines are used to determine temperature and surface gravity, the [Fe/H] abundance will be computed simultaneously. The derived metallicities are found to be in good agreement with literature values.

Microturbulence

Microturbulence is determined by fitting synthetic spectra to a combination of weak and strong lines. Because strong lines are more effected by microturbulence (Gray, 2005), the combination of weak and strong lines will be sensitive to the microturbulence.

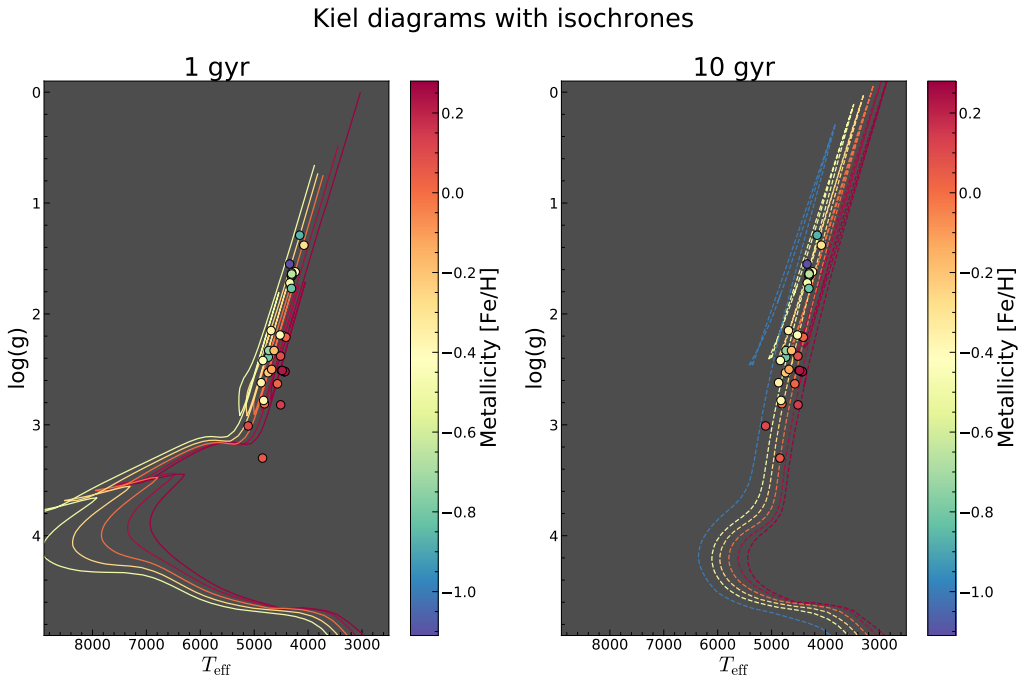

Figure 4.3: Kiel diagram showing the distribution of temperatures and surface gravities measured by Jönsson et al. (in prep.) for the stars observed in this thesis. Isochrones for a range of metallicities are also shown describing the expected location of stars in the diagram. The left plot shows isochrones for 1 Gyr with 10 Gyr for the right plot. Both sets of isochrones are computed using the calculator at `http://stev.oapd.inaf.it/cgi-bin/cmd` with data from Bressan et al. (2012).

4.2.2 Macroturbulence

As mentioned earlier in this thesis, what we refer to as macroturbulence describes a combination of large scale motions in the stellar atmosphere (stellar macroturbulence), stellar rotation and the instrumental profile. Values of macroturbulence value will not be transferable between observations with different instruments. The parameter is therefore not adopted from Jönsson et al. (in prep.) and instead determined specifically for the spectra within this thesis. Two different variations on the method used in Christensen (2020) were tried, using carefully selected sets of Si lines (called VmacSi) and Fe lines (called VmacFe). The two methods should give the same results as all lines are equally affected by macroturbulence. For unknown reasons this was not the case; this is illustrated in Figure 4.4, along with the abundance trends of Mg derived using VmacSi and VmacFe, shown to illustrate the impact on abundance analysis. A more in depth explanation of how to interpret abundance trends is given in section 5.2. The method used for the main results of the thesis is VmacFe, as abundances derived using those values showed better agreement with the abundances from Jönsson et al. (in prep.).

VmacSi

The first method of determining $v_{\rm mac}$ makes use of five Si I relatively unblended Si lines with Gaussian profiles: 16163.71, 16215.69, 16241.85, 16680.77 and 16828.18 Å. Theoretically, Si lines should be a good candidate for this type of measurement, as the elevated α abundances at lower metallicities should keep the lines strong enough for the most metal poor stars. Synthetic spectra are fitted to the lines, with both $v_{\rm mac}$ and Si abundance as free parameters. In an iterative process this was repeated after calibrating the strength of the spectral line (see section 4.4.1), until results converged. Lines were selectively chosen or discarded based on visual inspection of the spectra and inspection of the Si trend.

VmacFe

The second method of determining $v_{\rm mac}$ uses seven Fe I lines: 15207.53, 15343.80, 15648.51, 15980.72, 16009.61, 16153.24 and 16165.03 Å. The lines were selected based on the fact that they had updated van der Waals broadening data from Barklem (private communication). The same procedure as with VmacSi was used, constraining $v_{\rm mac}$ and Fe abundance simultaneously with intermittent calibration of the linestrength, and discarding lines based on visual inspection. The left panel of Figure 4.4 shows that contrary to expectation, there is a clear systematic difference between the values derived with VmacSi and VmacFe. The most metal rich stars appear to show some of the largest differences, but no clear trend is observed. The right panel shows an example of what effect this differences has on my abundance analysis by showing the abundance trend of magnesium (see section 5.2 for details on how to read abundance trends). The agreement between the abundances calculated using the VmacFe method and those of Jönsson et al., in prep. are notably better, especially for stars of supersolar metallicity, compared to the abundances calculated using VmacSi. Due to similar improvements in agreement for other elements the VmacFe method was selected for the final results.

4.3 Model atmospheres

The physical conditions of stellar photospheres are approximated by model atmospheres. In this thesis MARCS model atmospheres are used (Gustafsson et al., 2008), more specifically the MARCS2014 grid. The MARCS model atmospheres follow four main approximations:

- 1D: the photosphere is treated as being solely a function of depth, deviations from this is corrected by the microturbulence parameter.
- Spherical symmetry: this thesis focuses on giants, whose photosphere requires spherically symmetrical models due to the larger scale heights and extensions of the atmosphere (Heiter et al., 2006). This is in contrast to the simplified plane parallel models which work well for dwarfs.

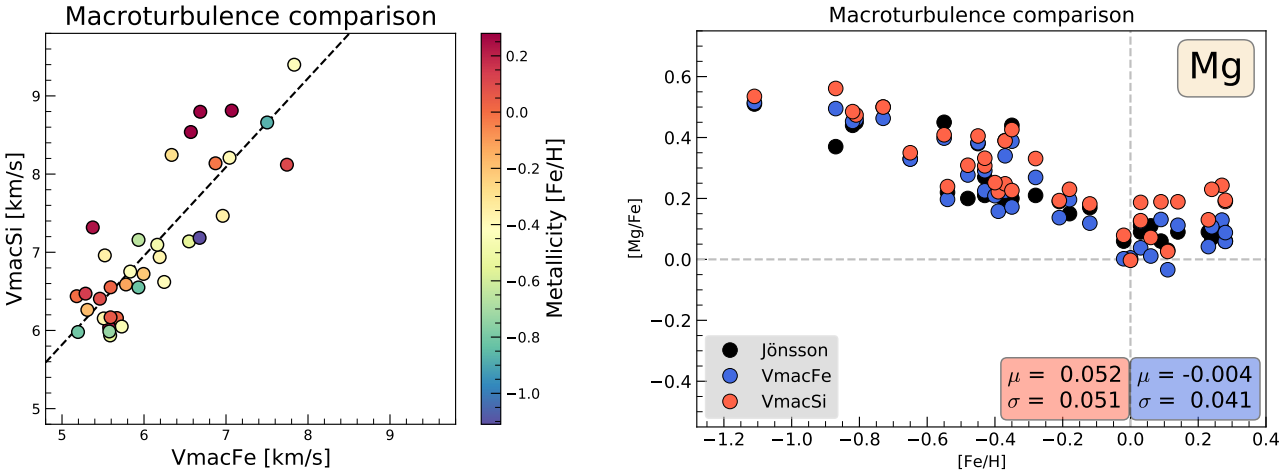

Figure 4.4: Left: Macroturbulences derived using the two methods described in section 4.2.2. No clear trend with metallicity is seen, note however the large difference for the most metal rich stars, seen in dark red.
Right: Comparison of magnesium abundance trends derived using the two techniques to determine macroturbulence investigated in this thesis, VmacSi and VmacFe, shown in red and blue respectively. The agreement with abundances from Jönsson et al., in prep. (shown in black) is notably better for VmacFe, especially for higher values of [Fe/H].

- Hydrostatic equilibrium: the forces of gravity and pressure are assumed to balance each other out, preventing the gas from predominantly moving in one direction.
- Local Thermodynamic Equilibrium (LTE): thermodynamic equilibrium describes a state where no net flow of energy occurs in the system, a condition which describes stars rather poorly as they radiate massive amounts of energy. LTE on the other hand, describes a system where although a net energy difference may be present, the change is slow enough that the temperature of an individual particle is still set by collisions with its immediate surroundings.

Using these assumptions, models are made which describe a number of different physical and thermodynamic parameters on a number of different depth points: temperature, gas pressure, electron pressure, radiation pressure and opacity etc. Each model corresponds to a different combination of the fundamental stellar parameters; effective temperature, surface gravity and metallicity. To adapt the model atmosphere to the precise parameters for each star, SME creates an interpolated model based on the MARCS2014 model grid. These LTE models are then used in the SME synthesis where the line formation can be computed in NLTE given departure coefficients for the line (see section 2.2.4), but the structure of the atmosphere will still be computed in LTE.

4.4 Linelists

The atomic physics data on the spectral lines in the studied wavelength region is gathered in a database commonly referred to as a linelist. The most essential parameters for each line are:

- The element and ionisation stage
- Central wavelength of the line
- Upper and lower excitation energies of levels involved in transition
- Linestrength, $\log(gf)$.

Additional information about the lines:

- Broadening parameters, estimating the lines susceptibility to different types of line broadening (see section 2.2.2)
- Energy level electron configurations, used for identifying transitions for possible NLTE corrections (see section 2.2.4)

The basis of the linelist used in this thesis is from VALD (Ryabchikova et al., 2015) which aggregates data from a large collection of sources. This linelist has then been improved in this work by both literature sources, and my own observational measurements. The main external addition is the improved values of the van der Waals broadening parameter calculated using ABO theory (see section 2.2.2), with new values from both Barklem, private communication and ones included in the spectral synthesis code BSYN (Gustafsson et al., 2008). References to the sources for the VALD data are given in the linelist in appendix A. Additions from literature sources consist mostly of more accurate wavelengths for a number of elements, also referenced in appendix A.

Molecular lines

The behaviour of spectral lines from molecules is somewhat different from that of atomic lines. Interactions inside the molecule such as rotation and vibration lead to very many spectral lines, meaning that molecular linelists can become very long. The second important consideration is that the number density of molecules is highly dependent on the stellar parameters, especially the temperature. Higher temperatures break molecules up into their constituent atoms, so that for a comparatively hot star like the Sun molecular lines do not appear as there are no molecules to see. Loading all available molecular data can therefore slow down calculations to little benefit. In this thesis linelists for $^{13}C^{14}N$ and $^{12}C^{14}N$ from Sneden et al. (2014), $^{13}C^{16}O$ and $^{12}C^{16}O$ from Goorvitch (1994) and ^{16}OH from Goldman et al. (1998) were used, as no other molecules show significant lines in the K giants spectra.

Despite the difference in how they form, molecular lines can be described using excitation energies and $\log(gf)$ values, just like lines from atoms and ions. Abundances could be derived using these lines, ideally by letting SME find the abundances of C, N and O simultaneously from a combination of the different molecular lines. This analysis has not been done in this thesis, where the molecular linelists have been included solely to help account for blends to atomic lines.

4.4.1 Astrophysical oscillator strength determination

The largest addition to the linelist are the $\log(gf)$ values astrophysically measured in this thesis, see section 2.2.1 for details on the need for these measurements. $\log(gf)$ values are determined using the same spectral synthesis method as when determining abundances (see section 4.1), with $\log(gf)$ being the parameter that is fitted to the lines as the solar abundances are already known.

The observation used for astrophysical $\log(gf)$ measurements in this thesis is a solar flux spectrum recorded with IGRINS from the sunlight reflected off the asteroid Ceres. A spectrum from reflected sunlight results in a more stellar like source, giving a integrated flux spectrum with no centre-of-disc or limb darkening effects present. There are several advantages to measuring $\log(gf)$ against the Sun; being several orders of magnitude closer than any other star, the Sun's abundances can be determined much more precisely (Asplund et al., 2009), and the stellar parameters can be obtained with high precision and accuracy, independently of the spectra. The Sun's increased temperature compared to K giants will also strongly reduce the risk of unknown molecular blends. To avoid any issues from the interpolation of model atmospheres, a Solar model atmosphere was constructed specifically for this purpose.

To the greatest extent possible, the lines used for abundance analysis in this thesis have had their $\log(gf)$ values measured astrophysically. For the elements where all lines were too weak in the Sun to get an accurate value, the $\log(gf)$ value was adjusted to reduce the mean difference between measured abundances of the giants and the values in Jönsson et al. (in prep.) to zero. Changing the $\log(gf)$ value only affects the scale of [X/Fe], meaning the shape of the trend is preserved and the scatter in the results can be compared to the optical values, even though the mean is not useful as a comparison between samples for elements shifted in this way. The elements with $\log(gf)$ values adjusted in this way in this thesis are: V, Co, Cu and Ce. Alternative approaches could have been to perform astrophysical measurements against α Boo or another well studied K giant, or to adopt laboratory or calculated linestrengths. The abundances and parameters of α Boo are less certain than those of the Sun and using it to measure $\log(gf)$ values will therefore introduce larger errors than the Sun does. For V, Co and Cu only semi-empirical $\log(gf)$ values are available, which are not accurate enough for abundance analysis. For the Ce II lines there exist astrophysical measurements by Cunha et al. (2017), measured against α Boo, for the lines within APOGEE's range. For the lines redwards of 17000 Å no measurements exist, and the method described above has to be used. The values from Cunha et al. (2017) were tried and found to give similar but slightly worse results than the method above. For

Nd, Hasselquist et al. (2016) uses a similar method and determines astrophysical values for infrared lines from the star 2MASS J16011638-1201525, by first measuring the Nd abundance from optical lines with lab measured $\log(gf)$ values. In this case, the values from Hasselquist et al. (2016) were better than my astrophysical results for one of the lines used for abundance analysis, 16053.63 Å.
For some wavelengths, there are observed spectral lines which are formed from not one, but several transitions. When the transitions come from different elements they are called blends and put the line at risk of being discarded, depending on the strength of the lines and how well they are modelled. Blends from lines of the same element pose no difficulty for abundance analysis, but they become a problem for astrophysical $\log(gf)$ measurements. This is because it is not immediately obvious how the strengths of different lines should be changed. For cases where the secondary line(s) come not only from the same element, but from the same LS multiplet, the relative oscillator strength between the lines can be calculated. The process developed in this thesis for calculating these relative strengths for both fine and hyperfine structure lines is described in appendix B, based on the theory described in Cowan (1981). In the H band this method has mostly been necessary for fine structure lines of Mg, S and K, and for the elements with hyperfine structure.
The method of astrophysically measuring $\log(gf)$ is not uncommon, but far from a universally adopted technique. The extra work involved, the need for a high resolution spectrum of a well known star and the risk of introducing an additional source of error, means that database values are often used instead.
The $\log(gf)$ values of many of the lines in the H band have been measured astrophysically in this thesis despite not being considered for abundance analysis. The benefits of this ranges from decreasing blending of nearby lines used to measure abundances and avoiding disruption of the local continuum calibrations, to the insight it gives through analysis of the errors in spectral lines. This kind of work is more commonly done for surveys, see Buder et al. (2020) and Smith et al. (2021), outside of which it is rarely done in the systematic manner which has been used in this thesis. For more information on this topic, see section 5.5.

4.5 Analysis of NLTE and HFS

A common procedure for spectral analysis is to adopt database values uncritically, making use of the available data, adding external literature sources if they are available. For the purpose of evaluating the impact of the hyperfine structure (HFS) splitting of energy levels and of NLTE corrections, I will instead be removing data when deriving abundances.
In the cases where data on the HFS lines of an element is available, two sets of results are calculated, with and without accounting for the elements HFS. $\log(gf)$ values are calculated for both sets of data in the manner described in section 4.4.1. The same applies for elements with NLTE corrections, where two sets of data are calculated with and without the elements NLTE departure coefficient grid, both when determining abundances and $\log(gf)$ values. The NLTE corrections for other elements have been applied for both sets of results. For the

elements where both HFS and NLTE have been considered, the effects have been assessed separately, meaning HFS has been included for both LTE and NLTE results, and vice versa.
Publishing the NLTE corrections that have been applied to your abundances is a common practice when using tools such as the Inspect Database (Lind et al., 2012), which calculates abundance corrections for results computed in LTE. Recently, with the advent of NLTE departure coefficient grids which do not require a manual correction to the abundance, it has become less common to publish such corrections. The impact of HFS is not commonly assessed, except in cases where the study of the hyperfine structure is the goal of the work (see Booth et al. (1983) for an example of a focused study of the impact of HFS in stellar abundance analysis).
An illustrative example of why highlighting the differences these effects cause is important, is the work by Thorsbro et al. (2018). In this article claims of scandium abundances exceeding [Sc/Fe] = 1 for galactic centre stars by Do et al. (2018) are dispelled by presenting an analysis which includes the effects of HFS. Accurately measured $\log(gf)$ values and excitation energies from Pehlivan et al. (2015) were used by Do et al. (2018) for the Sc lines. But as the lab measurements did not include HFS, the impact on line formation was neglected, leading to significant errors in the elemental abundance.

4.6 Uncertainties

The estimation of uncertainties in abundance analysis is not a trivial topic, due to the many different factors which can influence line formation. In this section I will discuss how I estimate the random errors from uncertainties in stellar parameters, how the instrumental errors can be estimated, and how correlations with stellar parameters are treated.

4.6.1 Stellar parameters

Based on benchmark values from the literature, the stellar parameters from Jönsson et al. (in prep.) are believed to be free from significant of systematic errors with a high level of precision.
This leaves random errors from the uncertainty in the analysis. The method used in this thesis to estimate the random errors is to generate sets of stellar parameters following a normal distribution of values, using the uncertainty in the parameter as the standard deviation, and to reanalyse the spectra using those parameters. A representative star is chosen, preferably one with a high signal to noise ratio to ensure that random fluctuations in the spectra do not affect the measurement of the error from stellar parameter definition. For this work I have chosen to use α Boo (Arcturus) and μ Leo (Rasalas), as they both have adequate S/N (155 & 169), are well studied benchmark stars with relatively well constrained stellar parameters, which are different enough that together they cover a large range of the stellar parameters of the stars in this work. The quoted uncertainties in the stellar parameters from Jönsson et al. (in prep.) can be seen in table 4.1 along with the

	$T_{\rm eff}$ [K]	log(g) [dex]	[Fe/H] [dex]	$v_{\rm mic}$ [km/s]
Uncertainty	50	0.15	0.05	0.1
α Boo	4308	1.66	-0.55	1.77
μ Leo	4494	2.51	0.27	1.53

Table 4.1: Uncertainties and stellar parameters adopted from Jönsson et al. (in prep.).

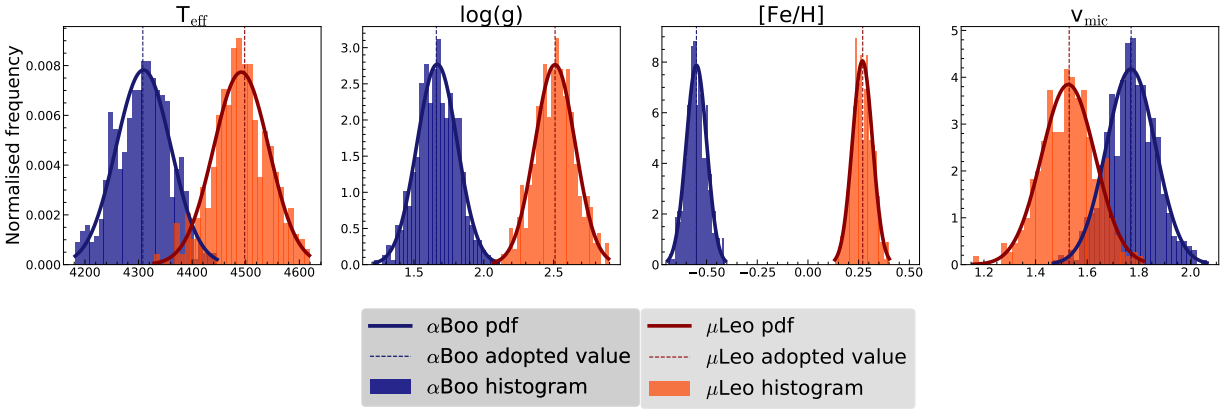

Figure 4.5: Adopted modified stellar parameters for Monte Carlo estimation of errors due to stellar parameters. 1000 sets of stellar parameters have been made in total, 500 each based on Arcturus and μ Leo respectively. The deviations in the parameters are based on the uncertainties in table 4.1.

adopted values for α Boo and μ Leo. For each star 500 sets of parameters have been generated in a normal distribution, using the adopted value as the mean and the quoted uncertainty as the standard deviation. Histograms of the values I have generated, along with a fitted Gaussian probability distribution function, can be seen in Figure 4.5; the dashed lines show the "true" values for the stars. The values based on α Boo are plotted in blue, while the ones for μ Leo are shown in red. The results of this analysis are shown in Figure 4.6. Note that it is not certain that the adopted values are in the middle of the distribution, as lines can have non-linear dependencies on stellar parameters. For μ Leo the minimum/mean/maximum spread in abundances is 0.042/0.078/0.19 dex. For α Boo the same numbers are 0.046/0.23/3.0; excluding a single extreme outlier for sulphur brings these values down to a minimum/mean/maximum of 0.046/0.074/0.16 dex. The errors for individual elements are further discussed in section 5.2, as other sources of error are assumed to be global.

Figure 4.6: (Shown on next page) Investigation of errors in abundance results from the uncertainty in stellar parameters. Results have been calculated from the spectra of α Boo and μ Leo with stellar parameters drawn from a normal distribution around their adopted values, shown in Figure 4.5.

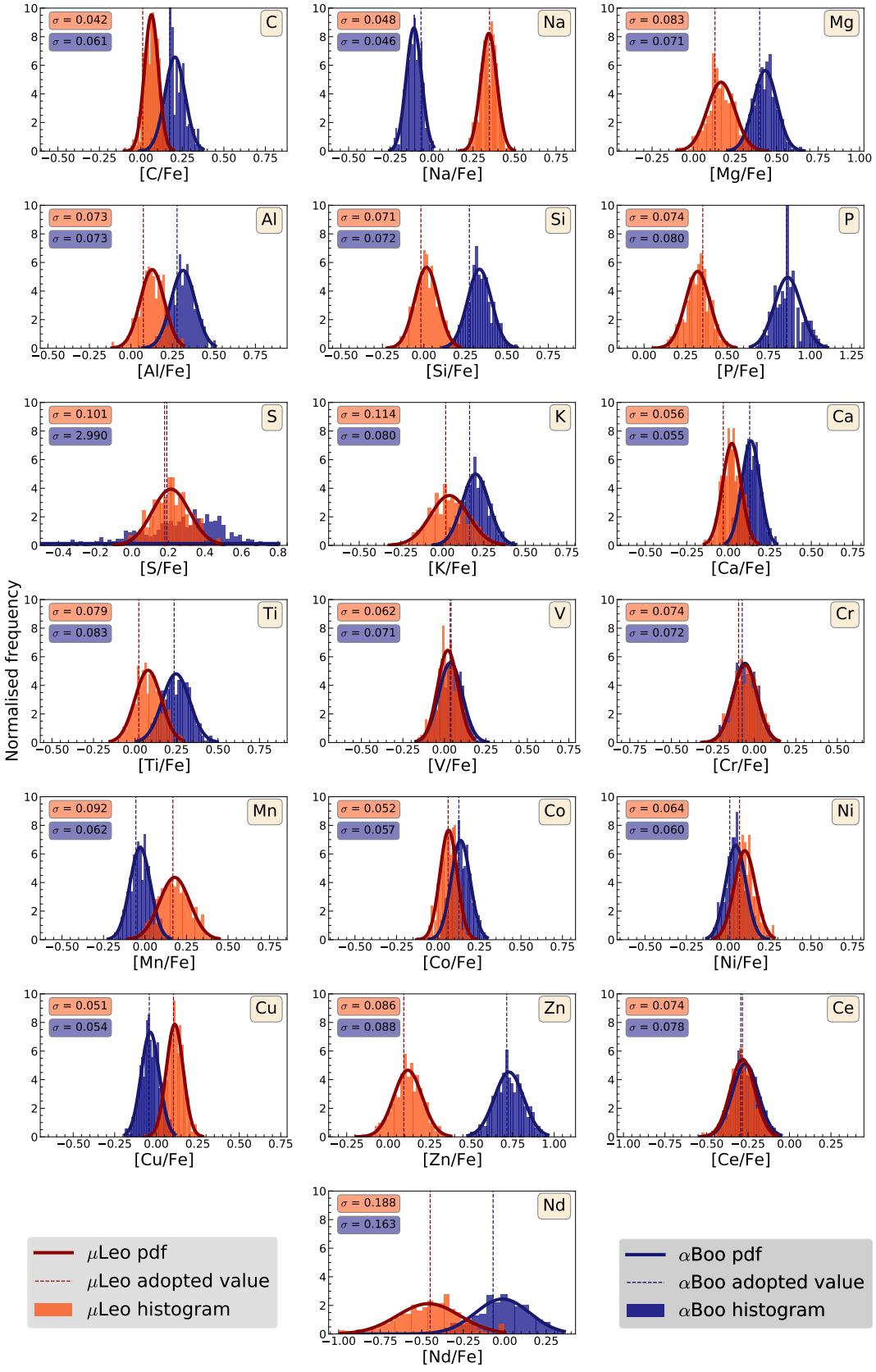
C
σ = 0.042
σ = 0.061
[C/Fe]
Na
σ = 0.048
σ = 0.046
[Na/Fe]
Mg
σ = 0.083
σ = 0.071
[Mg/Fe]
Al
σ = 0.073
σ = 0.073
[Al/Fe]
Si
σ = 0.071
σ = 0.072
[Si/Fe]
P
σ = 0.074
σ = 0.080
[P/Fe]
S
σ = 0.101
σ = 2.990
[S/Fe]
K
σ = 0.114
σ = 0.080
[K/Fe]
Ca
σ = 0.056
σ = 0.055
[Ca/Fe]
Normalised frequency
Ti
σ = 0.079
σ = 0.083
[Ti/Fe]
V
σ = 0.062
σ = 0.071
[V/Fe]
Cr
σ = 0.074
σ = 0.072
[Cr/Fe]
Mn
σ = 0.092
σ = 0.062
[Mn/Fe]
Co
σ = 0.052
σ = 0.057
[Co/Fe]
Ni
σ = 0.064
σ = 0.060
[Ni/Fe]
Cu
σ = 0.051
σ = 0.054
[Cu/Fe]
Zn
σ = 0.086
σ = 0.088
[Zn/Fe]
Ce
σ = 0.074
σ = 0.078
[Ce/Fe]
Nd
σ = 0.188
σ = 0.163
[Nd/Fe]
μLeo pdf
μLeo adopted value
μLeo histogram
αBoo pdf
αBoo adopted value
αBoo histogram

4.6.2 Instrumental errors

Instrumental errors are often quantified by analysing multiple spectra from the same star or measuring the abundances of cluster members. This has not been performed in this project as those observations have not been available. Böcek Topcu et al. (2016) has studied 12 K giants in the open cluster NGC 6940 using the same instrument used in this thesis, IGRINS. As open clusters are formed from the same material it is assumed that their abundances should be the same. The spread in investigated abundances for their stars is between 0.02 - 0.16 dex with a mean of 0.08 dex which could be adopted as a measure of the instrumental error (Jofré et al., 2019).

4.6.3 Bias from stellar parameters

Investigating abundance trends to see whether there is a detectable correlation to any of the adopted stellar parameters can be a good way of searching for systematic errors not detected by other methods. An issue with using this method for the sample of stars we have used, is that the sample is biased as a result of observational selection effects. The effect of this can be seen in Figure 4.7, where the abundance trend of magnesium is shown, with the stars coloured by $T_{\rm eff}$ and $\log(g)$ respectively. What can be seen in these plots is that low metallicity stars with a high relative magnesium abundance, features associated with the so-called thick disc, are biased towards lower temperatures and surface gravities. This bias exists because in the Solar neighbourhood thick disc stars are less common than stars from the thin disc, and are therefore statistically more likely to be far away. To compensate for this extra distance bright stars are targeted during observations to maintain high signal to noise ratios and reasonable observational times.
Because of this observational bias, there is little point to investigating whether there are correlations between abundances and parameters, as we already know this is the case for reasons other than systematic errors in the analysis. What I have done instead is to investigate whether there are any correlations between the stellar parameters and the deviation from the abundances derived by Jönsson et al. (in prep.). This will not verify that there are no correlations with stellar parameters, but it will verify whether there are "new" biases introduced that are not present in the optical results. Since this method relies on the results of Jönsson et al. (in prep.) it can only be used for elements measured by both studies.
The results of this analysis are shown in section 5.1.

4.7 Comparisons to other studies

In contrast to most stellar spectroscopic work, the primary results of this thesis are not the trends of the abundance ratios and their implications for galactic chemical evolution. Instead the main purpose is the comparison of the trends to results from optical spectra, to see how well they can be replicated and what the causes are for any discrepancies. Optical spectra have the advantages of many more decades of careful study and a wealth

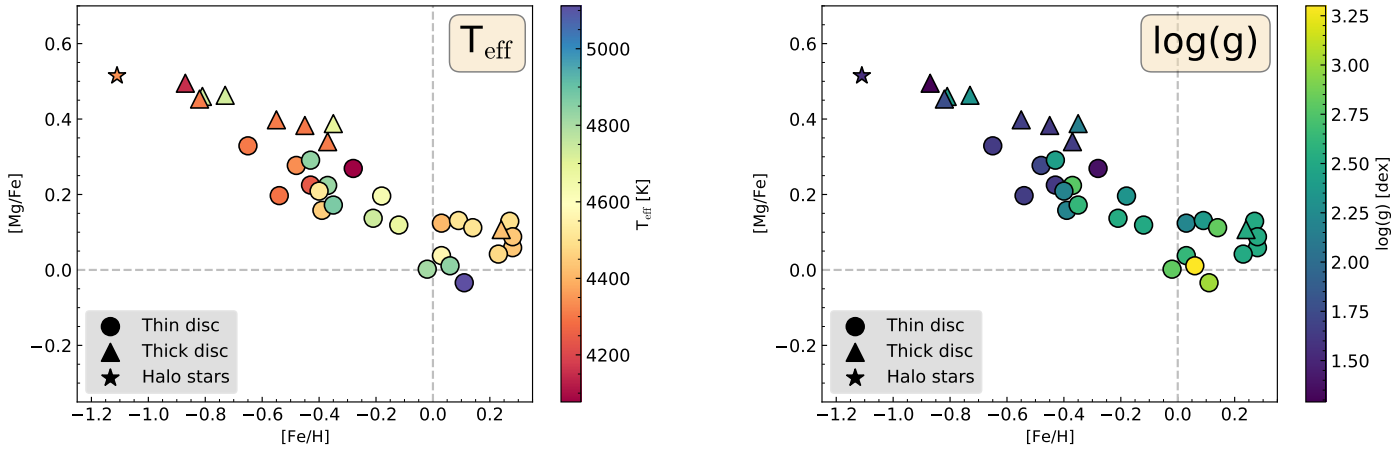

Figure 4.7: Abundance trend of Mg coloured by the stars effective temperature and surface gravity on the left and right respectively. The division into thin disc/thick disc/halo stars is made using Mg abundances and stellar kinematics by Forsberg (2019). The bias towards cooler stars with lower surface gravity towards lower metallicities can be explained by an observational bias towards observing brighter stars in the thick disc as they are rarer and thus more likely to be far away.

of lab measured atomic data not present for infrared lines, and it is therefore assumed the optical results will be better. However, there is no guarantee that this is the case; the reliability of abundance measurements depends to a substantial degree on the quality of the spectral lines, how strong they are, if they are blended, if the local continuum level is well established. In the light of this context; the optical abundances are treated as the best available data, elements where there is good agreement are considered to be measurable from H band spectra, while for elements where there are significant discrepancies further investigation is carried out to determine the cause, and which estimate is more reliable.
The optical results compared against are those presented in Jönsson et al. (in prep.), the same study which has determined the stellar parameters used in this thesis. The results come from high resolution optical spectra, with further details shown in section 3.2. The abundances have been derived using the same technique of manual spectroscopic analysis, using the same software (SME), with the same stellar parameters; the systematic errors between these two studies and the abundances derived in this thesis should therefore be minimised to as large a degree as possible.
A slight difference between the analyses are the treatment of NLTE effects and hyperfine structure lines, as updated values have been published during the thesis work which have not yet been incorporated into the optical analysis. In the optical analysis, NLTE grids have been used for O, Na, Mg, Si and Fe (Amarsi et al., 2016b; Lind et al., 2011; Osorio et al., 2016; Amarsi et al., 2017; Amarsi et al., 2016). These grids are mostly the same as those used for the infrared analysis in this thesis, but lacking the improvements and

standardisation made in Amarsi et al., 2020. Hyperfine structure lines have been included in the optical analysis for V, Mn, Co and Cu, while Na and Al lack HFS lines. The log(gf) values used in the optical analysis are mainly from the Gaia-ESO linelist (Heiter et al., 2021) with the addition of astrophysical values from Meléndez et al. (2009) for Fe II lines. The secondary comparison sample is from Christensen (2020), where APOGEE spectra of the same stars have been reanalysed using manual spectral synthesis with SME. The purpose of comparing to these results is mainly to study the impact of moving from APOGEE's resolving power $R \sim 22500$ to IGRINS $R \sim 45000$. The effect of such a change on the spectra can be seen in Figure 4.8, along with showing the resolution of a few current and upcoming spectrographs. The lower resolution spectra smears out a number of weak lines, blended lines become indistinguishable, finding the continuum emission level becomes more difficult. This combined with IGRINS increased wavelength range, means that more lines will be accessible for analysis in this thesis compared to Christensen (2020). As the results have been derived with a similar method and the same stellar parameters, it is the best available comparison in the infrared.

The analysis in Christensen (2020) differs from the one in this thesis in a few ways. The same NLTE grids used in Jönsson et al. (in prep.) have been used here, with the addition of an Al grid from Nordlander et al. (2017). No HFS lines have been included in the analysis. The log(gf) values used are a combination of semi-empirical values, lab values and astrophysical measurements carried out as part of the APOGEE survey (see table 5.1 in Christensen (2020)).

For elements which have not been measured by Christensen (2020) comparisons will be made to abundances obtained from APOGEE's latest data release, DR16 (Jönsson et al., 2020). APOGEE determines parameters and abundances simultaneously through the pipeline ASPCAP, described in García Pérez et al. (2016). ASPCAP is an industrial scale pipeline, optimised for the analysis of hundreds of thousands of spectra from a range of different types of stars, meaning that for individual stars the derived parameters can differ by a significant amount compared to the parameters from Jönsson et al. (in prep.). Because of the differences in method of analysis, finding the source of discrepancies between the results can be difficult, so comparisons to the APOGEE results will mostly be made when results from Christensen (2020) are not available. A summary of the differences between this work, Jönsson et al., in prep. and Christensen, 2020 can be seen in table 4.2.

	This work	Jönsson	Christensen
Spectral synthesis	SME	SME	SME
Base linelist	VALD3	Gaia-ESO	VALD3
Astrophysical $\log(gf)$	All lines used in analysis + extra	Only Fe II	Only Ce II
Hyperfine structure	Na, Al, V, Mn, Co and Cu	V, Mn, Co and Cu	None
NLTE corrections	C, Na, Mg, Al, Si, K, Ca and Mn	O, Na, Mg, Si and Fe	Na, Mg, Al, Si and Fe

Table 4.2: Differences in method between this thesis, Jönsson et al., in prep. and Christensen, 2020. Sources of different databases are given in section 4.7 and Appendix A.

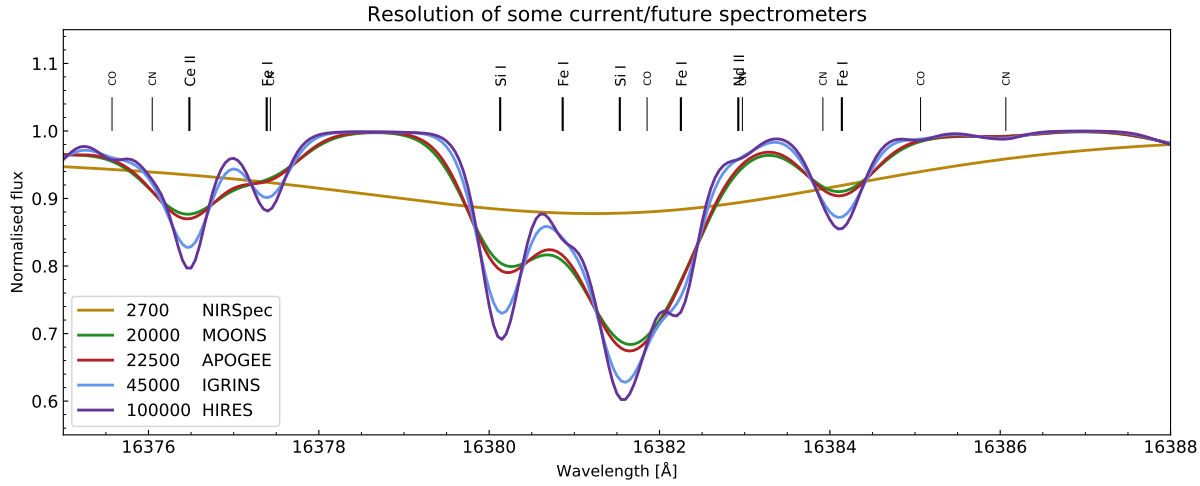

Figure 4.8: Comparison of how the different resolutions of current and future instruments would influence the Si I line at 16381 Å and associated blends and nearby lines. All the spectra have been synthesised by SME and adjusted to different resolutions with the built in instrumental profile parameter, no actual observations are shown in the figure. At the lower resolutions of MOONS and APOGEE the weaker lines blend together with the main line or do not show up at all. Resolutions higher than R $\sim$ 50000 have diminishing returns, as can be seen by comparing the spectra from IGRINS and the planned HIRES instrument for ELT. The spectra showing the resolution of the NIRSpec instrument on JWST does not resolve the lines at all, requiring a different method of analysis to determine abundances.

Chapter 5

Results and Discussion

The results of the thesis work are presented and discussed in this chapter. The subsections are structured as follows

- Tests for systematic bias in stellar parameters
- How to read the abundance trends
- Breakdowns of the results for individual elements, with discussion of NLTE and HFS when appropriate
- A note on a common outlier
- Further discussion of astrophysical $\log(gf)$ measurements

5.1 Parameter bias

As introduced in section 4.6.3, observational factors will bias the lowest metallicity stars towards low surface gravities and temperatures (see Figure 4.7). Because of this I have chosen to investigate whether there are correlations between stellar abundances and the deviation of my abundances from the values in Jönsson et al., in prep., instead of taking just the parameters and my abundances.
Figures 5.1-5.4 show the deviation from Jönsson et al. (in prep.)'s results plotted against $T_{\rm eff}$, $\log(g)$, [Fe/H] and $v_{\rm mic}$. A linear fit has been calculated for the plots, the slope of the fit k is given in the figures along with the correlation coefficient, r, calculated using the Python package Pandas (The pandas development team, 2020).
Where further discussion of the trends for individual elements is appropriate, it will be presented in the discussions of that element in section 5.2. A brief summary of some of the most statistically significant trends observed is presented below.

$T_{\rm eff}$

In Figure 5.1 we see that most elements show little correlation with $T_{\rm eff}$. Minor trends are seen in Mg and Ca and a slightly larger one in Al, but all with $r < 0.5$.

$\log(g)$

Figure 5.2 shows that the correlations with $\log(g)$ appear slightly more significant on average. Small trends are seen for Mg, Si and Ca with a moderate correlation. Al has a more noticeable trend with the highest significance of all the ones measured here.

[Fe/H]

The trends with metallicity in Figure 5.3 show the same results as the abundance trends presented in section 5.2 with the difference to Jönsson et al., in prep. easier to read out. Ca, Ti, Mn and Ni all show slight trends with a moderate significance. Al and Si show somewhat steeper trends with stronger correlations.

$v_{\rm mic}$

No major correlations are seen in $v_{\rm mic}$, the trend for Mn being the most significant. A noticeable feature in the plot for $v_{\rm mic}$ is that the star with the highest $v_{\rm mic}$ in the sample, HIP 63432, shows an overabundance of all elements but Co and V. This outlier is discussed further in section 5.3.

In general the analysis does not appear to introduce significant correlations to stellar parameters beyond what is present in Jönsson et al., in prep. The exception to this appears to be Al, which shows a statistically significant correlation to $\log(g)$ in particular. The trend for Nd shows large slopes in the linear fit for all parameters, but the high scatter of the trend means that none of the correlations are statistically significant. A similar effect is seen to a lesser degree for Cu.

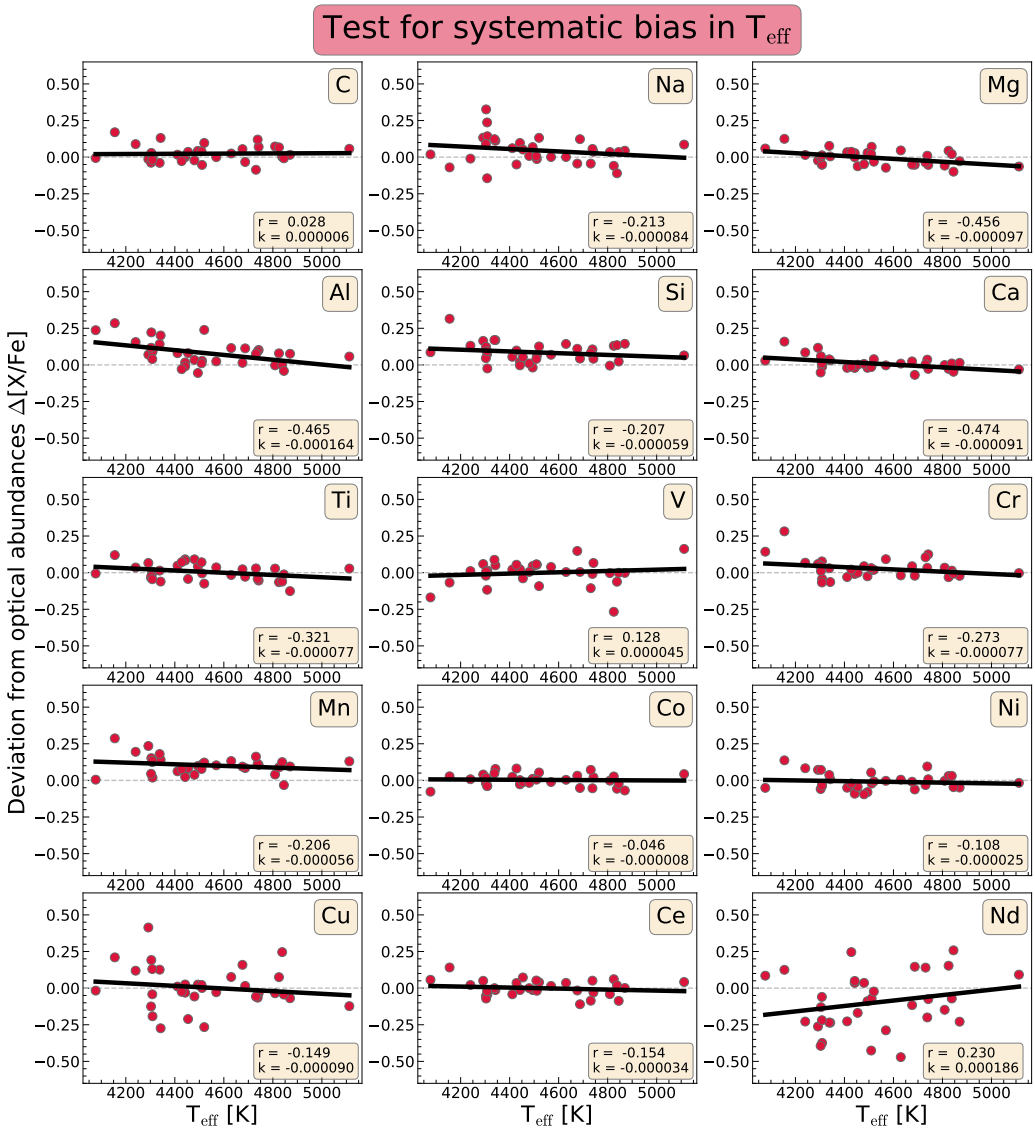

Figure 5.1: Deviation from the results of Jönsson et al. (in prep.) plotted against effective temperature, $T_{\rm eff}$.

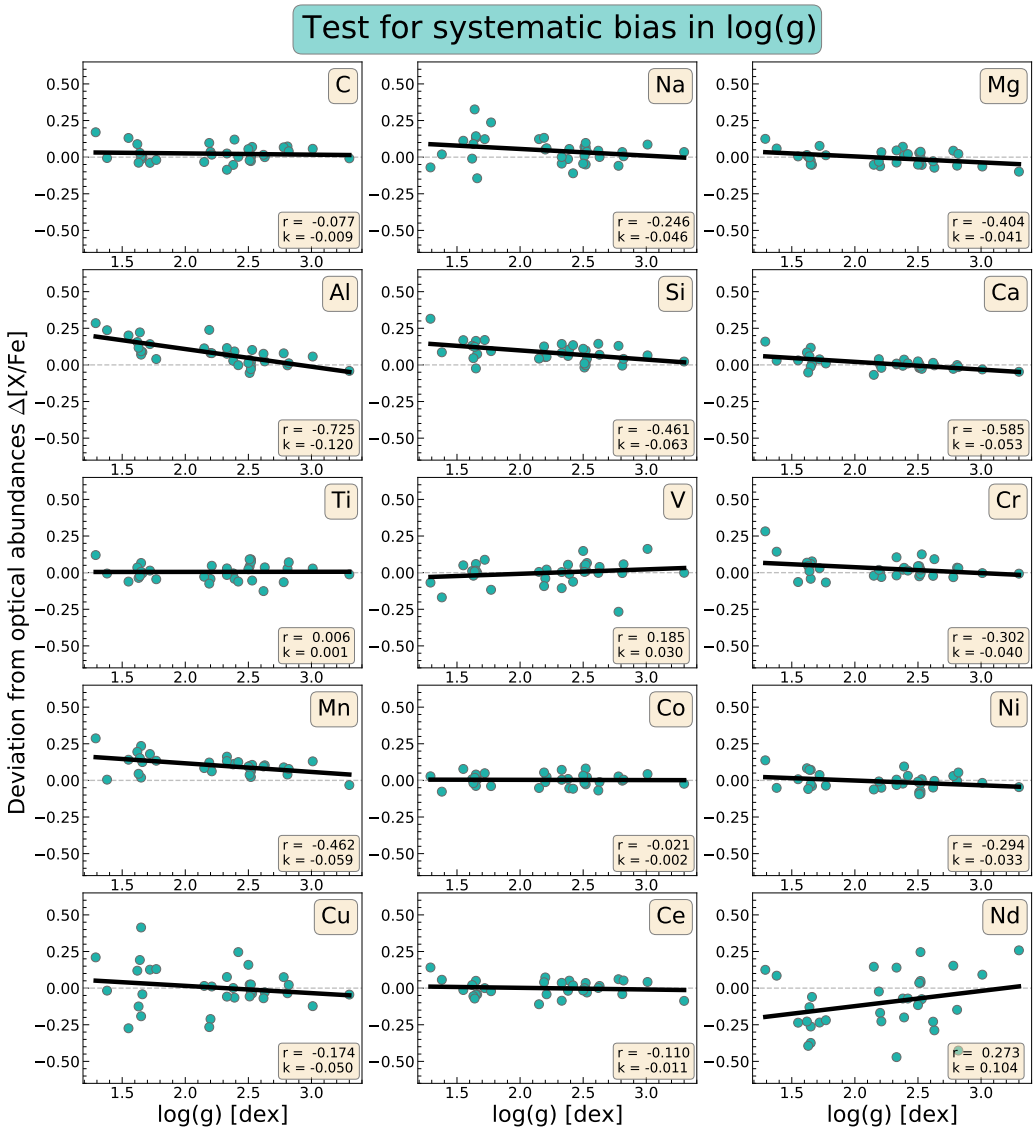

Figure 5.2: Deviation from the results of Jönsson et al. (in prep.) plotted against surface gravity, $\log(g)$.

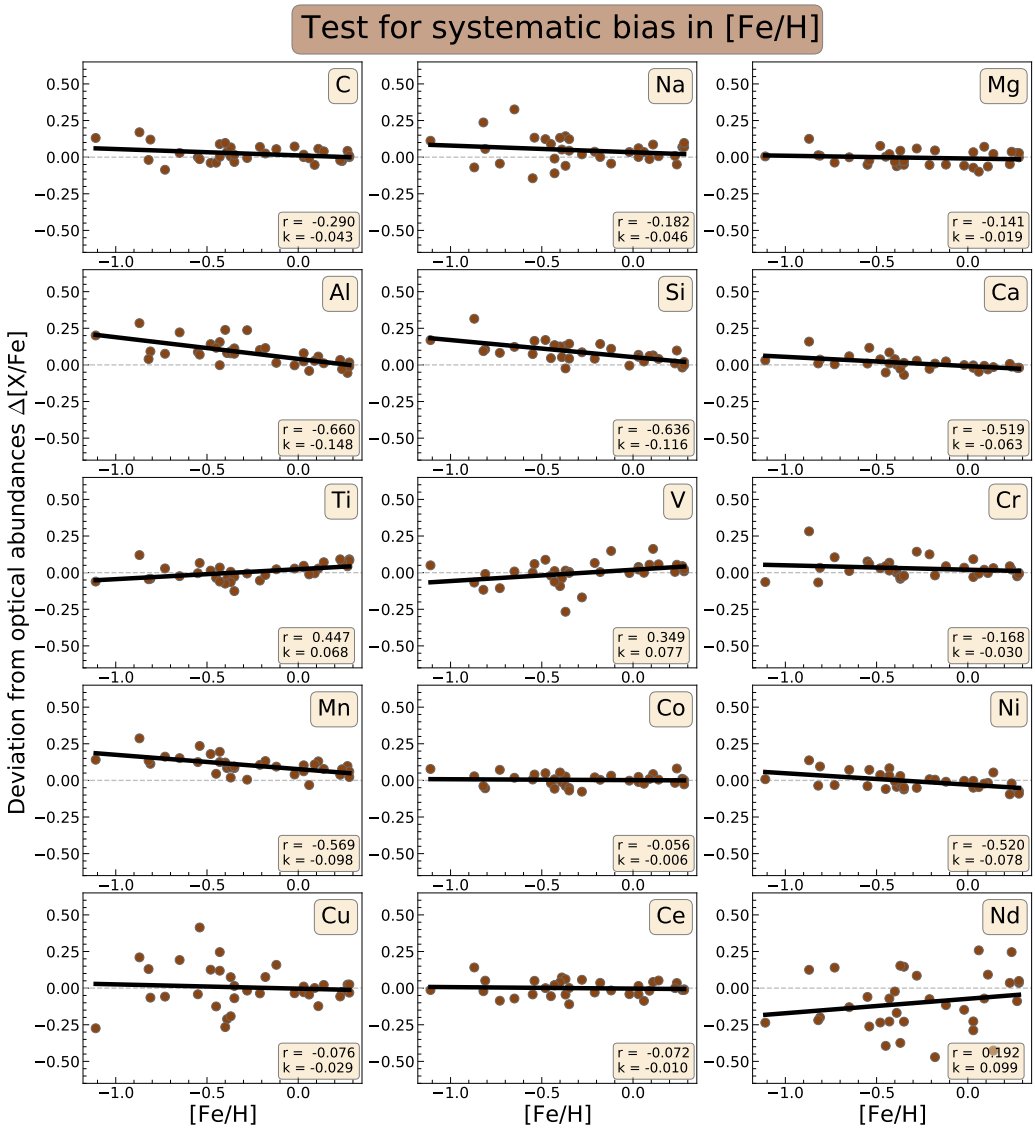

Figure 5.3: Deviation from the results of Jönsson et al. (in prep.) plotted against metallicity, [Fe/H].

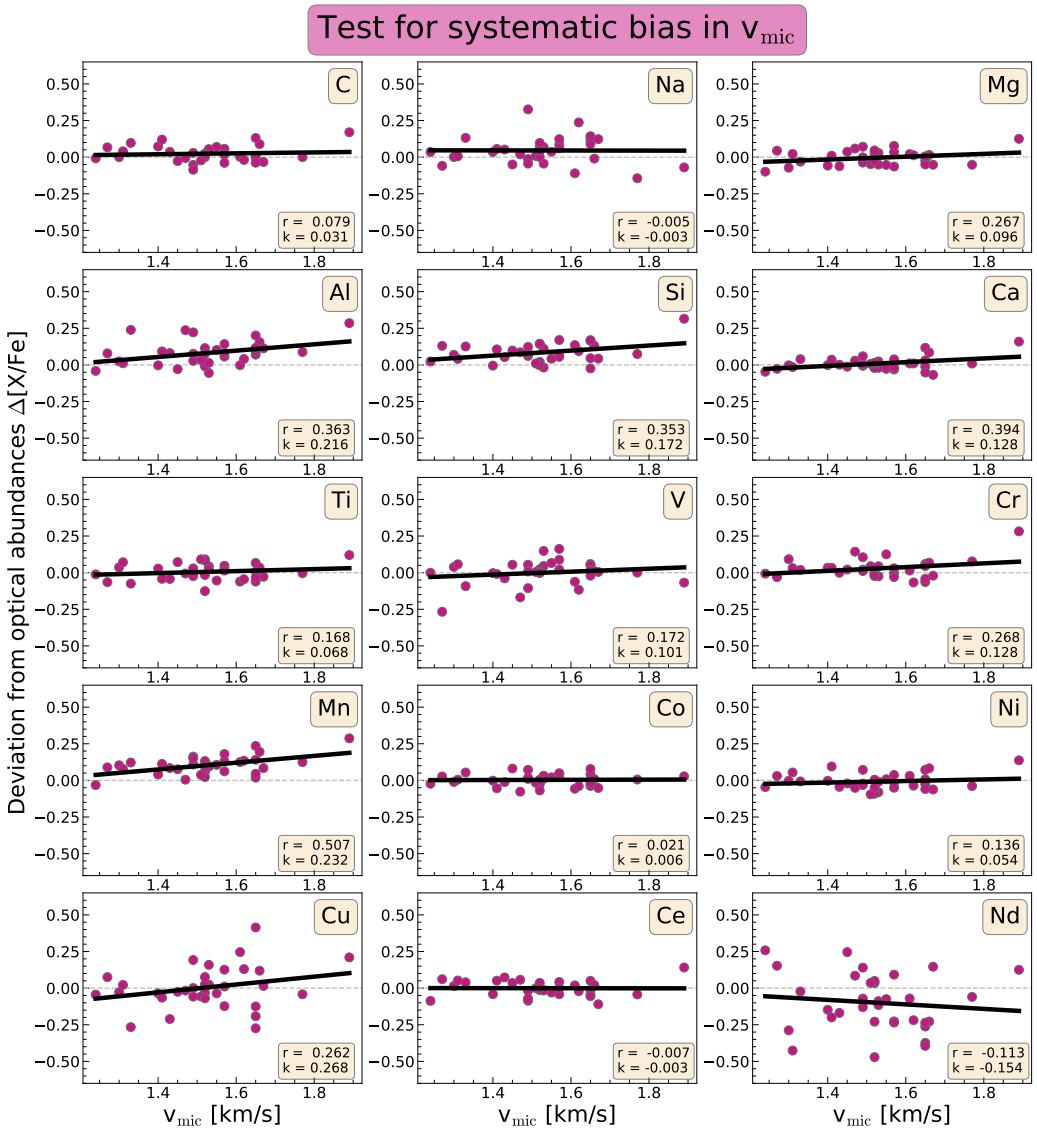

Figure 5.4: Deviation from the results of Jönsson et al. (in prep.) plotted against micro-turbulence, v_{mic}.

5.2 Abundance trends

In this section the abundances determined during the thesis work are presented and discussed. The abundance trends of all elements are shown in Figure 5.5, with each element being discussed in further detail in the following subsections. Below is an explanation of how to read the elemental abundance trends and how the comparison samples are presented.
The notation used for presenting elemental abundances in this thesis is [A/B], a shorthand for:

$$[\mathrm{A/B}] = \log_{10}\left(\frac{N_A}{N_B}\right)_\star - \log_{10}\left(\frac{N_A}{N_B}\right)_\odot \tag{5.1}$$

meaning the $\log_{10}$ value of the ratio between the number densities of the elements for a star, scaled to the values for the Sun. The results shown in this section all have the same parameter on the x-axis, [Fe/H], meaning the iron abundance or metallicity. The y-axes are all [X/Fe], meaning abundance of element X compared to the iron abundance. In the text when the abundance of X is mentioned, this refers to the relative, scaled [X/Fe] abundance, and not an absolute value.
A feature of using this notation is that the solar value will always be at (0, 0), dashed grey lines are shown in every plot intersecting this point. The scale of all subplots in Figure 5.5 are kept the same, with the values of the y-axis slightly shifted for some elements to better show all stars.
The abundance trend of each element is compared to abundances derived for the same stars with the same parameters from manually analysed high resolution optical spectra (Jönsson et al., in prep.); and medium-high resolution APOGEE spectra from Christensen (2020). Some additional comparisons are made to the official APOGEE DR16 results (Jönsson et al., 2020), derived using the ASPCAP pipeline (García Pérez et al., 2016). See section 3.2 for details on the different observations and section 4.7 for a description of the difference in the methodology used when analysing the spectra.
The results shown in the plots are:

- The abundances determined in of this thesis are shown in blue.
- The full sample of Jönsson et al. (in prep.) is displayed as smaller grey dots in the background for all available elements, to give a context for the values of the 34 stars I have measured.
- All stars studied in this thesis are present in the sample from Jönsson et al. (in prep.), the optical values for the overlapping stars have been highlighted with black dots.
- 25 stars overlap between this thesis and the work of Christensen (2020), those abundances are displayed in red for all elements where measurements have been performed. Some outliers are removed by Christensen (2020), meaning all 25 stars are not present for all elements.

- The same 25 stars have measurements from APOGEE DR16 (Jönsson et al., 2020), which are shown for elements where Christensen (2020) or Jönsson et al. (in prep.) lack measurements.

For elements with measurements by Jönsson et al. (in prep.), values of the mean and mean absolute deviation (labelled μ and σ in the figures) of the difference in [X/Fe] between the different samples and Jönsson et al. (in prep.)'s values are shown at the bottom of the figure. The boxes with these values have been colour coded in the same manner as the dots. The mean absolute deviation is used over the standard deviation to avoid influence from outliers and has been calculated using the implementation in Pandas (The pandas development team, 2020).
Note that as the same metallicities have been used for this work, Jönsson et al. (in prep.) and Christensen (2020), meaning they share an x-axis and dots on the same vertical line are measurements of the same star. APOGEE uses their own metallicities, and can not be identified in this fashion.
Elements with NLTE corrections or hyperfine structure lines have additional results shown in the elements subsections. The results without HFS are computed in NLTE where possible, and use astrophysically determined $\log(gf)$ values also using NLTE corrections. The same principle applies to the LTE results, which make use of HFS when available, both for abundances and astrophysical $\log(gf)$ values.
Due to an observational bias to intrinsically brighter stars at low metallicity, see section 4.6.3, it is possible that what appears as a correlation with metallicity is a correlation with a different parameter.

Figure 5.5: (Shown on next page) Abundance trends for all elements successfully measured in this project. The full sample from Jönsson et al. (in prep.) is shown in grey, with the stars present in the dataset used in this thesis marked in black. The results of my analysis are shown in blue. The results of Christensen (2020) are shown in red. The results of APOGEE's ASPCAP analysis are shown in green. The μ and σ values shown are the mean and mean absolute difference of the difference from the optical values of [X/Fe], colour coded to in the same manner as the abundance trends.

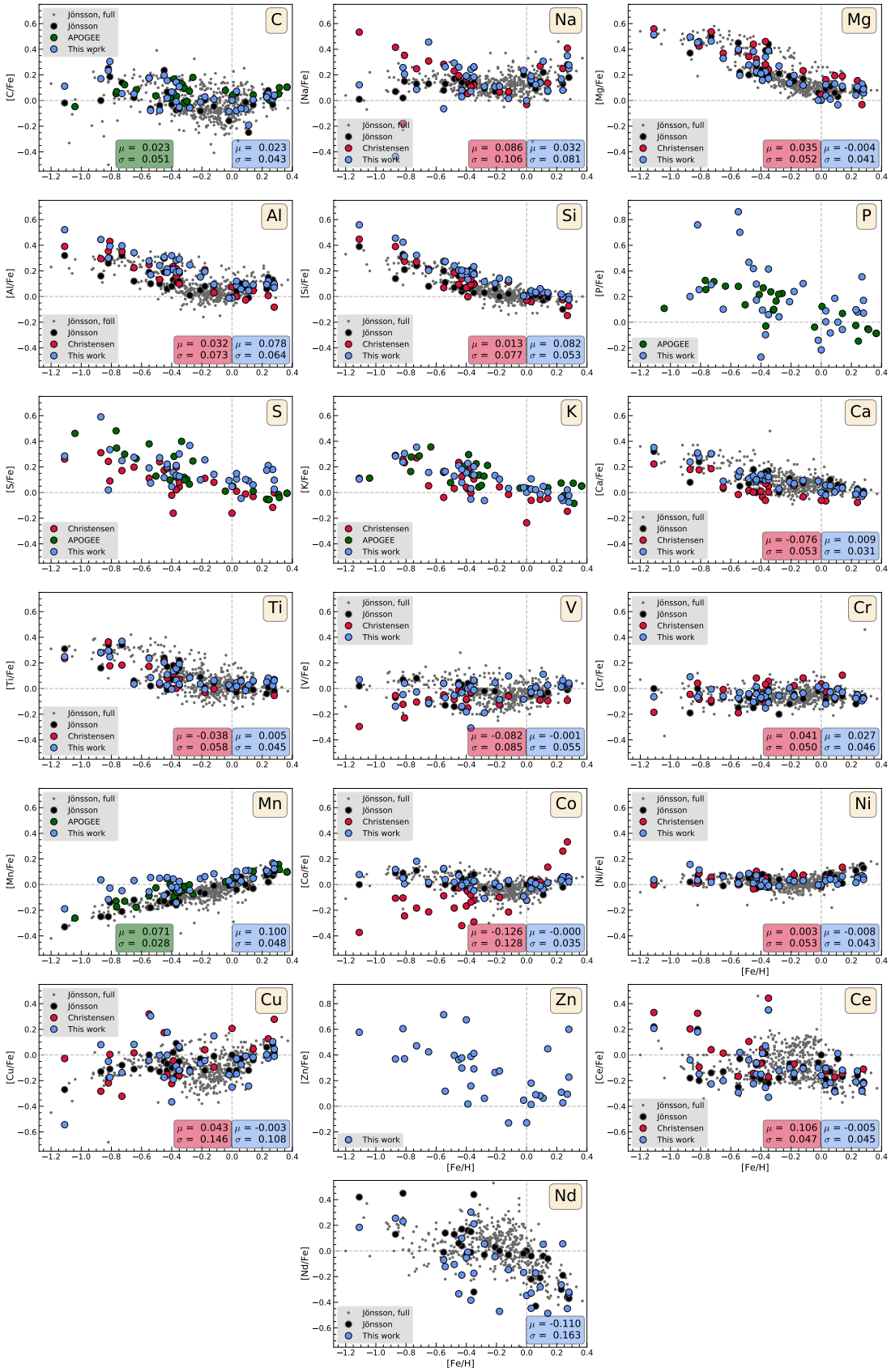
C
[C/Fe]
Jönsson, full
Jönsson
APOGEE
This work
μ = 0.023
σ = 0.051
μ = 0.023
σ = 0.043
Na
[Na/Fe]
Jönsson, full
Jönsson
Christensen
This work
μ = 0.086
σ = 0.106
μ = 0.032
σ = 0.081
Mg
[Mg/Fe]
Jönsson, full
Jönsson
Christensen
This work
μ = 0.035
σ = 0.052
μ = -0.004
σ = 0.041
Al
[Al/Fe]
Jönsson, full
Jönsson
Christensen
This work
μ = 0.032
σ = 0.073
μ = 0.078
σ = 0.064
Si
[Si/Fe]
Jönsson, full
Jönsson
Christensen
This work
μ = 0.013
σ = 0.077
μ = 0.082
σ = 0.053
P
[P/Fe]
APOGEE
This work
S
[S/Fe]
Christensen
APOGEE
This work
K
[K/Fe]
Christensen
APOGEE
This work
Ca
[Ca/Fe]
Jönsson, full
Jönsson
Christensen
This work
μ = -0.076
σ = 0.053
μ = 0.009
σ = 0.031
Ti
[Ti/Fe]
Jönsson, full
Jönsson
Christensen
This work
μ = -0.038
σ = 0.058
μ = 0.005
σ = 0.045
V
[V/Fe]
Jönsson, full
Jönsson
Christensen
This work
μ = -0.082
σ = 0.085
μ = -0.001
σ = 0.055
Cr
[Cr/Fe]
Jönsson, full
Jönsson
Christensen
This work
μ = 0.041
σ = 0.050
μ = 0.027
σ = 0.046
Mn
[Mn/Fe]
Jönsson, full
Jönsson
APOGEE
This work
μ = 0.071
σ = 0.028
μ = 0.100
σ = 0.048
Co
[Co/Fe]
Jönsson, full
Jönsson
Christensen
This work
μ = -0.126
σ = 0.128
μ = -0.000
σ = 0.035
Ni
[Ni/Fe]
Jönsson, full
Jönsson
Christensen
This work
μ = 0.003
σ = 0.053
μ = -0.008
σ = 0.043
[Fe/H]
Cu
[Cu/Fe]
Jönsson, full
Jönsson
Christensen
This work
μ = 0.043
σ = 0.146
μ = -0.003
σ = 0.108
Zn
[Zn/Fe]
This work
[Fe/H]
Ce
[Ce/Fe]
Jönsson, full
Jönsson
Christensen
This work
μ = 0.106
σ = 0.047
μ = -0.005
σ = 0.045
[Fe/H]
Nd
[Nd/Fe]
Jönsson, full
Jönsson
This work
μ = -0.110
σ = 0.163
[Fe/H]

5.2.1 C

One C I line at 16333.93 Å has been used to derive carbon abundances, NLTE corrections are included.
The C abundance in Jönsson et al. (in prep.) is derived from both C_2 and CN lines. Only atomic lines were considered in this thesis. Including the molecular CN and CO lines could markedly improve the results as more lines are available. The carbon trend follows the one in Jönsson et al. (in prep.) well, possibly appearing slightly tighter at solar metallicities and higher.
The estimated uncertainty based on errors in stellar parameters is 0.061 and 0.042 dex for α Boo and μ Leo respectively, reflecting the slightly elevated scatter at lower metallicities. Carbon does not show a systematic bias to stellar parameters, with some of the lowest correlations to $T_{\rm eff}$ and $\log(g)$ out of all elements.
The APOGEE "recommended" results shown are based on CO and CN lines. In Figure 5.6 the right hand plot shows an additional comparison, APOGEE's carbon results based on atomic C I lines, shown in pink. Overall both sets of results from APOGEE show good agreement with the results in this work and the optical results. Unfortunately the stars at solar metallicity which show subsolar C abundances in my results do not have measurements from APOGEE. The full APOGEE DR16 results do show a similar trend, with a more pronounced downwards curve in measurements from the C I lines (Jönsson et al., 2020).
NLTE corrections for the carbon line used are very small, as can be seen in the left hand plot of Figure 5.6 where the trends overlap almost perfectly.

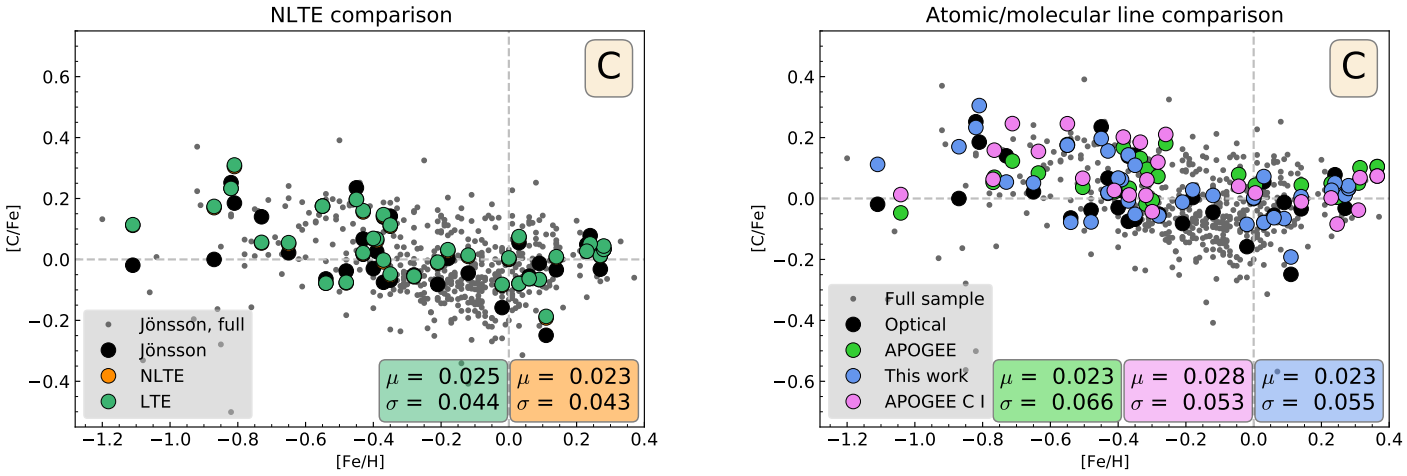

Figure 5.6: Left: Carbon abundances calculated with the NLTE grid from Amarsi et al. (2020) (orange markers), and in LTE (green markers), note the difference is small enough for the green dots to completely cover the orange ones.
Right: Carbon abundances compared to APOGEE data from both molecular (green markers) and atomic (pink markers) lines.

5.2.2 Na

One line at 16388.85 Å has been used to compute the sodium abundance, hyperfine structure and NLTE corrections are included.
The trend largely follows Jönsson et al. (in prep.), albeit with a significant scatter. The scatter is expected as the line used to compute the abundance is severely blended by both an Fe I and a Ni I line. At 16373.9 Å another Na I line can be considered for abundance analysis. Although it is less severely blended, it was excluded from this analysis because of interference from telluric lines causing large outliers in the data.
The estimated uncertainty based on errors in stellar parameters is 0.046 and 0.048 dex for α Boo and μ Leo respectively, among the lowest out of all the elements, excluding parameter error as the source of the observed scatter. No significant bias is observed in the results.
Christensen (2020) shows an anti-correlation with metallicity that is not present in the trend from Jönsson et al. (in prep.) or the results of this thesis. Christensen (2020) has used the same spectral line as this thesis. Figure 5.7 shows that neither the change in the NLTE correction grid nor the inclusion of hyperfine structure lines is likely to be the cause of this difference, as both changes are shown to have minor impacts. The difference in abundance for the most metal-poor stars in Christensen (2020) is significantly larger than the estimated errors from uncertainty in parameters. With similar Ni abundances and identical metallicity the blends for the line should be handled similarly. While it is unclear what the exact cause of the discrepancy between my results and those of Christensen (2020) is, it is likely to be rooted in the higher resolution spectra.

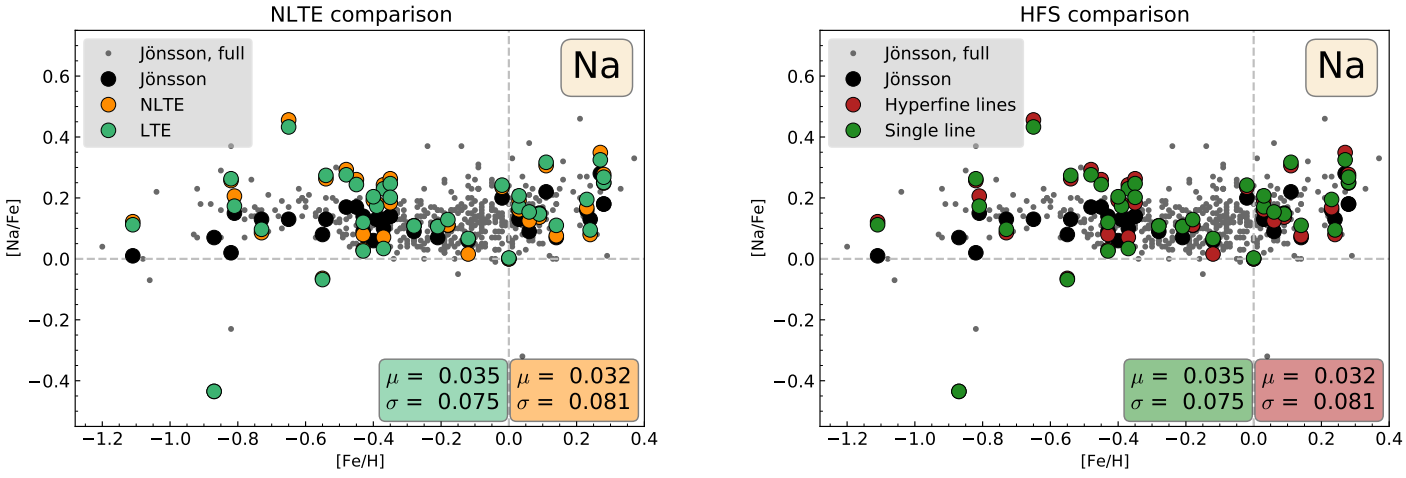

Figure 5.7: Left: Sodium abundances calculated with the NLTE grid from Amarsi et al. (2020) (orange markers), and in LTE (green markers). Both include hyperfine structure. Right: Sodium abundances calculated with the inclusion of hyperfine structure lines (red markers), and without including them (green markers). Both include NLTE corrections.

5.2.3 Mg

Three lines, at 15740.71, 15748.89 and 17108.63 Å, have been used to compute the magnesium abundance, NLTE corrections are included.
The abundance trend in Figure 5.5 shows excellent agreement with the values from Jönsson et al. (in prep.).
The estimated uncertainty based on errors in stellar parameters is 0.071 and 0.083 dex for α Boo and μ Leo respectively. There are some minor correlations between $T_{\rm eff}$, $\log(g)$ and the deviation from the results of Jönsson et al. (in prep.). The Mg lines are strong, with broad wings which are sensitive to stellar parameters, a likely cause for the bias.
In comparison with Christensen (2020) my values show a lower mean deviation from optical values and a significantly lower spread, especially at high metallicities. The improvement in mean deviation from optical values is likely due to the astrophysical linestrengths, despite Christensen (2020) using lab values for the Mg lines. The spread in values can be attributed to a combination of higher resolution, improvements in van der Waals broadening, updated NLTE corrections and access to the line at 17108.63 Å. The van der Waals broadening plays an important role for Mg as the lines in the H band are generally very strong.
The NLTE grid from Amarsi et al. (2020) is shown to have a noticeable impact on all stars in Figure 5.8, generally improving the accuracy of the measurements.

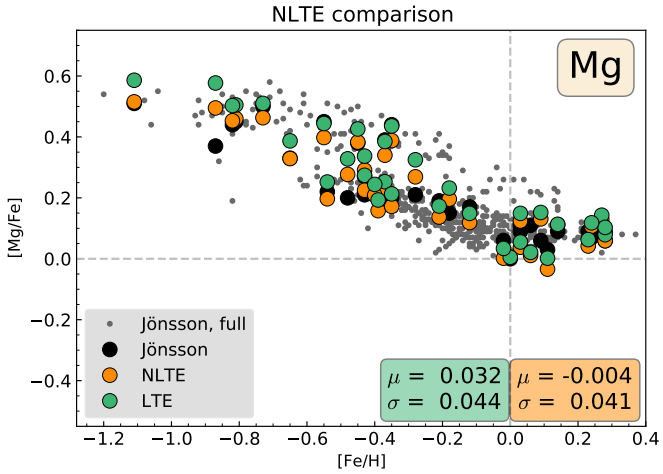

Figure 5.8: Magnesium abundances calculated with the NLTE grid from Amarsi et al. (2020) (orange markers), and in LTE (green markers).

5.2.4 Al

Three lines, at 16718.97, 16750.60 and 17699.05 Å, have been used to compute the aluminium abundance, hyperfine structure and NLTE corrections are included.
The Al trend is quite tight; matching the trend in Jönsson et al. (in prep.) at supersolar metallicities very well, but deviating significantly at subsolar metallicities. The cause of this discrepancy is not likely to stem from random errors in stellar parameters, as the analysis in Figure 4.6 shows an identical standard deviation of 0.074 dex for both α Boo and μ Leo, despite the difference in metallicity between the stars. Based on the trend in Figure 5.2 it is likely that this discrepancy has a relation to $\log(g)$, as it shows a correlation of -0.725. The lines at 16718 and 16750 Å are both strong and could be sensitive to $\log(g)$, but as the line at 17699 Å is much weaker and still shows a similar discrepancy for the stars with the lowest values of $\log(g)$ that explanation is unlikely. HFS effects have not been accounted for in Jönsson et al. (in prep.), something that needs to be done before a final judgement can be made on the reliability of the infrared lines for Al.
The trend from Christensen (2020) is slightly lower, giving it a better agreement with Jönsson et al. (in prep.) at subsolar metallicities, but worse for the supersolar values. The reason for the discrepancy is the choice of lines, with Christensen (2020) using a line at 16763.37 Å that is less sensitive to the NLTE and HFS effects accounted for in this work. The bottom left panel of Figure 5.9 confirms this, showing that the differences between the results for the line are quite minor.
The Al abundances for giants in APOGEE DR16 (Jönsson et al., 2020) have had a zero point calibration of -0.15 dex applied. Without this the mean deviation from the optical would essentially match the trend presented in this work, as can be seen in the bottom right panel of Figure 5.9.
The top row of Figure 5.9 shows that both NLTE corrections and hyperfine structure have big impacts on the derived abundances. An inverse metallicity dependence can be seen for both effects, with the difference between NLTE and LTE, or HFS and single line results getting smaller with higher metallicities. Typically the desaturating effects of HFS would be stronger for more metal rich stars. A possible explanation is that the lines for the most metal rich stars have reached the point where optically thin damping wings which are sensitive to the abundance are formed, so the desaturating effects of HFS is less impactful. For less metal rich stars where the lines are slightly weaker, the lines are saturated but without the abundance sensitive wings, the difference in derived abundance becomes larger as the line is less sensitive to changes in abundance.

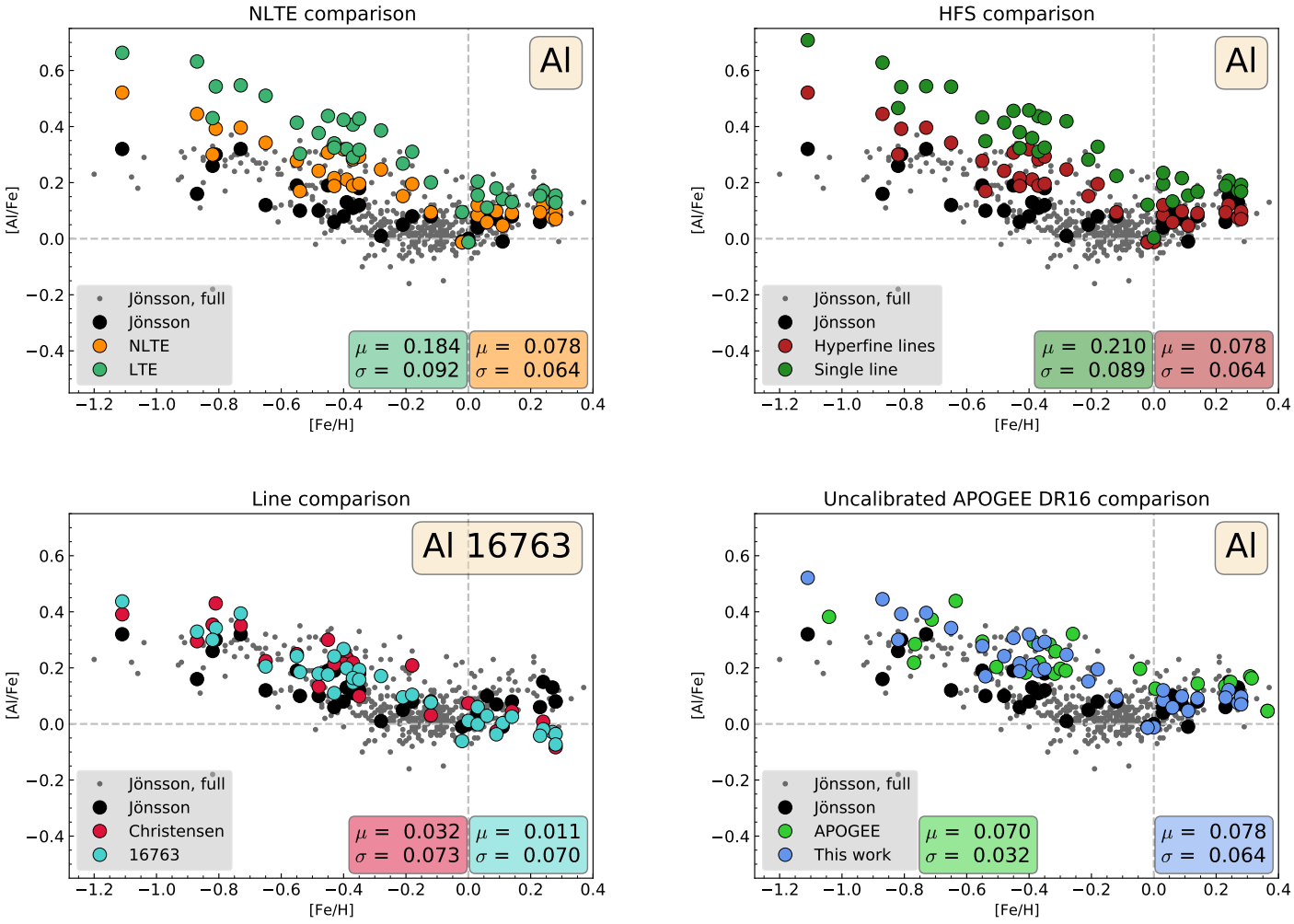

Figure 5.9: Top left: Aluminium abundances calculated with the NLTE grid from Amarsi et al. (2020) (orange markers), and in LTE (green markers). Both include HFS.
Top right: Aluminium abundances calculated with the inclusion of hyperfine structure lines (red markers), and without including them (green markers). Both include NLTE corrections.
Bottom left: Comparison between mine and Christensen (2020)'s results, both using only the Al I line at 16763.37 Å.
Bottom right: Comparison with APOGEE DR16 (Jönsson et al., 2020) without the zero point calibration.

5.2.5 Si

Five lines, at 15361.16, 16163.71, 16434.93, 16828.18 and 17225.63 Å, have been used to compute the silicon abundance, NLTE corrections are included.
The abundance trend in Figure 5.5 is quite tight, but shows significant discrepancies from the results of Jönsson et al. (in prep.) at subsolar metallicities.
The estimated error from parameter uncertainty is 0.072 and 0.071 dex for α Boo and μ Leo. A significant correlation is seen in Figure 5.3 between the difference to optical values and [Fe/H]. Because of the observational bias towards stars with lower $\log(g)$ at lower metallicities, this is also seen as a correlation with $\log(g)$ in Figure 5.2, although with less statistical significance.
A possible source of this discrepancy is the macroturbulence. As a significant difference has been observed between the values of v_{mac} determined using Si and Fe lines (see Figure 4.4), it is possible that an error in how the broadening for the Si lines are calculated was disguised by calculating the macroturbulence from them. Another possible contributing factor to the discrepancy is the astrophysical $\log(gf)$ value. If there are systematic effects that affect G dwarfs and K giant differently, the $\log(gf)$ value and thus the relative abundances could get shifted.
The Si line at 15884 Å gives a Si trend that aligns much closer with the results in Jönsson et al. (in prep.), shown in the left panel of Figure 5.10. The issue with measuring the Si results from this line is an OH blend which appears poorly modelled, as seen in the right panel of Figure 5.10, which shows the spectra of α Boo at 15884 Å. This is a good illustration of the strategy used for selecting lines for abundance analysis in this thesis; a good fit to the results of Jönsson et al. (in prep.) is the primary goal, but not the method of evaluating a spectral line. Visual inspection of the spectrum can not rule out any problems with the line formation, but it can spot many problems a computer has difficulty recognising.
The results from Christensen (2020) are better aligned with the trend from Jönsson et al. (in prep.), possibly because of the macroturbulence derived from Si lines. Despite this the scatter in the results are notably higher, an effect likely stemming from the use of two more spectral lines and a higher spectral resolution.
The NLTE grid from Amarsi et al. (2020) is shown to have a very limited impact on the abundance trend in Figure 5.11.

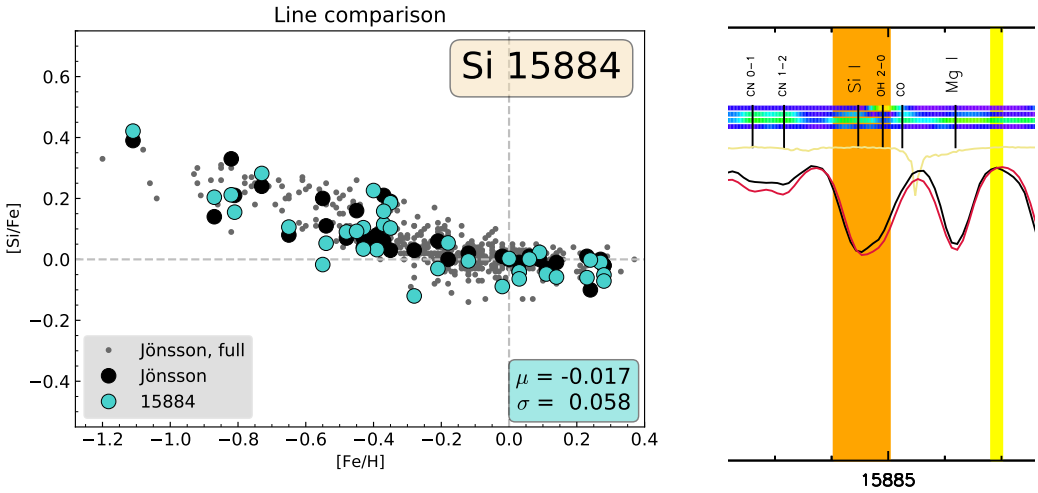

Figure 5.10: Left: Si abundances derived from a line at 15884 Å. A better alignment with the results of Jönsson et al. (in prep.) is shown than in Figure 5.5, but the line is not used as it has a significant OH blend which are the source of the lower abundances.
Right: the spectra of α Boo for at 15884 Å. The black line is the observed spectra, while the red line is the synthetic spectra fit to the observations to determine the Si abundance. Note that the red line goes below the black one at the OH lines wavelength. The Si derived Si abundance is lower for this line as SME compensates for the problem with the OH line.

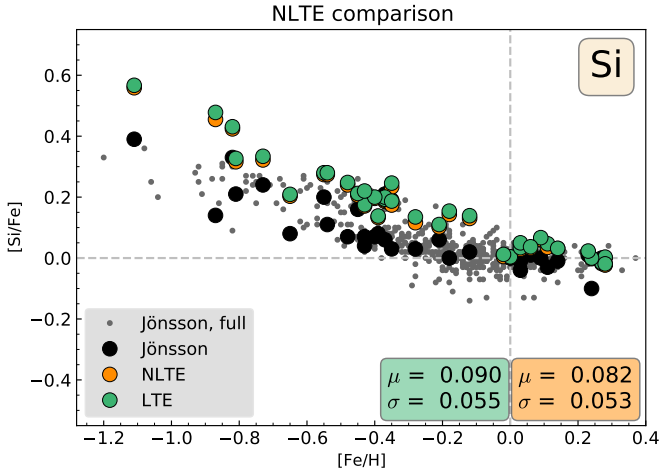

Figure 5.11: Silicon abundances calculated with the NLTE grid from Amarsi et al. (2020) (orange markers), and in LTE (green markers).

5.2.6 P

One line at 16482.93 Å has been used to compute the phosphorous abundance.
There are no measurements from Jönsson et al. (in prep.) to compare to, as there are no useable P lines in the optical wavelength region analysed. There are no measurements from Christensen (2020) either, so comparisons are made to APOGEE DR16 results (Jönsson et al., 2020). The trend shown in Figure 5.5 is very scattered, yet it appears to show some similarities to similar elements such as Al with enhanced abundances for stars with subsolar metallicity, but otherwise little to no discernible details.
The analysis of uncertainty from error in stellar parameters in Figure 4.6 shows uncertainties of 0.074 and 0.080 dex for μ Leo and α Boo respectively. The analysis for α Boo shows an unnatural spike at the adopted value of P. This is not a sign of a precise value, it is a sign of an error in the spectral synthesis. The reason for this error appearing is likely to be the significant CO blend present, sensitive to stellar parameters, making it difficult to find an abundance.
The results from APOGEE DR16 (Jönsson et al., 2020) appear to follow a much tighter trend. This is the result of APOGEE's ASPCAP pipeline determining abundances in a different way than SME, reducing scatter without determining abundances more precisely. The comparison is a good example of why comparing abundances analysed in a different manner can be dangerous.

5.2.7 S

One line at 15469.82 Å has been used to compute the sulphur abundance.
There are no sulphur measurements in Jönsson et al. (in prep.) as there are no useable lines in the FIES optical wavelength range. The abundance trend is quite scattered, this is expected as the S lines are blended with OH and Fe I lines of a comparable strength. The trend appears similar to other alpha elements such as Mg and Si as expected, see e.g. (Matrozis et al., 2013), with an enhancement of 0.1-0.4 dex for stars with subsolar metallicity.
The uncertainty due to errors in parameters for S is an outlier out of all elements analysed in this thesis. The OH line close to the line used for abundance analysis causes a very large dependence on stellar parameters, and temperature in particular. The error for μ Leo is 0.101 dex, and the error for α Boo is 0.38 dex (2.99 dex when a single extreme outlier is included, see section 4.6.1), the largest error of all elements by far. The difference between these errors is caused by the difference in temperature between the stars, towards the cooler end of the K spectral class OH lines become very strong.
In comparison with Christensen (2020) my abundances are notably higher, being more in line with the results from APOGEE for subsolar metallicities.
In contrast to Christensen (2020) and APOGEE my results show an upward trend for supersolar results, highlighted in Figure 5.12. Two literature sources are brought in to the comparison at supersolar metallicities. Matrozis et al. (2013) has used a forbidden line at 10821 Å to measure sulphur abundances; the two stars of supersolar metallicity in their

sample have sulphur abundances in good agreement with the upward trend observed here, albeit with large margins of error. Takada-Hidai et al. (2002) has studied dwarf stars, with the supersolar results being split between values higher and lower than those observed in this study. Neither study discusses the supersolar results in depth.
The chemical evolution model of Kobayashi et al. (2020) suggests an essentially flat model, in contrast to earlier work (Kobayashi et al., 2011b) where a downwards slope was predicted.
There is no NLTE grid available for the S lines in the H band. The lines share an upper level, 4p, with the sulphur triplets at 9237 and 10459 Å which are known to be affected by NLTE effects, see for example Duffau et al. (2017). A likely conclusion to draw from this is that there are some NLTE effects for this line which ideally would need to be accounted for before the S lines in the H band could be said to be reliable.

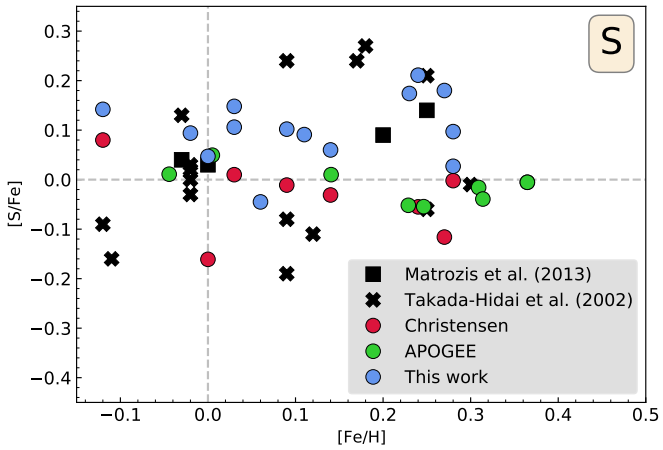

Figure 5.12: Closer view of the sulphur abundances for stars with supersolar metallicities. Additional comparisons have been added: Matrozis et al. (2013) (black squares), the stars included in this figure are K-giants; and Takada-Hidai et al. (2002) (black crosses), the stars are G and F dwarfs.

5.2.8 K

Two lines, at 15163.09 and 15168.40 Å, have been used to compute the potassium abundance, NLTE corrections are included.
There are no potassium measurements in Jönsson et al. (in prep.) as there are no useable lines in the FIES optical wavelength range. Christensen (2020) does not measure K abundances either, forcing us to mainly compare to APOGEE's values. Both trends show very similar results, with an anti-correlated increase of [K/Fe] for lower metallicities, reaching a maximum around [K/Fe] = 0.3 - 0.4 dex at [Fe/H] = -0.7 dex. The spectrum of the lowest metallicity star in the sample, at [Fe/H] = -1.11 dex, is quite heavily afflicted by

interference from telluric lines and this abundance should likely be significantly higher. The trend appears to flatten out at supersolar metallicities with a slight downwards tilt. The error analysis shown in Figure 4.6 estimates the error in potassium from parameter uncertainty to be 0.080 dex for α Boo and 0.114 dex for μ Leo. The error in potassium for μ Leo is larger than for most elements, possibly indicating that the slight downwards turn seen at supersolar metallicities should be taken with a grain of salt.
Zhao et al. (2016) have derived K abundances using equivalent width measurements from optical spectra of F and G dwarfs. Their results show an enhancement for subsolar metallicity stars about 0.1 dex lower than the results for this thesis, but also show a similar downwards turn for supersolar metallicities. This trend are in conflict with the galactic chemical evolution models of Kobayashi et al. (2020), which predict a slight upwards turn. The theoretical models severely underproduce K, possibly due to unaccounted for effects of neutrinos in supernovae (Kobayashi et al., 2011).
Figure 5.13 shows that the NLTE corrections from Amarsi et al. (2020) have a noticeable impact on K abundances, shifting them down by 0.043 dex on average. However, this correction is much smaller than the NLTE effect measured for optical lines which can show corrections of up to 0.7 dex (Zhao et al., 2016).

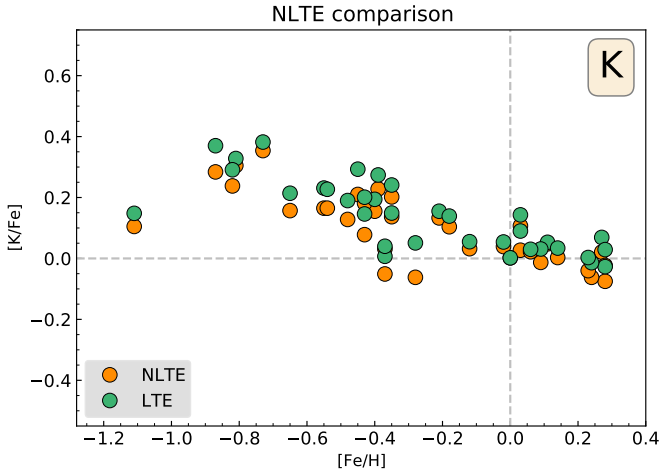

Figure 5.13: Potassium abundances calculated with the NLTE grid from Amarsi et al. (2020) (orange markers), and in LTE (green markers).

5.2.9 Ca

Three lines, at 16136.82, 16150.76 and 16155.24 Å, have been used to compute the calcium abundance, NLTE corrections are included.
The abundance trend in Figure 5.5 agrees very well with Jönsson et al. (in prep.) while maintaining an arguably tighter trend. No NLTE corrections have been used for Jönsson et al. (in prep.)'s Ca lines, meaning the infrared results could be more reliable in this case.

The errors due to stellar parameter uncertainty are also small, 0.055 and 0.056 dex for α Boo and μ Leo respectively. There is a small correlation between the difference to Jönsson et al. (in prep.)'s abundances and the stellar parameters $T_{\rm eff}$, $\log(g)$ and [Fe/H], although the bias appears to be minor.

The difference between this work and Christensen (2020) is primarily caused by the use of astrophysical $\log(gf)$ values, as the only literature values are semi-empirical measurements. The results from this work appear significantly tighter. This can be attributed to a combination of a higher resolution, the astrophysical $\log(gf)$ values reducing the line by line scatter and the use of NLTE corrections.

Ca is one of the elements which show a clear difference between the abundances computed using different values of the macroturbulence. The left panel of Figure 5.14 shows the results using the different methods described in section 4.2.2. The clearest difference is in the $\log(gf)$ value, with the VmacSi trend showing a value that is 0.022 dex higher. The scatter in the VmacSi trend is also clearly higher for supersolar metallicities, combined these effects make the trend appear to flatten out or even increase at supersolar metallicities in contrast to the downwards turn seen in the trends of Jönsson et al. (in prep.) and that using VmacFe.

The left panel of Figure 5.14 shows the impact of Amarsi et al. (2020)'s NLTE grid for Ca. The mean difference between NLTE and LTE results is -0.024 dex and appears to be smoothly distributed.

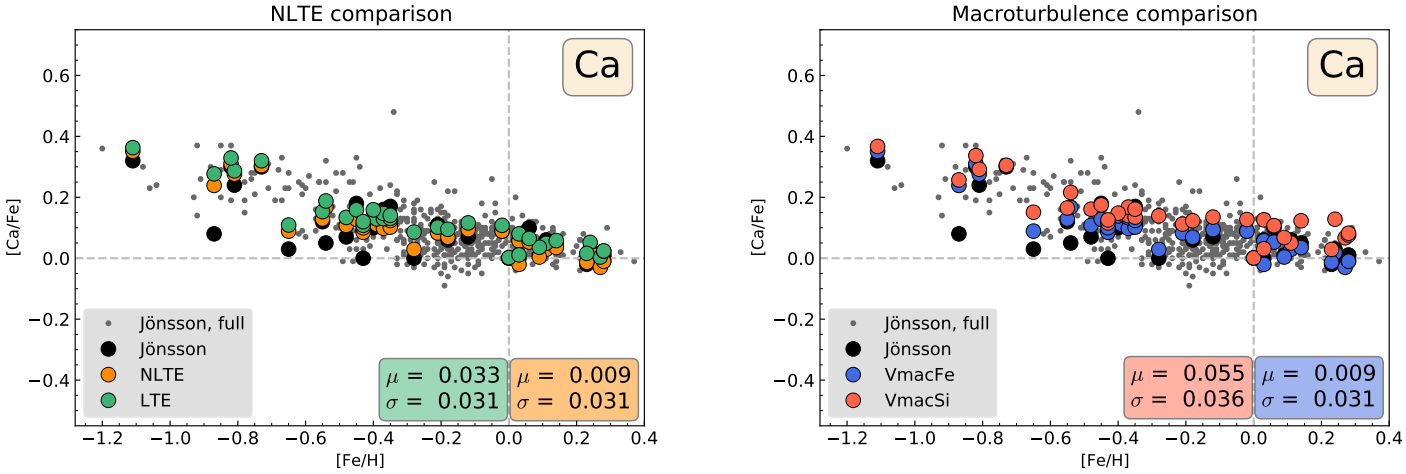

Figure 5.14: Left: Calcium abundances calculated with the NLTE grid from Amarsi et al. (2020) (orange markers), and in LTE (green markers).
Right: Ca abundances derived with different macroturbulences, red and blue dots marking the VmacSi and VmacFe methods respectively.

5.2.10 Ti

Two Ti I lines, at 15602.84 and 16330.54 Å, have been used to compute the titanium abundance.
A good agreement with the abundances in Jönsson et al. (in prep.) as seen in Figure 5.5. A minor difference is seen for supersolar abundances where my results show a slight increase in Ti abundance with metallicity, seen more clearly in Figure 5.3.
Figure 4.6 shows that a moderate uncertainty of 0.083 and 0.079 dex for α Boo and μ Leo has been estimated due to parameter error. No systematic bias is seen in $T_{\rm eff}$ or $\log(g)$.
Astrophysical $\log(gf)$ measurements are difficult to perform against the Sun for Ti, as most lines in the H band are from Ti I, while a significant fraction of the solar Ti is ionised to Ti II. The the cooler K giants do not have this problem, and the Ti I lines in their spectra are well suited to abundance analysis.
Astrophysical measurement of the one unblended Ti II line in the H band, 15873.84 Å, gives a value of -1.997, just outside the limits of the lab measured value of -1.90±0.08 from Wood et al. (2014). Abundances derived using the astrophysical value show a deviation of 0.186 dex from the results of Jönsson et al. (in prep.), shown in Figure 5.15. Combined, these two differences suggest that there is an NLTE effect affecting this line which, as there is no NLTE grid for Ti in Amarsi et al. (2020), has not been mitigated.
The results agree quite well with those of Christensen (2020), improving both the mean deviation from Jönsson et al. (in prep.) and the spread, while maintaining a similar shape to the trend. Christensen (2020) uses two additional Ti lines, including the Ti II line discussed above, which were not not used in this work due to poorly fitting astrophysical $\log(gf)$ value.

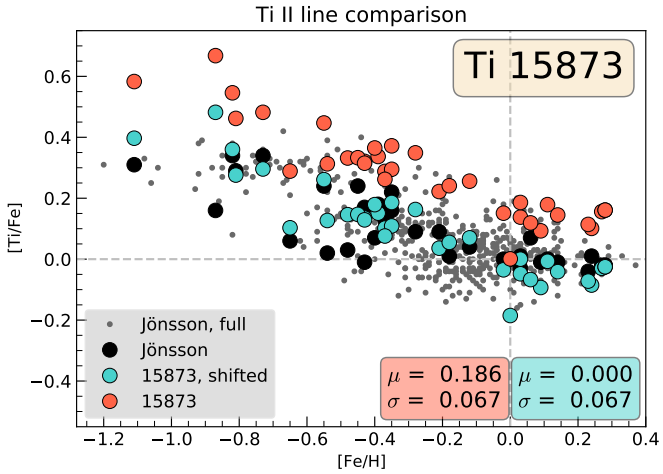

Figure 5.15: Ti abundances derived from the Ti II line at 15873.84 Å shown in red, and also recalibrated to match Jönsson et al. (in prep.) shown in turquoise. Note the gap between the Sun at (0,0) and the giants.

5.2.11 V

One line at 15924.81 Å has been used to compute the vanadium abundance, hyperfine structure is included.
Astrophysical $\log(gf)$ values have not been derived successfully for the V lines. The $\log(gf)$ value has instead been shifted to align the derived abundances with the values of Jönsson et al. (in prep.) and the Sun has been excluded from the figures. The overall trend matches quite well, with a number of outliers. Abundances for stars with supersolar metallicities are slightly higher in this work.
The estimated error from parameter uncertainty is 0.071 and 0.062 dex for α Boo and μ Leo. No significant bias is observed in the results.
In the trend from Christensen (2020) a slight downwards trend with decreasing metallicity not present in the trend from Jönsson et al. (in prep.) is seen. The trend is not seen in my results despite using the same spectral line. The cause of this has not been identified.
Figure 5.16 shows the impact of including HFS for V. Both trends have been adjusted to match the optical value. The difference between the results is very small, with the most notable feature being a minor increase in V abundance at supersolar metallicities which is corrected by accounting for HFS.

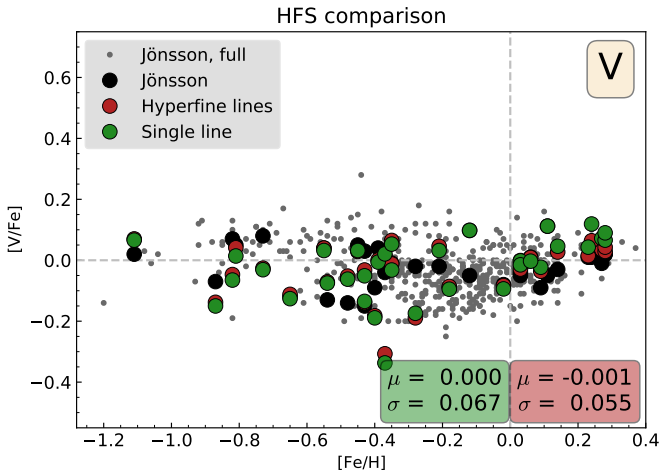

Figure 5.16: V abundances calculated with the inclusion of hyperfine structure lines (red markers), and without including them (green markers).

5.2.12 Cr

One line at 15860.21 Å has been used to compute the chromium abundance.
The abundance trend follows the slightly s-shaped curve of Jönsson et al. (in prep.) very well, the most prominent difference being the minor shift of 0.027 dex upwards.
The estimated error from parameter uncertainty is 0.072 and 0.074 dex for α Boo and μ Leo. No significant bias is observed in the results.

The results from Christensen (2020) show a largely similar trend despite using another line, 15680.06 Å, which was not used in this work due to a poorly fitting astrophysical linestrength. Both the mean deviation and the spread are decreased by a significant amount.
The chemical evolution model for Cr by Kobayashi et al. (2020) does not show the slight s-shaped curve of the trend, but are consistent with trend that slopes slightly downwards with metallicity. This is not present in all studies, see e.g. Bensby et al. (2014) where a very slight upwards tilt is measured.

5.2.13 Mn

Two lines, at 15217.74 and 15262.49 Å, have been used to compute the manganese abundance, hyperfine structure and NLTE corrections are included.
Manganese shows a quite tight trend in Figure 5.5, with abundances markedly higher than those of Jönsson et al. (in prep.). The differences are especially significant for metallicities lower than -0.25: my results level out around [Mn/Fe] = 0 until [Fe/H] = -0.7 before decreasing slightly; while the trend of Jönsson et al. (in prep.) continually decreases. An explanation for this is the lack of NLTE corrections for Jönsson et al. (in prep.)'s Mn lines. Bergemann et al. (2019) suggest that the NLTE corrections for the Mn I lines at 6013 and 6021 Å, used in part for the analysis in Jönsson et al. (in prep.), are metallicity dependent, going from ∼0.3 dex at [Fe/H] = -1 to ∼0.2 dex at solar metallicities for K giants ($T_{\rm eff}$ = 4500, log(g) = 1.5). Applying such a NLTE correction to the results from Jönsson et al. (in prep.) would give a flatter trend, more in line with the one measured in this thesis.
The estimated error from parameter uncertainty is 0.062 and 0.092 dex for α Boo and μ Leo. The metallicity dependent effects are clearly seen in Figure 5.3, while the minor correlation to log(g) in figure 5.2 is likely a result the correlation between the parameters. Figure 5.17 shows relatively minor NLTE corrections for Mn, and very significant hyperfine structure effects. Note that the y-scale on the right hand frame has been expanded upwards to show the full trend from the results without HFS. The change arising from including HFS presents with a strong dependence on metallicity, from showing similar results at [Fe/H] = -0.8, to a difference of 0.64 dex at [Fe/H] = 0.28. The changes are not distributed evenly, with the stronger line 15217.74 Å showing a larger difference. In Figure 5.18 the impact on the line shape of 15217.74 is shown for μ Leo, a metal rich star. The two synthetic spectra, with HFS in red and without in green, show some minor differences but are remarkably similar. Compared to the observed spectra they could be said to fit equally well, with the red line fitting better in the line centre and worse at the lower right edge. Despite this, the derived Mn abundances differ by an order of magnitude, 0.18 with HFS and 1.16 without. This is one of the clearest examples of the importance of including hyperfine lines, as they can make an enormous difference, even without changing the line shape by a large amount.

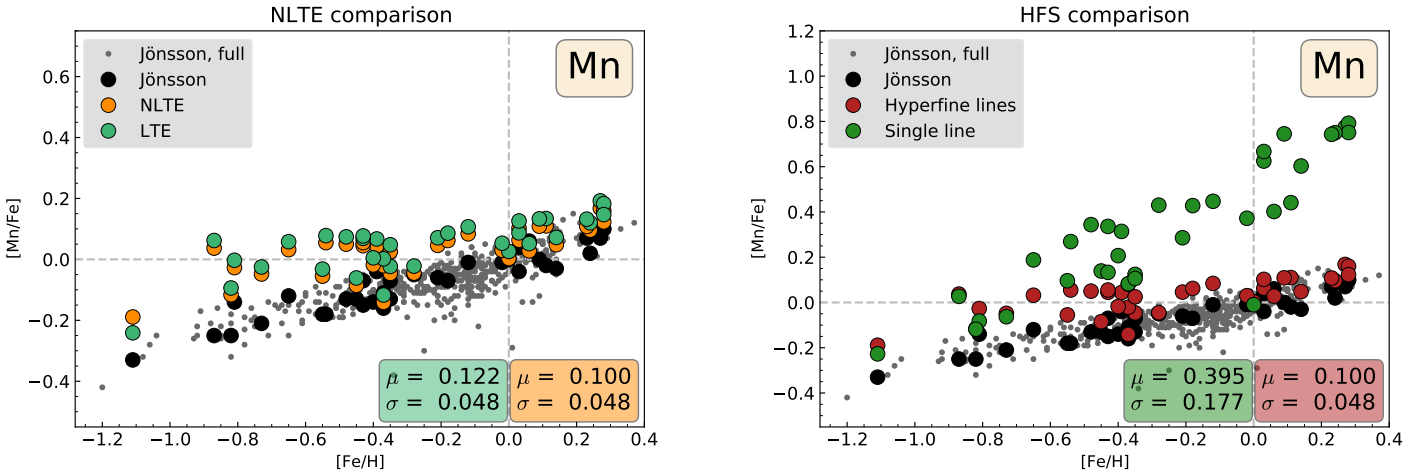

Figure 5.17: Left: Manganese abundances calculated with the NLTE grid from Amarsi et al. (2020) (orange markers), and in LTE (green markers). Both include HFS.
Right: Manganese abundances calculated with the inclusion of hyperfine structure lines (red markers), and without including them (green markers). Both include NLTE corrections. Note the changed scale of the y-axis.

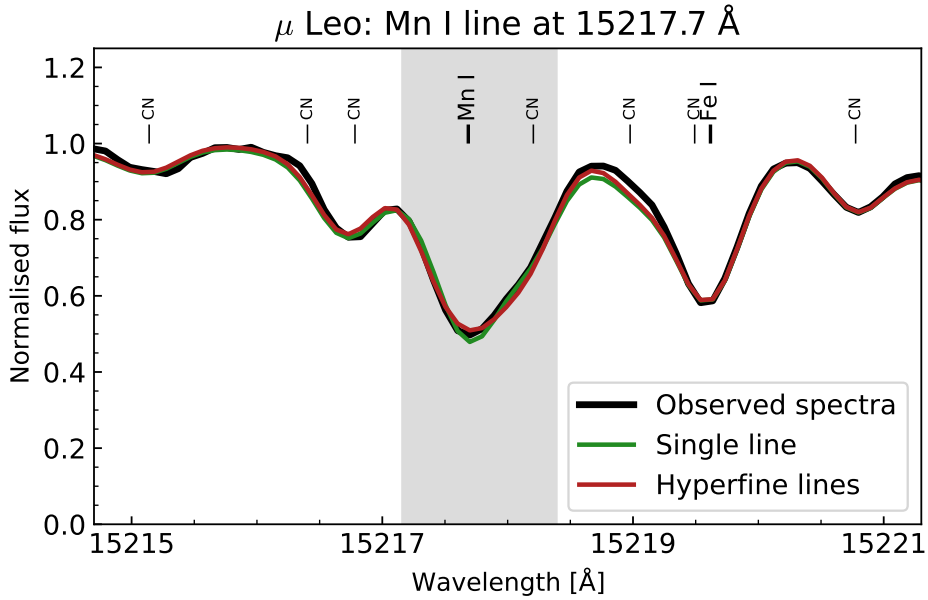

Figure 5.18: Example of synthesised spectra of the Mn line at 15217.74 Å for the star μ Leo, both with and without accounting for HFS. Despite similar goodness of fit the abundances derived from the spectra are 1.16 dex for the single line and 0.18 when including HFS lines.

5.2.14 Co

One line at 16757.64 Å has been used to compute the chromium abundance, hyperfine structure is included.
The astrophysical $\log(gf)$ value from the Sun causes a large mean deviation from Jönsson et al., in prep.'s values of 0.133 dex. The value was therefore adjusted to remove this discrepancy. The only other value of $\log(gf)$ is from the semi-empirical calculations of Kurucz et al. (1995), using this causes an even larger deviation of 0.198 dex.
The results show a tight trend that matches the s-shaped curve from Jönsson et al. (in prep.) very well. No significant deviations or outliers are seen.
The estimated error from parameter uncertainty is 0.057 and 0.052 dex for α Boo and μ Leo, among the lowest of all elements. No correlation between the difference between my results and those of Jönsson et al. (in prep.) and the stellar parameters is found.
The left panel of Figure 5.19 shows the impact of HFS on the Co trend. The difference is quite small for subsolar metallicities, but starts to increase around solar values up to a difference of 0.24 dex at [Fe/H] = 0.28 dex.
Christensen (2020) has a scattered trend in poor agreement with Jönsson et al. (in prep.), primarily because HFS is not accounted for. In the right panel of Figure 5.19 my results without accounting for HFS are compared to those of Christensen (2020), recalibrated to account for the difference in $\log(gf)$ value. For subsolar metallicities the trends seem to match well, while at supersolar metallicities the results from Christensen (2020) appear to show an even larger effect from the HFS. The reason for this discrepancy is not known, but it appears to be clear that the main effects that needed to be accounted for are HFS and the semi-empirical $\log(gf)$ value.

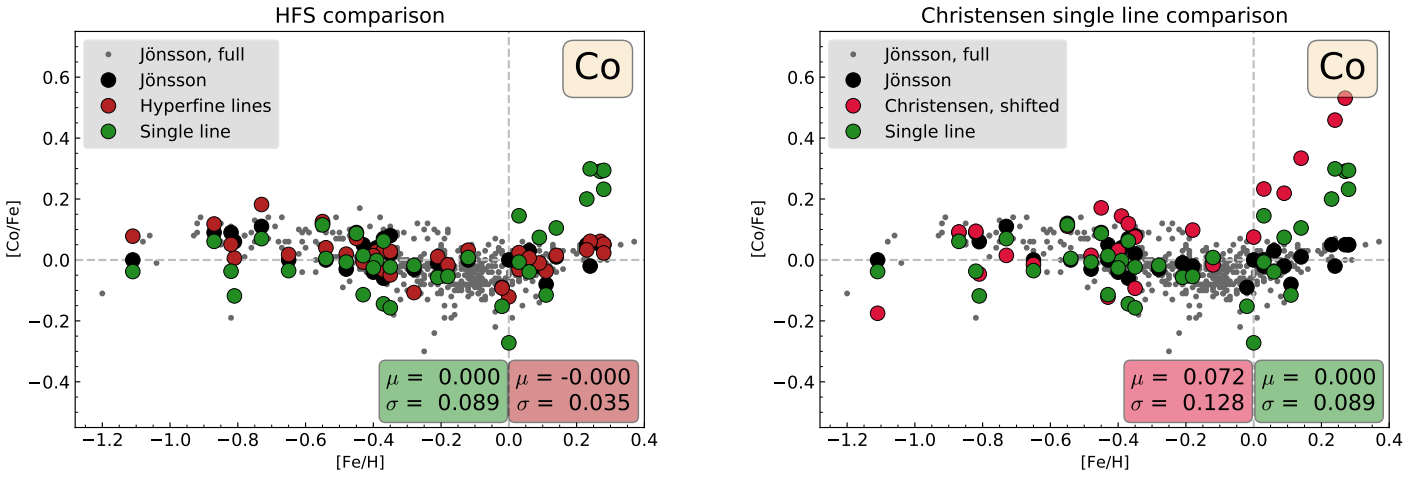

Figure 5.19: Left: Cobalt abundances calculated with the inclusion of hyperfine structure lines (red markers), and without including them (green markers).
Right: Cobalt abundances calculated without HFS and the results of Christensen (2020) shifted to use the same $\log(gf)$ value.

5.2.15 Ni

Four lines, at 16310.50, 16363.09, 16815.46 and 16818.75 Å, have been used to compute the nickel abundance.
The Ni abundance trend in Figure 5.5 shows a mostly excellent agreement with Jönsson et al. (in prep.). A small exception is the minor increase in [Ni/Fe] displayed in measurements of stars with supersolar metallicity by Jönsson et al. (in prep.), which is not present to the same degree in this work. Depending on the choice of lines used such a trend can be derived from the infrared spectra, with two lines initially showing trends matching the one from Jönsson et al. (in prep.) well at these high metallicities, 15555.38 and 16363.09 Å. Upon review of the spectra it became apparent that the upwards trend in [Ni/Fe] was caused by blends, CN lines for 15555.38 Å and a nearby, very poorly modelled, Mg multiplet for 16363.09 Å. Reducing the linestrengths of the Mg lines influencing the Ni line at 16363.09 Å improved the fit to observations significantly and reduced the slope of the upwards trend at supersolar metallicities. The reduced upwards trend in my results reaches a Ni abundance of 0.06-0.07 for stars at [Fe/H]≈0.27, which is consistent with the optical measurements of F and G dwarfs by Bensby et al. (2014), whose Ni abundance plateau slightly below [Ni/Fe]=0.10 dex.
The estimated error from parameter uncertainty is 0.060 and 0.064 dex for α Boo and μ Leo. The difference between the trends can be seen in the test for bias in [Fe/H] in Figure 5.3, but the trend appears to be otherwise uncorrelated with stellar parameters.
Only 2 stars of supersolar metallicity are shared with the sample in Christensen (2020) for Ni; they show a closer alignment to the values of Jönsson et al. (in prep.) than my values, possibly because the line at 15555 Å has been used. The rest of the trend is in good agreement with my trend, with a slightly larger scatter, likely to be the result of a combination of the lower resolution and the choice of lines.

5.2.16 Cu

Two lines, at 16005.64 and 16638.98 Å, have been used to compute the copper abundance, hyperfine structure is included as well as isotope shifts.
Accurate astrophysical measurements of the $\log(gf)$ value have not been successful for Cu, as the lines are very weak in the Sun. The $\log(gf)$ values have been shifted to match the trend from Jönsson et al. (in prep.).
The results presented in Figure 5.5 largely follow the trend from Jönsson et al. (in prep.), with a large amount of significant outliers. The Cu lines available in the H band all suffer from significant issues: the line at 16005 Å is weak and in the wings of much stronger lines on both sides; the line at 16638 Å is unblended but very weak.
The estimated error from parameter uncertainty is 0.054 and 0.051 dex for α Boo and μ Leo, some of the lowest values out of all the elements, showing that the scatter in the results are not a product of the stellar parameters, but of blending lines and noise in the spectra. The large scatter in the Cu results leads to significant slopes in the tests for bias in stellar parameters, no major correlation is found however.

Comparing against the trend from Christensen (2020) the general shape is very similar, with the interesting difference that for a number of the large outliers in my results, equally large deviations from the results of Jönsson et al. (in prep.) are seen by Christensen (2020), but in the opposite direction (see stars at [Fe/H] = -1.1, -0.87, -0.12 and 0.0). Note that the same lines have been used in the analysis.
Figure 5.20 shows the rather limited impact of including HFS for Cu. After VALD updated their HFS database based on a suggestion from me, information on both ^{63}Cu and ^{65}Cu is available and has been used in the calculations. The corrections appear to be slightly asymmetrical, increasing abundances for lower metallicities and decreasing them at super-solar values. The single line results for the most metal rich stars appear similar to those of Christensen (2020), indicating that those outliers may have been caused by HFS.

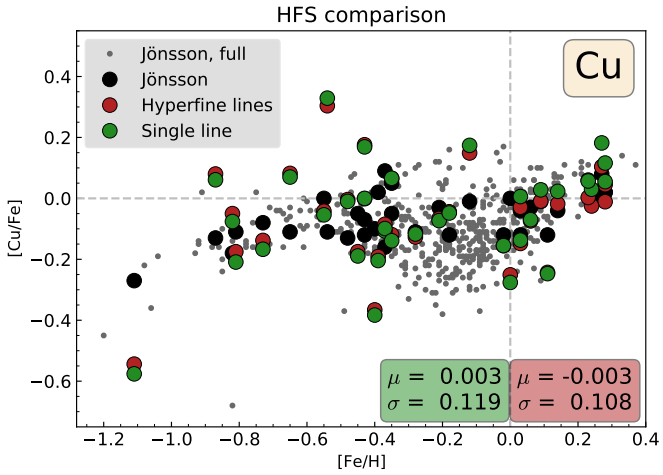

Figure 5.20: Cu abundances calculated with the inclusion of hyperfine structure lines (red markers), and without including them (green markers).

5.2.17 Zn

Two lines, at 16483.43 and 16505.18 Å, have been used to compute the zinc abundance.
Precise astrophysical measurement of the log(gf) values for Zn have not been successful. As there are no Zn results in either Jönsson et al. (in prep.), Christensen (2020) or Jönsson et al. (2020), the values of log(gf) have been shifted to make the stars at solar metallicity pass through origo.
The estimated error from parameter uncertainty is 0.088 and 0.086 dex for α Boo and μ Leo, slightly higher than the mean uncertainty, but not high enough to explain the large scatter in the results. As there are no Zn abundances from Jönsson et al. (in prep.), there is no data on the correlation with stellar parameters.
Zn abundances for dwarfs generally follow a trend similar to the nearby Cu, see results by Reddy et al. (2003) or Bensby et al. (2014). The analysis by Duffau et al. (2017) shows

a substantial difference to this general trend for giants, instead seeing a trend resembling that of alpha elements. Comparing results from two lines, at 4810 and 6262 Å, they find a lower scatter for stars with solar metallicity using only the results from the line at 4810 Å as the line at 6362 Å is affected by an auto ionising Ca I line at 6361 Å. Their results with the line at 4810 Å are shown overlain on my trend in Figure 5.21. I have applied a zero point shift of 0.3 dex to their abundances to ease comparison.
With the exception of the outliers at supersolar metallicity in my sample the results agree remarkably well: stars with subsolar metallicity plateau at a similar enhancement of around 0.4 dex; a "knee" similar to those in alpha elements is seen at approximately [Fe/H] = -0.4. Duffau et al. (2017) analyse their stars in terms of their galactocentric radius and the height above the disc, as a their sample are distributed out to 16 kpc (compare to the distances of my more local stars shown in Figure 3.1). Due to my lack of inner disc stars a similar analysis can not be performed.

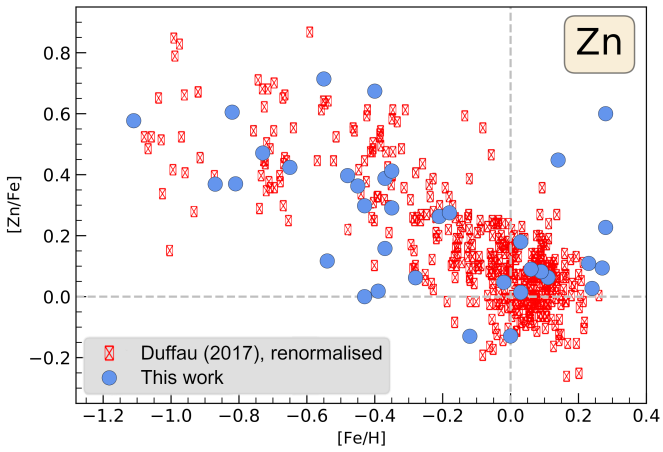

Figure 5.21: Comparison between my Zn abundances and those of Duffau et al. (2017), derived from high resolution optical spectra for red giants close to the K spectral range. The results shown are those derived using only the spectral line at 4810 Å. The results have been copied and adjusted to fit the grid used in my plots, and zero point adjusted by 0.3 dex to align with the results of this thesis.

5.2.18 Ce

Two lines, at 16595.18 and 17058.88 Å, have been used to compute the cerium abundance. The Ce II lines in the Sun have not been of sufficient quality to derive astrophysical $\log(gf)$ values. For the line at 16595.18 Å astrophysical measurements against α Boo have been calculated by Cunha et al. (2017), but as APOGEE's wavelength range does not cover wavelengths longer than 17000 Å there is no data for 17058.88 Å. In this thesis both lines have instead had their $\log(gf)$ values adjusted so that the derived abundances match those

of Jönsson et al. (in prep.).
The abundance trend of Ce in Figure 5.5 largely agrees with the one in Jönsson et al. (in prep.). The trend shows a significantly higher amount of scatter, but appears to give accurate abundances for the s-enhanced stars shown above the rest of the trend (see Forsberg (2019) for details on s-enhanced stars).
The estimated error from parameter uncertainty is 0.078 and 0.074 dex for α Boo and μ Leo. No significant bias is observed in the results.
The abundance trend from Christensen (2020) shows very similar results, the major difference being the $\log(gf)$ values used, and a somewhat notable reduction in the scatter.

5.2.19 Nd

Two lines, at 16053.63 and 16262.04 Å, have been used to compute the neodymium abundance. SME has not been able to constrain the abundances of three stars which have been excluded from the sample.
For the line at 16262.04 Å an astrophysical $\log(gf)$ value has been determined, the line at 16053.63 Å is significantly weaker and was not detected in the Sun. The $\log(gf)$ value for 16053.63 Å was instead sourced from Hasselquist et al. (2016), which has determined it astrophysically against the metal poor K giant 2MASS J16011638-1201525.
Figure 5.5 shows that the agreement with the results of Jönsson et al. (in prep.) is quite poor, in part because of the uncertainty in the $\log(gf)$ values. Both lines used for abundance analysis have large outliers which distort the data. A more careful analysis choosing the lines used for each star individually could improve the results for a number of stars. The general trend of a mostly flat trend with sharply decreasing abundances for stars with supersolar metallicities is distinguishable in the scattered data. This general pattern is also seen in the galactic chemical evolution models by Kobayashi et al. (2020).
The estimated error from parameter uncertainty is 0.163 and 0.188 dex for α Boo and μ Leo, the largest in this work by a significant margin (excluding the outlier of α Boo's sulphur results). Due to the large scatter in the results it is near impossible to determine whether the difference compared to Jönsson et al. (in prep.) is correlated with stellar parameters.
Neither Christensen (2020) nor APOGEE DR16 (Jönsson et al., 2020) have published abundances of Nd, and as such no comparison can be made to other infrared results.

5.3 Note on HIP 63432

For most of the elements presented so far, the star HIP 63432 (9 Draconis, 2MASS J12595500+6635502), appears as a significant outlier compared to the optical results. At a metallicity of [Fe/H] = -0.87 it is the star with the second lowest metallicity in the sample and is thus often easily distinguishable as an outlier in the abundance trends, and an important marker of the trends direction. The deviations shown are often several times larger than the expected errors based on variations in stellar parameters. For Al, Si, Cr, Mn and Cu the error is larger than any of the models based on α Boo, with C, Na and Ca

coming close to that limit.
In terms of stellar parameter the star has $T_{\rm eff}$, log(g), [Fe/H], $v_{\rm mic}$ = 4155 K, 1.29 dex, -0.87 dex, 1.89 km/s from Jönsson et al. (in prep.), standing out as having the lowest log(g) and highest $v_{\rm mic}$ in the stellar sample, making it clearly visible in figures 5.2 and 5.4. I have only been able to find one other estimation of the stars parameters, from Sharma et al. (2016) which gives values of $T_{\rm eff}$, log(g), [Fe/H] = 4269 ± 53 K, 1.47 ± 0.18 dex, -0.81 ± 0.08 dex. These values have been derived from spectra with a resolution of $R \sim 2000$, markedly lower than the FIES spectra used by Jönsson et al. (in prep.), meaning they should be less reliable. Given that the values are outside each others margins of error in log(g) and especially $T_{\rm eff}$, it could be an indication that there is an issue with the parameters.

5.4 Additional Elements

The periodic table shown in Figure 2.1 indicates that there are spectral lines present in the H band for Ge, Rb and Yb which have not been accounted for so far. In this section the reason for excluding these elements are given, along with a description of the work done to analyse the lines present in the spectra. As described in section 2.1.1 it is possible that there are even more elements which could possibly have detectable spectral lines in the H band, but their lines have not yet been identified, see for example Smith et al. (2021).

5.4.1 Ge

Germanium only has one detectable spectral line in the H band , at 16759.76 Å. It is positioned in the wings of a much stronger, but still Gaussian, line which has been identified as Fe I by Biemont et al. (1985). The identification of this Fe I line is uncertain, as it is not seen in later Fe I studies (Nave et al., 1994), and lacks level identification. Without knowing the properties of this unknown line, the germanium line cannot be measured. The Ge line appears to be strong enough that with a proper identification of the blending line and high resolution spectra it should be possible to derive an abundance trend.
A second spectral line, which should be only slightly weaker, exists at 17214.34 Å (Humphreys et al., 1964). Unfortunately the line is blended by a CO line and it has not been possible to get good fits to the spectra.

5.4.2 Rb

Two lines of Rb I are available in the H band, at 15288.43 and 15289.48 Å (Johansson, 1961). The line at 15288 is blended by a CN line and I have not been able to get good fits to the spectra. The line at 15289 Å is supposedly the stronger of the two based on log(gf) values from Kurucz et al. (1995), but as they are marked with the same relative intensity in the lab measurements by Johansson (1961) it it difficult to confirm this. The line itself is impossible to measure at the moment, as there is an unidentified Fe I line which has been observed by Nave et al. (1994) at 15289.469 Å. With the unidentified line so close in

wavelength it is impossible to perform any measurements of the Rb line.

5.5 Additional astrophysical log(gf) measurements

Although not directly used for abundance analysis, I have measured the log(gf) values of most of the identified spectral lines in the H band astrophysically. The benefit of doing this is that as most of the lines only have semi-empirical log(gf) values from Kurucz et al. (1995), their values can have errors large enough that they affect nearby spectral lines or the local normalisation of the continuum.
An illustrative example to demonstrate the impact this has is to look specifically at the Fe I lines, as they are by far the most numerous and as all of the Fe I lines in VALD come from the semi-empirical calculations of Kurucz et al. (1995) there are fewer factors to consider in the analysis. A total of 550 Fe I lines have been measured in this thesis. Figure 5.22 shows the log(gf) from Kurucz on the x axis and the difference between the Kurucz and astrophysical values on the y-axis. The results are colour coded with the upper levels excitation energy, as there appears to be some correlation to the error. It is possible that this correlation is a result of the semi-empirical methods reliance on extrapolations from lab measurements of lower levels to calibrate the higher levels, but a more in-depth analysis of the energy levels would be needed to verify this assertion. The energy levels also give an indication of the strength of the spectral lines as both log(gf) and the excitation energy contribute to the line strength, see section 2.2.1 for more details.
There is a bias in which lines get measured, causing some of the asymmetry in the figure. If a spectral line is seen in the observed spectrum but not in the synthesised one, it is an indication that there may be a line with a log(gf) value that is too low. But even if there is only one line in the linelist which matches the wavelength of the observed line it is not certain that there isn't an undiscovered line which is the real cause of the observed spectral line. Due to the risk of misidentifying lines, all lines with $\Delta \log(gf) \leqslant -1$ have been verified to exist and to have a matching relative intensity in the Fe I lab measurements of Nave et al. (1994). In summary, for a line to have its log(gf) value increased, an identification that a line of that element should be visible is required. For lines with the opposite problem, a log(gf) value that is too high, identification is simply a matter of picking the strongest line in the relevant area and decreasing its linestrength to match observed the spectrum. In some cases the influence of other lines is not negligible and no log(gf) value can be determined; these lines have been excluded from this analysis.
The results in Figure 5.22 show that even for the very strongest Fe I lines with $\log(gf)_{\text{Kurucz}} \geqslant 0$, the mean difference from the astrophysical measurements is 0.22 dex, meaning the semi-empirical value is too high. This difference is much higher than the estimated error from instrumental errors of 0.08 dex (see section 4.6.2), and significantly higher than the uncertainty from errors in stellar parameters for all elements. What this shows is that even for the strongest lines, where errors are the smallest, semi-empirical values should not be used.
For the weaker lines the difference between the log(gf) values grow to several orders of

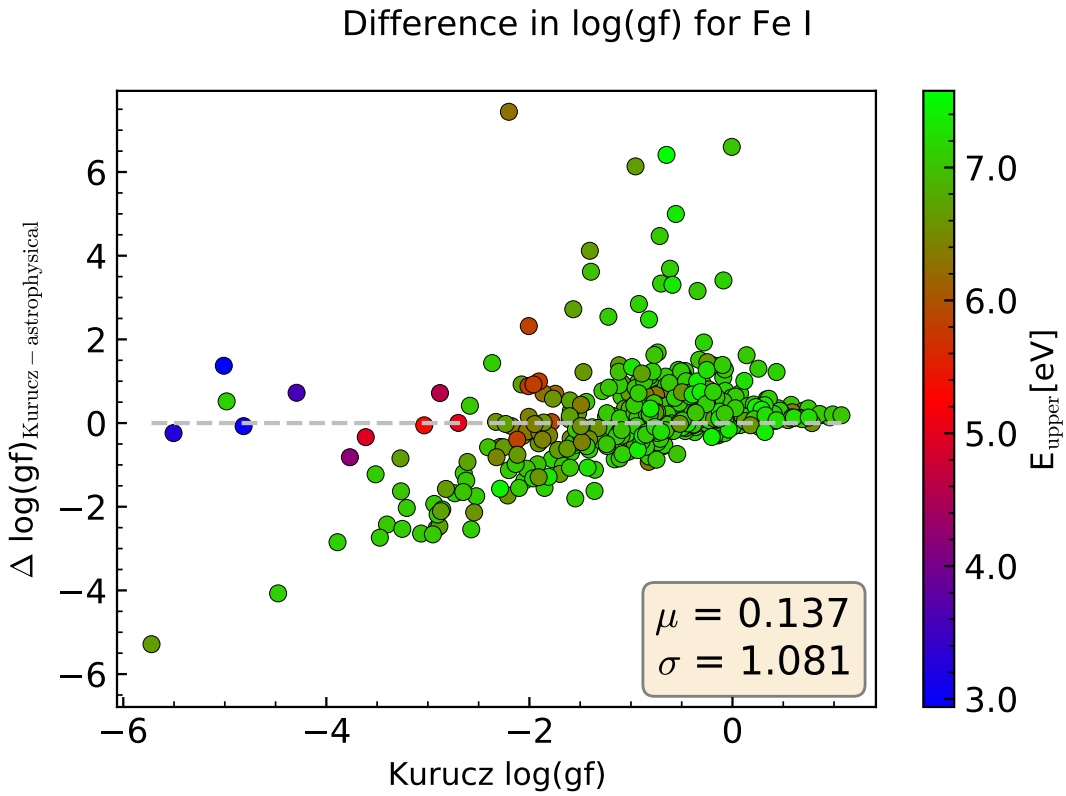

Figure 5.22: The difference between astrophysically measured and semi-empirically calculated $\log(gf)$ values for Fe I lines. The energy of the upper excitation levels are used to colour the plot, showing a better agreement for astrophysical values with lower excitation levels.

magnitude, both too strong and too weak. The lines which are too strong are less interesting, the main objective is to make sure they do not interrupt spectral lines of interest, which rarely requires precise measurement. The lines which are too weak are more interesting: besides being a potential source of disruption for other lines, they are potentially useful for determining abundances or stellar parameters.
For comparison, see the analysis performed by Lind et al. (2017) which evaluates the semi-empirical values for both Fe I and Fe II lines in the optical against experimentally determined values. A very similar pattern is shown, only lacking the values at $\Delta \log(gf) > 2$, as lab measurements for such weak lines is generally not performed.

Chapter 6

Conclusions

The aim of this thesis has been to lay the groundwork for further infrared spectroscopy by evaluating the level of agreement between abundance trends derived from the H band and those derived from optical spectra. To better understand the reasons for agreement and discrepancies in the abundance analysis a thorough examination of different aspects of line formation has been conducted; focusing on the hyperfine structure (HFS) splitting of energy levels; corrections to the Local Thermodynamic Equilibrium (LTE) approximation by non-LTE departure coefficient grids; astrophysical determination of spectral line strength; macroturbulence determination techniques; and the impact of using higher resolution spectra.
To achieve these goals the spectra from 34 K giants, measured by the spectrograph IGRINS, have been manually analysed using SME. To reach the lowest possible level of systematic errors in the comparison to optical abundance trends, the results are compared to high resolution optical analysis of the same stars by Jönsson et al. (in prep.). Both studies use the same accurate stellar parameters, minimising systematic uncertainties further.
Additional comparisons have been made to the infrared analysis of Christensen (2020), where a method similar to the one in this work has been used to analyse lower resolution H band spectra. The same stellar parameters are again utilised to minimise systematic differences. The comparison is meant to show the impact of both the resolution and changes in method such as astrophysical linestrength measurements.

Agreement with Jönsson et al. (in prep.)

Good agreement with the abundance measurements of Jönsson et al. (in prep.) is found for:

- C, Na, Mg, Ca, Ti, V, Cr, Co, Ni, Cu and Ce

Significant differences from the values in Jönsson et al. (in prep.) have been found for:

- Al, Si, Mn and Nd

For Al, Si and Mn the exact cause of this is not conclusively established, and better agreement could be found by further studies. For Nd the cause is likely the poor quality

of the lines in the H band.
Elements measured in this thesis which are not measured by Jönsson et al. (in prep.) are:

- P, S, K and Zn

Hyperfine structure

The impact of accounting for HFS has been investigated for Na, Al, V, Mn, Co and Cu. Minor differences, smaller than 0.1 dex for all stars, have been detected for Na, V and Cu. A moderate difference is observed for Co, increasing to up to 0.24 dex at supersolar metallicities. Differences of a similar magnitude are observed for Al, showing an inverse correlation with metallicity. Very large differences are measured for Mn, ranging from 0.002 dex at low metallicities all the way up to 0.65 dex for supersolar metallicities.
Accounting for HFS does not give a predictable impact on the abundance trend, results appear to be highly dependent on metallicity, sometimes in a non-linear manner. The "direction" of the correction is not set either, with $A_{\mathrm{HFS}} - A_{\mathrm{single}}$ decreasing with metallicity for Mn, and increasing with metallicity for Al.

NLTE corrections

Corrections to the LTE approximation calculated using the NLTE departure coefficient grid by Amarsi et al. (2020) have been investigated for C, Na, Mg, Al, Si, K, Ca and Mn. Corrections smaller than 0.06 dex for all stars have been measured for C, Na, Si, Ca and Mn. Moderate corrections, smaller than 0.11 dex have been measured for Mg and K. Large corrections have been measured for Al, ranging from 0.004 dex for metal rich stars up to 0.2 dex for metal poor stars.
The use of the NLTE grids has shown to improve the agreement with the optical abundances of Jönsson et al. (in prep.) in all cases.

Astrophysical linestrengths

Astrophysical calibration of linestrengths has been an essential tool for analysing infrared spectral lines as many lines only have semi-empirically determined values with large uncertainties. The effect is seen most clearly in elements where the agreement between my results and those of Jönsson et al., in prep. and Christensen, 2020 is generally good, e.g. Mg and Ca. Despite otherwise similar trends the mean deviation from Jönsson et al., in prep.'s values are notably lower for my trend compared to Christensen, 2020, indicating that the astrophysical $\log(gf)$ value has improved the results.
Adjusting nearby lines has been an effective tool for reducing ill-fittings lines influence on lines' used for abundance analysis and improving continuum normalisation. These effects have been especially important for improving the abundance trends for stars with supersolar metallicity.
The procedure for correctly distributing line strength across fine and hyperfine structure multiplets has been a useful tool, especially for handling the strong Mg lines.

Despite the promising results of the astrophysical method presented in this thesis, it is also clear that there are deficiencies, especially for lines that are too weak to measure in the Sun. The need for more extensive lab measurements and theoretical calculations of linestrengths is clear, with astrophysical measurements ideally functioning as a complement and not as a replacement.

Macroturbulence

Values of the macroturbulence have been computed with two different strategies using carefully selected samples of Si and Fe lines respectively. Comparing the results of the macroturbulence determination from Si and Fe lines respectively, it appears that there are significant differences, both in the values of the macroturbulence and in the abundance trends derived using those values. The abundance trends derived using macroturbulence from Fe lines appears to show less scatter and better agreement with the values from Jönsson et al. (in prep.). This is unexpected, as macroturbulence should affect all lines equally.
Accurate estimates of the van der Waals broadening are an essential component for getting a good estimate of the macroturbulence and should be a primary consideration when choosing lines to calculating macroturbulence from.

Resolution

The impact of using higher resolution spectra has been studied by comparing results to Christensen (2020), as the same stars are studied, with similar methodology and often with an overlap in the lines used. For certain elements the resolution is not the primary source of discrepancies, work has been done to explain what that source is. A general pattern of tighter trends with a smaller scatter compared to the results of Jönsson et al. (in prep.) is observed, which indicates the benefit from higher resolution.

6.1 Future Prospects

Much of the work done in this thesis is intended to be a stepping stone to build on, with many parts that can be utilised: the precisely derived abundances, the carefully curated linelist, and the insights into the importance of different features of line formation.
Knowing which elements can be accurately measured from infrared spectra with good agreement to optical results will let us measure regions optical light can't access, and to be confident in that potential differences are not caused by errors in the line formation. Observed differences are one part of a complex search for distinguishing between different theories of galaxy formation, requiring many fields of study such as computer simulations (see e.g. Agertz et al., 2020), chemical evolution models (see e.g. Kobayashi et al., 2020) and observational studies of other galaxies (see e.g. Scott et al., 2021), for a full understanding. Seeing whether simulations and models matching the observed trends is the only way of constraining what can otherwise be very variable areas of research.

Which elements will display differences cannot be known until measurements have been performed, but here are some science cases where the good agreement we have found with optical results could assist in further studies:

- The excellent agreement for Mg and Ca will allow for further study of the alpha element enhancement in the thin and thick discs at smaller galactocentric radii. This could help answer some of the many questions regarding the origin of the two discs, whether they are the result of mergers, accretion events or radial migration.

- Using optical spectra Lomaeva, 2018 has found a significant enhancement of iron-peak elements such as V and Co in the bulge, compared to the local thick disc. With the good agreement we have seen for both V and Co a larger sample of bulge giants could more easily be obtained using infrared observations, for further study of the connection between the formation of the thick disc and the bulge.

- The good agreement with optical results for Ce is very important, as it is formed by neutron capture processes. In galactic chemical evolution models such elements are used for constraining the physics of a number of different processes including AGB star winds, neutron star - black hole mergers and magnetorotational supernovae (Kobayashi et al., 2020). Finding discrepancies in such an element could therefore give clues to the relative importance of such processes in the region.

When it comes to continuing the analysis performed in this thesis, a first step to take is to use the insights into line formation to improve the optical analysis of Jönsson et al. (in prep.); expanding the use of hyperfine structure lines, updating the NLTE correction grids, and measuring astrophysical linestrengths where they are needed. Seeing the impact these techniques would have on the optical spectra could give further clarifications of where there are disagreements with the infrared results, and why.
A natural extension of the work is to find strategies for accurately determining stellar parameters from IR spectra. When reliable methods have been developed and benchmarked, infrared spectra can be analysed without needing to adopt stellar parameters from optical studies. This will unlock the full potential of observing in the infrared, enabling observations of the furthest reaches of the galaxy through the dust clouds, and potentially beyond using adaptive optics. Work has already begun on determining parameters using the same H band spectra used in this thesis, utilising the linelist I have created during this thesis work (Puspure, in prep.). Work is also in progress to determine stellar parameters for solar like stars from APOGEE spectra, with the aim of improving analysis of exoplanets and planet formation, making use of my linelist (Forsberg, in prep.).
Extending the work done here to other wavelength regions is another important step. Work has begun on the K band using IGRINS data and the methods developed during this thesis (Nandakumar et al., in prep.), but similar analysis should be extended to the other infrared wavelength bands as well.
With the thesis showing the necessity of a deep understanding of the line formation and the atomic data it is built on, furthering the measurement of everything from wavelengths,

linestrengths and hyperfine structure constants, to the calculation of van der Waals broadening parameters and NLTE departure grids, is an essential step for infrared spectral analysis to reach the same level of reliability as optical. Simply measuring the infrared spectra of more elements so that unidentified lines can be identified and the direction for further studies can be decided, would also be of great use.
The final step to take from this work is to redo it with better data, when new instruments such as HIRES for the ELT are online, bringing a new level of precision and much greater wavelength coverage. With the guidance of earlier work, a new stepping stone can be laid. Comparing optical and infrared measurements taken with the same instrument, will reduce the systematic errors to the highest possible degree and allow for more accurate parameter determinations as a wider selection of lines would be available. With benchmark values from such a study the work of determining the finest details of chemical evolution of our galaxy can be done.

Acknowledgements

I would like to thank my supervisors Nils Ryde and Henrik Jönsson for letting me find my own wings, for always being there to lift me when I've fallen. In a difficult year their support has been essential. I would also like to thank the other members of the ISA group: Ivalu Barlach Christensen, Rebecca Forsberg, Henrik Hartman and Brian Thorsbro. Without the good cheer and excellent advice in the weekly meetings, little progress would have been made.
I would also like to thank Paul Barklem for sending over updated values of the van der Waals broadening, which turned out to be very important to the thesis.
Finally I would like to thank my family and friends who have had to put up with me talking about nothing but spectral lines for the last year and a half, your support has been sorely needed.

Bibliography

Agertz, Oscar et al. (June 2020). "VINTERGATAN I: The origins of chemically, kinematically and structurally distinct discs in a simulated Milky Way-mass galaxy". In: *arXiv e-prints*, arXiv:2006.06008, arXiv:2006.06008. arXiv: 2006.06008 [astro-ph.GA].

Amarsi, A. M. & M. Asplund (Jan. 2017). "The solar silicon abundance based on 3D non-LTE calculations". In: *MNRAS* 464.1, pp. 264–273. DOI: 10.1093/mnras/stw2445. arXiv: 1609.07283 [astro-ph.SR].

Amarsi, A. M., M. Asplund, R. Collet & J. Leenaarts (Feb. 2016b). "Non-LTE oxygen line formation in 3D hydrodynamic model stellar atmospheres". In: *MNRAS* 455.4, pp. 3735–3751. DOI: 10.1093/mnras/stv2608. arXiv: 1511.01155 [astro-ph.SR].

Amarsi, A. M., K. Lind, M. Asplund, P. S. Barklem & R. Collet (Dec. 2016). "Non-LTE line formation of Fe in late-type stars - III. 3D non-LTE analysis of metal-poor stars". In: *MNRAS* 463.2, pp. 1518–1533. DOI: 10.1093/mnras/stw2077. arXiv: 1608.06390 [astro-ph.SR].

Amarsi, A. M. et al. (Oct. 2020). "The GALAH Survey: non-LTE departure coefficients for large spectroscopic surveys". In: *Astronomy Astrophysics* 642, A62. ISSN: 1432-0746. DOI: 10.1051/0004-6361/202038650. URL: http://dx.doi.org/10.1051/0004-6361/202038650.

Anstee, S. D. & B. J. O'Mara (Dec. 1991). "An investigation of Brueckner's theory of line broadening with application to the sodium D lines". In: *MNRAS* 253, pp. 549–560. DOI: 10.1093/mnras/253.3.549.

— (Oct. 1995). "Width cross-sections for collisional broadening of s-p and p-s transitions by atomic hydrogen". In: *MNRAS* 276.3, pp. 859–866. DOI: 10.1093/mnras/276.3.859.

Asplund, Martin, Nicolas Grevesse, A. Jacques Sauval & Pat Scott (Sept. 2009). "The Chemical Composition of the Sun". In: *ARA&A* 47.1, pp. 481–522. DOI: 10.1146/annurev.astro.46.060407.145222. arXiv: 0909.0948 [astro-ph.SR].

Barklem, Paul S. (May 2016). "Accurate abundance analysis of late-type stars: advances in atomic physics". In: 24.1, 9, p. 9. DOI: 10.1007/s00159-016-0095-9. arXiv: 1604.07659 [astro-ph.SR].

— (private communication). In: *TBD*.

Bengtsson, J., J. Larsson, S. Svanberg & C.-G. Wahlstrom (Jan. 1990). "Hyperfine-structure study of the 3d10 5p 2P3/2 level of neutral copper using pulsed level-crossing spectroscopy at short laser wavelengths". In: *Phys. Rev. A* 41. (BLSW estimated A

and B taken from Cu 63 with factors 1.064A and 1.075B), pp. 233–242. DOI: 10.1103/PhysRevA.41.233.

Bengtsson, J., J. Larsson, S. Svanberg & C.-G. Wahlstrom (Jan. 1990b). "Hyperfine-structure study of the 3d10 5p 2P3/2 level of neutral copper using pulsed level-crossing spectroscopy at short laser wavelengths". In: *Phys. Rev. A* 41, pp. 233–242. DOI: 10.1103/PhysRevA.41.233.

Bensby, T., S. Feltzing & M. S. Oey (Feb. 2014). "Exploring the Milky Way stellar disk. A detailed elemental abundance study of 714 F and G dwarf stars in the solar neighbourhood". In: *A&A* 562, A71, A71. DOI: 10.1051/0004-6361/201322631. arXiv: 1309.2631 [astro-ph.GA].

Bergemann, Maria & Thomas Nordlander (Mar. 2014). "Non-LTE radiative transfer in cool stars. Theory and applications to the abundance analysis for 24 chemical elements". In: *arXiv e-prints*, arXiv:1403.3088, arXiv:1403.3088. arXiv: 1403.3088 [astro-ph.SR].

Bergemann, Maria et al. (Nov. 2019). "Observational constraints on the origin of the elements. I. 3D NLTE formation of Mn lines in late-type stars". In: *A&A* 631, A80, A80. DOI: 10.1051/0004-6361/201935811. arXiv: 1905.05200 [astro-ph.SR].

Bergström, H., W. X. Peng & A. Persson (Sept. 1989). "Two different types of hollow-cathode discharges used for high resolution laser spectroscopy on copper". In: *Zeitschrift fur Physik D Atoms Molecules Clusters* 13, pp. 203–206. DOI: 10.1007/BF01436957.

Biemont, E. & J. W. Brault (Dec. 1986). "The infrared spectrum of magnesium (1800 ¡ σ ¡ 9000cm^{-1}) and an extension of the term systems of Mg I and Mg II". In: 34, p. 751. DOI: 10.1088/0031-8949/34/6B/007.

Biemont, E., P. Quinet & C. J. Zeippen (Dec. 1993). "DELTA-N2 Allowed Transitions in Neutral Sulphur Within the Visible and Infrared Spectral Ranges". In: 102. (BQZ), pp. 435–+.

Biemont, E., G. Roland, L. Delbouille & J. W. Brault (July 1985). "An investigation of iron in the infrared solar spectrum based on FTS laboratory measurements". In: 61, pp. 107–125.

Blackwell-Whitehead, R. J., J. C. Pickering, O. Pearse & G. Nave (Apr. 2005). "Hyperfine Structure Measurements of Neutral Manganese with Fourier Transform Spectroscopy". In: *Astrophysical Journal Supplement Series* 157, pp. 402–409. DOI: 10.1086/427924.

Blanco-Cuaresma, Sergi (June 2019). "Modern stellar spectroscopy caveats". In: *MNRAS* 486.2, pp. 2075–2101. DOI: 10.1093/mnras/stz549. arXiv: 1902.09558 [astro-ph.SR].

Böcek Topcu, G., M. Afşar & C. Sneden (Aug. 2016). "The chemical compositions and evolutionary status of red giants in the open cluster NGC 6940". In: *Monthly Notices of the Royal Astronomical Society* 463.1, pp. 580–597. ISSN: 0035-8711. DOI: 10.1093/mnras/stw1974. eprint: https://academic.oup.com/mnras/article-pdf/463/1/580/18756643/stw1974.pdf. URL: https://doi.org/10.1093/mnras/stw1974.

Booth, A. J. & D. E. Blackwell (Aug. 1983). "The effect of hyperfine structure on stellar abundance analysis". In: *MNRAS* 204, pp. 777–781. DOI: 10.1093/mnras/204.3.777.

Borrero, J. M., L. R. Bellot Rubio, P. S. Barklem & J. C. del Toro Iniesta (June 2003). "Accurate atomic parameters for near-infrared spectral lines". In: *A&A* 404, pp. 749–762. DOI: 10.1051/0004-6361:20030548.

Bressan, Alessandro et al. (Nov. 2012). "PARSEC: stellar tracks and isochrones with the PAdova and TRieste Stellar Evolution Code". In: *MNRAS* 427.1, pp. 127–145. DOI: 10.1111/j.1365-2966.2012.21948.x. arXiv: 1208.4498 [astro-ph.SR].

Buder, Sven et al. (Nov. 2020). "The GALAH+ Survey: Third Data Release". In: *arXiv e-prints*, arXiv:2011.02505, arXiv:2011.02505. arXiv: 2011.02505 [astro-ph.GA].

Chang, E. S. (Jan. 1990). "Energy Levels of Atomic Aluminum with Hyperfine Structure". In: *Journal of Physical and Chemical Reference Data* 19, pp. 119–125. DOI: 10.1063/1.555870.

Christensen, Ivalu Barlach (2020). *Accurate Abundances of Giant Stars in the Local disk: A manual analysis of IR APOGEE spectra*. eng. Student Paper.

Chromey, Frederick R. (2010). *To measure the sky : an introduction to observational astronomy.* Cambridge University Press. ISBN: 9780521763868. URL: http://ludwig.lub.lu.se/login?url=https://search.ebscohost.com/login.aspx?direct=true&db=cat07147a&AN=lub.1926058&site=eds-live&scope=site.

Commons, Wikimedia (2013). *The Discovery Channel Telescope*. File: LambdaPlaques.jpg. URL: https://upload.wikimedia.org/wikipedia/commons/4/48/Discovery_Channel_Telescope.JPG.

Corliss, Charles H. (July 1978). "Wavelengths and Energy Levels of the Second Spectrum of Cerium (Ce II)". In: *Journal of Research of the National Bureau of Standards - A. Physics and Chemistry* 4, pp. 419–546.

Cowan, Robert Duane (1981). *The theory of atomic structure and spectra.* Los Alamos series in basic and applied sciences. University of California P. ISBN: 0520038215. URL: http://ludwig.lub.lu.se/login?url=https://search.ebscohost.com/login.aspx?direct=true&db=cat07147a&AN=lub.241100&site=eds-live&scope=site.

Cunha, Katia et al. (Aug. 2017). "Adding the s-Process Element Cerium to the APOGEE Survey: Identification and Characterization of Ce II Lines in the H-band Spectral Window". In: *ApJ* 844.2, 145, p. 145. DOI: 10.3847/1538-4357/aa7beb.

Do, Tuan et al. (Mar. 2018). "Super-solar Metallicity Stars in the Galactic Center Nuclear Star Cluster: Unusual Sc, V, and Y Abundances". In: *ApJ* 855.1, L5, p. L5. DOI: 10.3847/2041-8213/aaaec3. arXiv: 1802.08270 [astro-ph.GA].

Duffau, S. et al. (Aug. 2017). "TheGaia-ESO Survey: Galactic evolution of sulphur and zinc". In: *Astronomy Astrophysics* 604, A128. ISSN: 1432-0746. DOI: 10.1051/0004-6361/201730477. URL: http://dx.doi.org/10.1051/0004-6361/201730477.

Elbel, M. & W. Fischer (Apr. 1961). "Zur Isotopieverschiebung im Kupfer I- und II-Spektrum". In: *Zeitschrift fur Physik* 165, pp. 151–170. DOI: 10.1007/BF01377677.

Falkenberg, B. & P. Zimmermann (1979). "The Perturbed Hyperfine Structure of the $3s^2$ 3d 2D- and $3s^2$ 4d 2D-States of AI I". In: *Z. Naturforsch. A* 34, pp. 1249–1250.

Forsberg, Rebecca (2019). *Detailed chemical abundances of neutron-capture elements - from 523 local giant stars*. eng. Student Paper.

— (in prep.). PhD thesis. Lund Observatory.

Gaia Collaboration et al. (Aug. 2018). "Gaia Data Release 2. Summary of the contents and survey properties". In: *A&A* 616, A1, A1. DOI: 10.1051/0004-6361/201833051. arXiv: 1804.09365 [astro-ph.GA].

García Pérez, Ana E. et al. (May 2016). "ASPCAP: THE APOGEE STELLAR PARAMETER AND CHEMICAL ABUNDANCES PIPELINE". In: *The Astronomical Journal* 151.6, p. 144. ISSN: 1538-3881. DOI: 10.3847/0004-6256/151/6/144. URL: http://dx.doi.org/10.3847/0004-6256/151/6/144.

Goldman, A. et al. (May 1998). "Updated line parameters for OH $X^2\Pi$-$X^2\Pi$ ($v v'$) transitions." In: 59.3-5, pp. 453–469. DOI: 10.1016/S0022-4073(97)00112-X.

Goorvitch, D. (Dec. 1994). "Infrared CO Line List for the X 1 Sigma + State". In: 95, p. 535. DOI: 10.1086/192110.

Gray, David F. (2005). *The observation and analysis of stellar photospheres.* Cambridge Univ. Press. ISBN: 0521851866. URL: http://ludwig.lub.lu.se/login?url=https://search.ebscohost.com/login.aspx?direct=true&db=cat07147a&AN=lub.1619252&site=eds-live&scope=site.

Gustafsson, B. et al. (Aug. 2008). "A grid of MARCS model atmospheres for late-type stars. I. Methods and general properties". In: *A&A* 486.3, pp. 951–970. DOI: 10.1051/0004-6361:200809724. arXiv: 0805.0554 [astro-ph].

Guthöhrlein, G. H. & H. P. Keller (Sept. 1990). "Doppler-free laserspectroscopic investigations of hyperfine structure in the atomic cobalt spectrum". In: *Zeitschrift fur Physik D Atoms Molecules Clusters* 17, pp. 181–193. DOI: 10.1007/BF01437898.

Hasselquist, Sten et al. (Dec. 2016). "Identification of Neodymium in the Apogee H-Band Spectra". In: *ApJ* 833.1, 81, p. 81. DOI: 10.3847/1538-4357/833/1/81.

Heiter, U. & K. Eriksson (June 2006). "Geometry of giant star model atmospheres: a consistency test". In: *A&A* 452.3, pp. 1039–1048. DOI: 10.1051/0004-6361:20064925. arXiv: astro-ph/0603273 [astro-ph].

Heiter, U. et al. (Jan. 2021). "Atomic data for the Gaia-ESO Survey". In: *A&A* 645, A106, A106. DOI: 10.1051/0004-6361/201936291. arXiv: 2011.02049 [astro-ph.IM].

Huber, Daniel et al. (Mar. 2014). "Revised Stellar Properties of Kepler Targets for the Quarter 1-16 Transit Detection Run". In: 211.1, 2, p. 2. DOI: 10.1088/0067-0049/211/1/2. arXiv: 1312.0662 [astro-ph.EP].

Huber, M.C.E. (1) & R.J. Sandeman (1986). "The measurement of oscillator strengths." In: *Reports on Progress in Physics* 49.4, pp. 397–490. ISSN: 00344885. URL: http://ludwig.lub.lu.se/login?url=https://search.ebscohost.com/login.aspx?direct=true&db=edselc&AN=edselc.2-52.0-0000823002&site=eds-live&scope=site.

Humphreys, Curtis J. & Kenneth L. Andrew (Sept. 1964). "Extension of Observations and Analysis of Ge i†". In: *J. Opt. Soc. Am.* 54.9, pp. 1134–1140. DOI: 10.1364/JOSA.54.001134. URL: http://www.osapublishing.org/abstract.cfm?URI=josa-54-9-1134.

Jofré, P. et al. (May 2017). "Gaia FGK benchmark stars: opening the black box of stellar element abundance determination". In: *A&A* 601, A38, A38. DOI: 10.1051/0004-6361/201629833. arXiv: 1612.05013 [astro-ph.SR].

Jofré, Paula, Ulrike Heiter & Caroline Soubiran (Aug. 2019). "Accuracy and Precision of Industrial Stellar Abundances". In: *ARA&A* 57, pp. 571–616. DOI: 10.1146/annurev-astro-091918-104509. arXiv: 1811.08041 [astro-ph.SR].

Johansson, I. (1961). "Spectra of the Alkali Metals in the Lead-Sulphide Region". In: *Arkiv för Fysik* 20, pp. 135–145.

Jönsson, G., S. Kröll, H. Lundberg & S. Svanberg (Oct. 1984). "Hyperfine structure and radiative lifetimes in the 3 s ^{2} n p ^{2} P $_{3/2}$ sequence of^{27}Al using time resolved laser spectroscopy". In: *Zeitschrift fur Physik A Hadrons and Nuclei* 316. (extrapolated JKLS), pp. 259–263. DOI: 10.1007/BF01439898.

— (Oct. 1984b). "Hyperfine structure and radiative lifetimes in the 3 s ^{2} n p ^{2} P $_{3/2}$ sequence of^{27}Al using time resolved laser spectroscopy". In: *Zeitschrift fur Physik A Hadrons and Nuclei* 316, pp. 259–263. DOI: 10.1007/BF01439898.

Jönsson, Henrik et al. (July 2020). "The 16th Data Release of the Sloan Digital Sky Surveys: First Release from the APOGEE-2 Southern Survey and Full Release of eBOSS Spectra". In: 249.1, 3, p. 3. DOI: 10.3847/1538-4365/ab929e. arXiv: 1912.02905 [astro-ph.GA].

Jönsson, Henrik et al. (in prep.). In: *TBD*.

Kobayashi, Chiaki, Amanda I. Karakas & Maria Lugaro (Sept. 2020). "The Origin of Elements from Carbon to Uranium". In: *ApJ* 900.2, 179, p. 179. DOI: 10.3847/1538-4357/abae65. arXiv: 2008.04660 [astro-ph.GA].

Kobayashi, Chiaki, Amanda I. Karakas & Hideyuki Umeda (July 2011b). "The evolution of isotope ratios in the Milky Way Galaxy". In: *MNRAS* 414.4, pp. 3231–3250. DOI: 10.1111/j.1365-2966.2011.18621.x. arXiv: 1102.5312 [astro-ph.GA].

Kobayashi, Chiaki et al. (Oct. 2011). "Evolution of Fluorine in the Galaxy with the ν-process". In: *ApJ* 739.2, L57, p. L57. DOI: 10.1088/2041-8205/739/2/L57. arXiv: 1108.3030 [astro-ph.SR].

Kurucz, R. L. (May 1973). "Semiempirical Calculation of gf Values: sc II (3d+4s)^2 - (3d+4s) 4p, a Detialed Example". In: *SAO Special Report* 351.

Kurucz, Robert & B. Bell (Jan. 1995). "Atomic Line Data". In: *Atomic Line Data (R.L. Kurucz and B. Bell) Kurucz CD-ROM No. 23. Cambridge* 23.

Kurucz, Robert L. (Jan. 1981b). "Semiempirical Calculation of gf Values, IV: Fe II". In: *SAO Special Report* 390.

Lawler, J. E., A. Guzman, M. P. Wood, C. Sneden & J. J. Cowan (Apr. 2013). "Improved Log(gf) Values for Lines of Ti I and Abundance Determinations in the Photospheres of the Sun and Metal-Poor Star HD 84937 (Accurate Transition Probabilities for Ti I)". In: 205, 11, p. 11. DOI: 10.1088/0067-0049/205/2/11.

Lefèbvre, P.-H., H.-P. Garnir & E. Biémont (June 2003). "Hyperfine structure for neutral manganese lines of astrophysical interest". In: *Astron. and Astrophys.* 404, pp. 1153–1158. DOI: 10.1051/0004-6361:20030592.

Li, Wai-Kee & S. M. Blinder (2014). *Atomic electronic states: the L-S and j-j coupling schemes and their correlation.* arXiv: 1409.2032 [physics.chem-ph].

Lind, K., M. Asplund, P. S. Barklem & A. K. Belyaev (Apr. 2011). "Non-LTE calculations for neutral Na in late-type stars using improved atomic data". In: *A&A* 528, A103, A103. DOI: 10.1051/0004-6361/201016095. arXiv: 1102.2160 [astro-ph.SR].

Lind, K. et al. (July 2017). "Non-LTE line formation of Fe in late-type stars - IV. Modelling of the solar centre-to-limb variation in 3D". In: *MNRAS* 468.4, pp. 4311–4322. DOI: 10.1093/mnras/stx673. arXiv: 1703.04027 [astro-ph.SR].

Lind, Karin et al. (2012). *INSPECT database*. http://http://www.inspect-stars.com/.

Lindegren, Lennart & Sofia Feltzing (2013). "The case for high precision in elemental abundances of stars in the era of large spectroscopic surveys". eng. In: Astronomy Astrophysics 553. ISSN: 0004-6361. DOI: 10.1051/0004-6361/201321057. URL: http://dx.doi.org/10.1051/0004-6361/201321057.

Litzén, Ulf (1964). "The Si I spectrum in the lead-sulphide region". In: *Arkiv för Fysik* 28, pp. 239–248.

Lomaeva, Maria (2018). *Abundances of iron-peak elements in disk and bulge giant stars from high-resolution optical spectra*. eng. Student Paper.

Majewski, Steven R. et al. (Sept. 2017). "The Apache Point Observatory Galactic Evolution Experiment (APOGEE)". In: *AJ* 154.3, 94, p. 94. DOI: 10.3847/1538-3881/aa784d. arXiv: 1509.05420 [astro-ph.IM].

Matrozis, E., N. Ryde & A. K. Dupree (Nov. 2013). "Galactic chemical evolution of sulphur. Sulphur abundances from the [S i] λ1082 nm line in giants". In: *A&A* 559, A115, A115. DOI: 10.1051/0004-6361/201322317. arXiv: 1309.0114 [astro-ph.GA].

Meléndez, J. & B. Barbuy (Apr. 2009). "Both accurate and precise gf-values for Fe II lines". In: *A&A* 497.2, pp. 611–617. DOI: 10.1051/0004-6361/200811508. arXiv: 0901.4451 [astro-ph.SR].

Mozurkewich, D. et al. (Nov. 2003). "Angular Diameters of Stars from the Mark III Optical Interferometer". In: *AJ* 126.5, pp. 2502–2520. DOI: 10.1086/378596.

Nandakumar, Govind & et al. (in prep.). In: *TBD*.

Nave, G., S. Johansson, R. C. M. Learner, A. P. Thorne & J. W. Brault (Sept. 1994). "A New Multiplet Table for Fe i". In: 94, p. 221. DOI: 10.1086/192079.

Nordlander, T. & K. Lind (Nov. 2017). "Non-LTE aluminium abundances in late-type stars". In: *A&A* 607, A75, A75. DOI: 10.1051/0004-6361/201730427. arXiv: 1708.01949 [astro-ph.SR].

Osorio, Y. & P. S. Barklem (Feb. 2016). "Mg line formation in late-type stellar atmospheres. II. Calculations in a grid of 1D models". In: *A&A* 586, A120, A120. DOI: 10.1051/0004-6361/201526958. arXiv: 1510.05165 [astro-ph.SR].

Pakhomov, Yu. V., T. A. Ryabchikova & N. E. Piskunov (2019). "Hyperfine Splitting in the VALD Database of Spectral-line Parameters." In: URL: http://ludwig.lub.lu.se/login?url=https://search.ebscohost.com/login.aspx?direct=true&db=edsarx&AN=edsarx.1911.03189&site=eds-live&scope=site.

Palmeri, P., E. Biemont, A. Aboussaid & M. Godefroid (Sept. 1995). "Hyperfine structure of infrared vanadium lines". In: *Journal of Physics B Atomic Molecular Physics* 28, pp. 3741–3752. DOI: 10.1088/0953-4075/28/17/013.

Park, Chan et al. (July 2014). "Design and early performance of IGRINS (Immersion Grating Infrared Spectrometer)". In: vol. 9147. Society of Photo-Optical Instrumentation Engineers (SPIE) Conference Series, p. 91471D. DOI: 10.1117/12.2056431.

Pehlivan, A., H. Nilsson & H. Hartman (Oct. 2015). "Laboratory oscillator strengths of Sc i in the near-infrared region for astrophysical applications". In: *A&A* 582, A98, A98. DOI: 10.1051/0004-6361/201526813. arXiv: 1509.06341 [astro-ph.IM].

Perryman, M. et al. (June 1997). "The Hipparcos Catalogue". In: *Astronomy and Astrophysics* 323, pp. L49–L52.

Pickering, J. C. (Dec. 1996). "Measurements of the Hyperfine Structure of Atomic Energy Levels in CO i". In: *Astrophysical Journal Supplement Series* 107, p. 811. DOI: 10.1086/192382.

Piskunov, Nikolai & Jeff A. Valenti (Jan. 2017). "Spectroscopy Made Easy: Evolution". In: *A&A* 597, A16, A16. DOI: 10.1051/0004-6361/201629124. arXiv: 1606.06073 [astro-ph.IM].

Puspure, Ieva (in prep.). Upcoming B.Sc. thesis.

Ralchenko, Yu., A.E. Kramida, J. Reader & NIST ASD Team (Sept. 2010). *NIST Atomic Spectra Database (ver. 4.0.0), [Online].*

Reddy, Bacham E., Jocelyn Tomkin, David L. Lambert & Carlos Allende Prieto (Mar. 2003). "The chemical compositions of Galactic disc F and G dwarfs". In: *MNRAS* 340.1, pp. 304–340. DOI: 10.1046/j.1365-8711.2003.06305.x. arXiv: astro-ph/0211551 [astro-ph].

Rieke, G. H. (Aug. 2009). "History of infrared telescopes and astronomy". In: *Experimental Astronomy* 25.1-3, pp. 125–141. DOI: 10.1007/s10686-009-9148-7.

Rutten, Robert J. (2003). *Radiative Transfer in Stellar Atmospheres.*

Ryabchikova, T. et al. (May 2015). "A major upgrade of the VALD database". In: 90.5, 054005, p. 054005. DOI: 10.1088/0031-8949/90/5/054005.

Santos-Peral, P., A. Recio-Blanco, P. de Laverny, E. Fernández-Alvar & C. Ordenovic (July 2020). "The AMBRE Project: Spectrum normalisation influence on Mg abundances in the metal-rich Galactic disc". In: *A&A* 639, A140, A140. DOI: 10.1051/0004-6361/202037522. arXiv: 2006.08544 [astro-ph.GA].

Scott, Nicholas et al. (May 2021). "Identification of an [/Fe]—Enhanced Thick Disk Component in an Edge-on Milky Way Analog". In: *The Astrophysical Journal Letters* 913.1, p. L11. ISSN: 2041-8213. DOI: 10.3847/2041-8213/abfc57. URL: http://dx.doi.org/10.3847/2041-8213/abfc57.

Sharma, Kaushal, Philippe Prugniel & Harinder P. Singh (Jan. 2016). "New atmospheric parameters and spectral interpolator for the MILES cool stars". In: *A&A* 585, A64, A64. DOI: 10.1051/0004-6361/201526111. arXiv: 1512.04882 [astro-ph.SR].

Smith, Verne V. et al. (Mar. 2021). "The APOGEE Data Release 16 Spectral Line List". In: *arXiv e-prints*, arXiv:2103.10112, arXiv:2103.10112. arXiv: 2103.10112 [astro-ph.SR].

Sneden, Christopher, Sara Lucatello, Ram S. Ram, James S. A. Brooke & Peter Bernath (Oct. 2014). "Line Lists for the A $^2\Pi$-X $^2\Sigma^+$ (Red) and B $^2\Sigma^+$-X $^2\Sigma^+$ (Violet) Systems

of CN, $^{13}C^{14}N$, and $^{12}C^{15}N$, and Application to Astronomical Spectra". In: 214.2, 26, p. 26. DOI: 10.1088/0067-0049/214/2/26. arXiv: 1408.3828 [astro-ph.SR].

Stoehr, F. et al. (Aug. 2008). "DER_SNR: A Simple & General Spectroscopic Signal-to-Noise Measurement Algorithm". In: *Astronomical Data Analysis Software and Systems XVII*. Ed. by R. W. Argyle, P. S. Bunclark & J. R. Lewis. Vol. 394. Astronomical Society of the Pacific Conference Series, p. 505.

Stück, H. L. & P. Zimmermann (Aug. 1970). "Level crossing investigations in the 4 d ^{2} D $_{5/2,3/2}$-states of the A1 I-spectrum". In: *Zeitschrift fur Physik* 239, pp. 345–350. DOI: 10.1007/BF01398246.

Svendenius, Nils (1980). "The Spectrum and Term Analysis of Neutral Phosphorus, P I." In: *Physica Scripta* 22.3, p. 1. ISSN: 00318949. URL: http://ludwig.lub.lu.se/login?url=https://search.ebscohost.com/login.aspx?direct=true&db=edb&AN=98331761&site=eds-live&scope=site.

Takada-Hidai, Masahide et al. (July 2002). "Behavior of Sulfur Abundances in Metal-poor Giants and Dwarfs". In: *ApJ* 573.2, pp. 614–630. DOI: 10.1086/340748. arXiv: astro-ph/0103481 [astro-ph].

The pandas development team (Feb. 2020). *pandas-dev/pandas: Pandas*. Version latest. DOI: 10.5281/zenodo.3509134. URL: https://doi.org/10.5281/zenodo.3509134.

Thorne, A. P., J. C. Pickering & J. Semeniuk (Jan. 2011). "The Spectrum and Term Analysis of V I". In: 192.1, 11, p. 11. DOI: 10.1088/0067-0049/192/1/11.

Thorsbro, B. et al. (Oct. 2018). "Evidence against Anomalous Compositions for Giants in the Galactic Nuclear Star Cluster". In: *ApJ* 866.1, 52, p. 52. DOI: 10.3847/1538-4357/aadb97. arXiv: 1808.07489 [astro-ph.GA].

Unkel, P., P. Buch, J. Dembczyński, W. Ertmer & U. Johann (Dec. 1989). "Sternheimer free determination of the ^{51}V nuclear quadrupole moment from hyperfine structure measurements". In: *Zeitschrift fur Physik D Atoms Molecules Clusters* 11, pp. 259–271. DOI: 10.1007/BF01438497.

Unsöld, Albrecht (1955). *Physik der Sternatmospharen, MIT besonderer Berucksichtigung der Sonne.*

Valenti, J. A. & N. Piskunov (Sept. 1996). "Spectroscopy made easy: A new tool for fitting observations with synthetic spectra." In: 118, pp. 595–603.

Wagner, S. (Feb. 1955). "Zur Isotopieverschiebung im Cul-Spektrum". In: *Zeitschrift fur Physik* 141, pp. 122–145. DOI: 10.1007/BF01327293.

Wiese, W. L., M. W. Smith & B. M. Miles (1969). *Atomic transition probabilities. Vol. 2: Sodium through Calcium. A critical data compilation*. Ed. by Wiese, W. L., Smith, M. W., & Miles, B. M. (WSM). US Government Printing Office.

Wood, M. P., J. E. Lawler & M. D. Shetrone (June 2014). "A Laboratory log(gf) Measurement of the Ti II 15873.84 Å H-Band Line in Support of SDSS-III Apogee". In: *ApJ* 787.2, L16, p. L16. DOI: 10.1088/2041-8205/787/2/L16. arXiv: 1404.5944 [astro-ph.SR].

Zhao, G. et al. (Dec. 2016). "Systematic Non-LTE Study of the -.6 $\leqslant$ [Fe/H] $\leqslant$ 0.2 F and G Dwarfs in the Solar Neighborhood. II. Abundance Patterns from Li to Eu". In:

ApJ 833.2, 225, p. 225. DOI: 10.3847/1538-4357/833/2/225. arXiv: 1610.00193 [astro-ph.SR].

Appendix A

Linelist sources

Data	Reference
Na, K: wavelengths	Johansson (1961)
Mg: wavelength	Biemont et al. (1986)
Mg: wavelengths	Ralchenko et al. (2010)
Al, K: wavelengths	Wiese et al. (1969)
Al: hfs	Chang (1990)
Al: hfs	Stück et al. (1970)
Al: hfs	Falkenberg et al. (1979)
Al: hfs	Jönsson et al. (1984)
Al: hfs	Jönsson et al. (1984b)
P: wavelengths	Svendenius (1980)
Si: wavelength	Litzén (1964)
S: wavelength	Biemont et al. (1993)
Ti: wavelength	Lawler et al. (2013)
V: wavelength	Thorne et al. (2011)
V: hfs	Unkel et al. (1989)
V: hfs	Palmeri et al. (1995)
Mn: hfs	Lefèbvre et al. (2003)
Mn: hfs	Blackwell-Whitehead et al. (2005)
Co: hfs	Pickering (1996)
Co: hfs	Guthöhrlein et al. (1990)
Cu: wavelengths	Wagner (1955)
Cu: hfs	Elbel et al. (1961)
Cu: hfs	Bergström et al. (1989)
Cu: hfs	Bengtsson et al. (1990)
Cu: hfs	Bengtsson et al. (1990b)
Ce: wavelengths, excitation energies	Corliss (1978)
Nd: wavelengths, excitation energies	Hasselquist et al. (2016)
Other data	Kurucz et al. (1995)

Table A.1: References to the papers which have contributed data to the lines used in abundance analysis, both through VALD and as supplemental literature sources.

Appendix B

LS Multiplet Divider

This appendix will describe how the two main problems of calculating relative linestrengths and applying them to astrophysical linestrength measurements, have been solved in this thesis. The problem of applying relative linestrengths is described first, as it is necessary to understand the procedure used for the formulation of the calculations to make sense.

B.1 Applying relative linestrengths

The problem of applying the ratios to the astrophysical measurement of linestrength is mostly an issue of time. With enough time, a reliable system of incorporating the relative linestrengths into the scripts used to run SME could have been developed, so that the process is fully automatised. Unfortunately there was not enough time to do this work, especially as SME is written in IDL which I personally have not yet mastered. Therefore the procedure developed requires manual input and iteration. The procedure works as follows:

1. Masks designating lines of interest, continuum and segments are set up as described in section 4.1.

2. The IDL code sme_adjustlines is called to adjust the $\log(gf)$ value of the line. The code picks out the strongest line of the given element within the specified linemask, refered to as the primary line, and varies the $\log(gf)$ value until a minimum in goodness of fit evaluated by χ^2 has been reached.

3. Using the newly calculated $\log(gf)$ value for the primary, a set of new $\log(gf)$ values for the other lines in the multiplet, the secondary lines, is calculated.

4. As the changed linestrengths of the secondary lines will have changed the goodness of fit to the observed spectra, steps 2-4 are repeated until convergence is achieved.

Given this procedure, the sought after quantity is not just the relative linestrengths of LS multiplet, but the scaled $\log(gf)$ values for the multiplet given the $\log(gf)$ value of the strongest line.

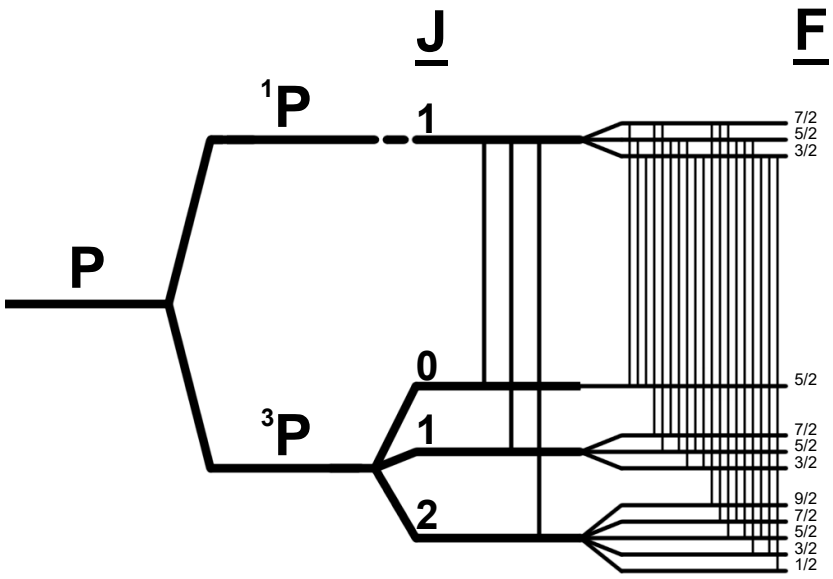

Figure B.1: Illustration of how a P orbital is split up, starting with the split into singlet and triplet states based on the electron spin. Spin-orbit interaction splits the triplet state into fine structure levels, with the J quantum number distinguishing the levels. As the spin of the electron in the singlet state is paired with another the level is not split. The three allowed transitions between the fine structure states are shown. The hyperfine structure splitting of the fine structure levels is illustrated for an element with intrinsic nuclear spin I=5/2. The interaction between the magnetic fields splits all the fine structure levels, with the total number of states depending on the quantum number $F = |I - J|, I + J + 1$. A total of 18 hyperfine structure lines are shown.

B.2 Relative linestrengths

In section 4.4.1 the need for a method to accurately divide linestrength across fine and hyperfine structure lines is described. The theoretical basis for doing so is described in Cowan (1981). The basis of this method is the LS coupling scheme, meaning it is an approximation of sorts and the results will depend on how well LS coupling describes the involved energy states. In general it works best for light elements and gets progressively worse for heavier elements, which after the first four periods are better described by $j-j$ coupling (Li et al., 2014). With the exception of Ce, Nd and Yb whose energy levels are poorly described by LS coupling, the approximation should be reasonable for the elements investigated in this thesis.
Assuming that the energy levels are well described by a pure LS coupling scheme, the relative linestrengths of the lines in the multiplet can be calculated. The equation for doing so for fine structure lines is described by Cowan (1981) in Appendix I as equation 14.50, reproduced here:

$$(D_{\text{line}})^2 = \delta_{\text{SS}'}[J, J'] \begin{Bmatrix} L & S & J \\ L' & S' & J' \end{Bmatrix} \tag{B.1}$$

- $(D_{\text{line}})^2$ is the square of the line factor, representing something like the relative linestrength
- $\delta_{\text{SS}'}$ is a Kronecker delta for the upper and lower spin quantum numbers, restricting the formulas use to eg. transitions between two triplets
- $[J, J'] = (J^2 + 1) * (J'^2 + 1)$
- $\begin{Bmatrix} L & S & J \\ L' & S' & J' \end{Bmatrix}$ is a Wigner 6-j symbol which describes the coupling of angular momenta, the full definition can be found in equations 5.23 and 5.24 in Cowan (1981)

For a multiplet of hyperfine structure lines a similar relative intensity parameter factor can be constructed:

$$(D_{\text{line}})^2 \propto [F, F'] \begin{Bmatrix} J & I & F \\ F' & 1 & J' \end{Bmatrix} \tag{B.2}$$

- $[F, F'] = (F^2 + 1) * (F'^2 + 1)$
- The I in the Wigner 6-j symbol is the nuclear spin for the particular isotope giving rise to the line.

Identifying the relevant quantum numbers for the fine or hyperfine structure lines which have been blended together, the relative linestrengths can be calculated and converted to relative $\log(gf)$ values, which is what is commonly read into spectral synthesis codes. The line factor $(D_{\text{line}})^2$ is analogous to the transition probability A_{ul} for a transition from an upper u to a lower l level. A_{ul} is related to g and f as

$$A_{ul} \propto \frac{g_l}{g_u} \frac{f_{lu}}{\lambda^2} \tag{B.3}$$

The ratio of the transition probabilities from two lines $A_{ul,1}$ and $A_{ul,2}$ can therefore be expreesed as,

$$\frac{A_1}{A_2} = \frac{g_{l,1}g_{u,2}}{g_{l,2}g_{u,1}}\frac{f_{lu,1}}{f_{lu,2}}\frac{\lambda_2^2}{\lambda_1^2} \approx \frac{g_{u,2}}{g_{u,1}}\frac{gf_1}{gf_2} \tag{B.4}$$

where the wavelength dependence has been neglected, as $\frac{\lambda_2^2}{\lambda_1^2}$ should be ≈ 1 for lines close enough to blend together, and the quantity $gf = g_l f_{lu}$ has been introduced. By solving for the gf-value, taking the log10 value of both sides and converting the statistical weight $g = (2J + 1)$ an expression for the $\log(gf)$ value for line 1 given the value for line 2 is derived,

$$log(gf_1) = log\left(10^{log(gf_2)} \cdot \frac{2J_{u,1} + 1}{2J_{u,2} + 1}\frac{A_1}{A_2}\right) \tag{B.5}$$

B.3 Predictive adjustment

To make the process of iterating the measurements easier I have implemented a small adjustment to the relative $\log(gf)$ values. The first step is to define to what extent the multiplet is dominated by the primary line, by dividing the linestrength of the primary line by the sum of all the linestrengths in the multiplet,

$$R = \frac{D^2_{\text{Primary}}}{\sum D^2_{\text{Multiplet}}}. \tag{B.6}$$

The linestrength of the primary line is then recalculated, taking the weighted impact of the secondary lines into account,

$$log(gf)_{\text{final}} = log(gf)_{\text{measured}} - (1 - R)\Delta log(gf) \tag{B.7}$$

The idea is to reduce the amount of overcompensation SME has to do to account for the fact that only the primary lines strength is adjusted in the fitting process. $(1 - R)$ gives the combined strength of the secondary lines, while $\Delta log(gf)$ is the difference between the primary lines $\log(gf)$ value before and after being adjusted astrophysically. The process improves the estimate of the linestrength by a significant amount, but the process still requires some iteration.
The code used for calculating relative linestrength can be found at my GitHub: `https://github.com/mablscmo/SME_Scripts/blob/master/LSMultiplet/lsmult.py`

Appendix C

Poster

Made for Cool Stars 20.5, 2-4 March 2021. Available at: https://zenodo.org/record/4569121

Towards a high resolution view of infrared line formation

Martin Montelius[1] Nils Ryde[1] Henrik Jönsson[2]

[1]Lund Observatory, Department of Astronomy and Theoretical Physics, Lund University, Box 43, SE-221 00 Lund
[2]Department of Materials Science and Applied Mathematics, Malmö University, SE-205 06, Malmö

Introduction

High resolution infrared spectroscopy is still in its infancy. There is a lot of work to do: validating that abundances derived from IR spectra are **consistent with optical data**, and investigating **from which processes differences arise**. This is especially important in the context of upcoming IR surveys such as MOONS, but also for IR spectroscopy in general.

Stellar Sample

Number of stars:	34
Spectral class:	K-giants
Spectrometer:	IGRINS
Spectral resolution:	∼45000
Spectral range:	1.49 - 1.80 μm
Telescope:	Lowell Discovery
S/N min/median/max:	85/184/413

Method

The spectra are manually analysed with the spectral synthesis code **SME** [1]. Stellar parameters have been predetermined from **high resolution optical spectra** [2], as methods for doing so are currently lacking in IR. The same optical analysis has determined abundances, which I **benchmark** my results against.

Investigated issues

- **Measuring:** C, Na, Mg, Al, Si, P, S, K, Ca, Ti, Cr, Mn, Co, Ni, Cu, Zn
- **Macroturbulence determination**
  - Testing Si and Fe lines
- **Astrophysical line strengths**
  - Measuring lines for all H-band elements
- **NLTE corrections**
  - Investigating C, Na, Mg, Al, Si, K, Ca, Mn
- **Hyperfine structure**
  - Investigating Na, Al, V, Mn, Co, Cu

Macroturbulence – v_{mac}

For R $\gtrsim$50 000 the instrumental profile no longer dominates line broadening, easing investigation of the broadening from the star.

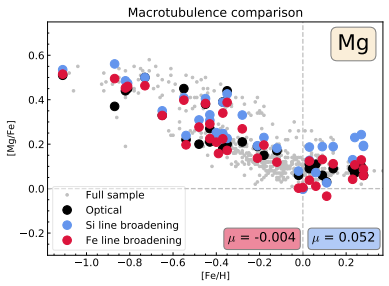

I have tried using both Si and Fe lines to determine v_{mac} for my stars. Highly accurate van der Waals broadening data [3] was used to minimise errors from the other major source of broadening for cool stars. The figure shows the abundance trend for Mg, note the **improved supersolar results using Fe lines**.

Astrophysical line strength

Inaccuracies in atomic data is cited as a top concern for abundance analysis [4], chiefly the line strength – log(gf). **Lab measurements** offer the highest levels of precision, but **are rarely available for IR lines**. Astrophysical log(gf) measurements use the spectra of a star with known abundances (the Sun) and solve for line strength instead of the abundance.
I have developed a method that **takes fine and hyperfine structure into account** when performing astrophysical log(gf) measurements, building on relative line strengths in LS multiplets to adjust secondary lines log(gf) [5].

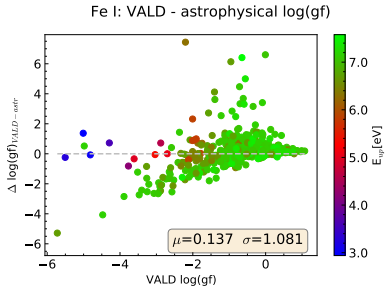

Astrophysical measurements **can be very important**; above, the differences between astrophysical measurements and values from the VALD database for 551 Fe I lines are shown. Not accounting for the inaccuracies in database values, risks the accuracy of studies.

Non - LTE corrections

To simplify calculations, spectral synthesis codes typically assume Local Thermodynamic Equilibrium (LTE), that temperature changes happen slowly enough that equilibrium can be assumed at each point. Further out in a star's photosphere, that assumption breaks down. Corrections to account for the resulting Non - LTE effects can be estimated, with updated values published in 2020 [6].

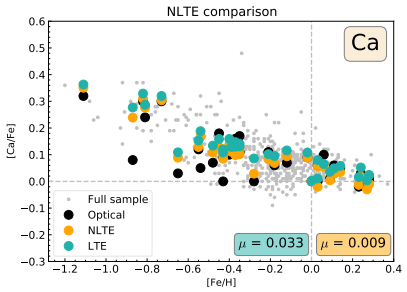

Above is an example of how I have assessed the impact of NLTE corrections. The two sets of results have been computed with and without NLTE corrections, including when measuring the astrophysical log(gf) values, with otherwise identical input. The difference in the Ca abundances are significant, with the LTE results showingm systematically higher abundances compared to the optical results.

Hyperfine structure – HFS

The nuclear spin of nuclei with odd Z or A, interacts with the angular momentum of the electrons, and splits the atom's energy levels into their hyperfine components. The HFS can warp the line profile, but also **desaturate strong lines, drastically affecting the derived abundance**.

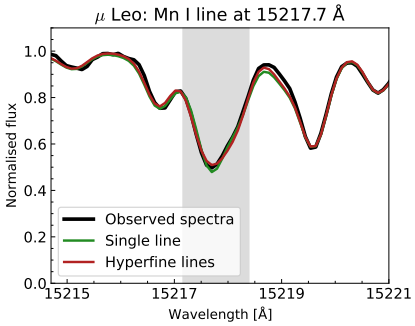

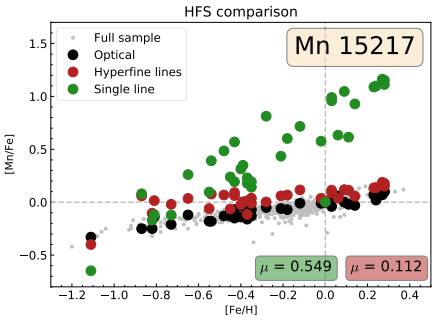

In the example shown above, two synthetic spectra of the star μ Leo have been computed, one with a single Mn I line and one with 16 hyperfine Mn I lines. The two synthetic **spectra appear similar**, but the **derived abundances differ by almost a whole order of magnitude!** The abundance trends shows the stark difference for the rest of the stars; the HFS effect shows a strong metallicity dependence, resulting in everything from similar abundances to an order of magnitude in difference.

Future prospects

- Investigating and comparing techniques for parameter determination in the IR
- Extending studies to available K band data
- Replicating studies for stars of different spectral classes, investigating differences
- Consistently studying the impact of HFS / NLTE / v_{mac} on optical spectra
- Calculating van der Waals broadening data for IR lines to test v_{mac} determination
- Extending laboratory measurements of more IR spectral lines

References

[1] Piskunov, N. Valenti, J. (2017). "Spectroscopy Made Easy: Evolution". *AA* 597
[2] Jönsson, H., et al. (in prep.)
[3] Barklem, P. (private communication)
[4] Barklem P. (2016) "Accurate abundance analysis...". *Astron. Astrophys. Rev.* 21:9.
[5] Cowan, R. D. (1981). "The theory of atomic structure and spectra".
[6] Amarsi, A., et al. (2020). "The GALAH Survey: non-LTE departure coefficients for large spectroscopic surveys". *AA* 642.

Appendix D

Arcturus line fits

The fits of the synthetic spectra to the observations of α Boo has been included in this appendix to show a number of things of interest: the strength and shape of the used spectral lines; nearby features of the spectra which could be important for abundance analysis; the location of the masks designating lines of interest, continuum and segments; and the continuum normalisation.
The area marked in orange marks the spectral line of interest, while the yellow areas mark the continuum level. The blue line is the solar spectrum while the dark grey line is the metal-rich giant μ Leo. The thin yellow line close to the continuum level shows the atmospheric spectra, to show where potential issues can arise from so called telluric lines. Due to the radial velocity of the stars the yellow line will not be accurate for all of the stars, but it is a good indicator of regions where telluric lines may appear. The coloured lines above the spectra indicate that particular wavelength's sensitivity to stellar parameters, $T_{\rm eff}$, $\log(g)$, [Fe/H] and $v_{\rm mic}$
Many of the lines in the spectra have been identified as being caused by a particular element and ionisation stage and have been marked with that information. Note that there are many unidentified lines which have not been marked, and especially important for this appendix; there are also identified lines which are not marked, including ones used in abundance analysis. The unmarked lines used in abundance analysis are: C I at 16333.93 Å, Zn I at 16483.43 and 16505.18 Å, Ce II at 17058.88 Å.

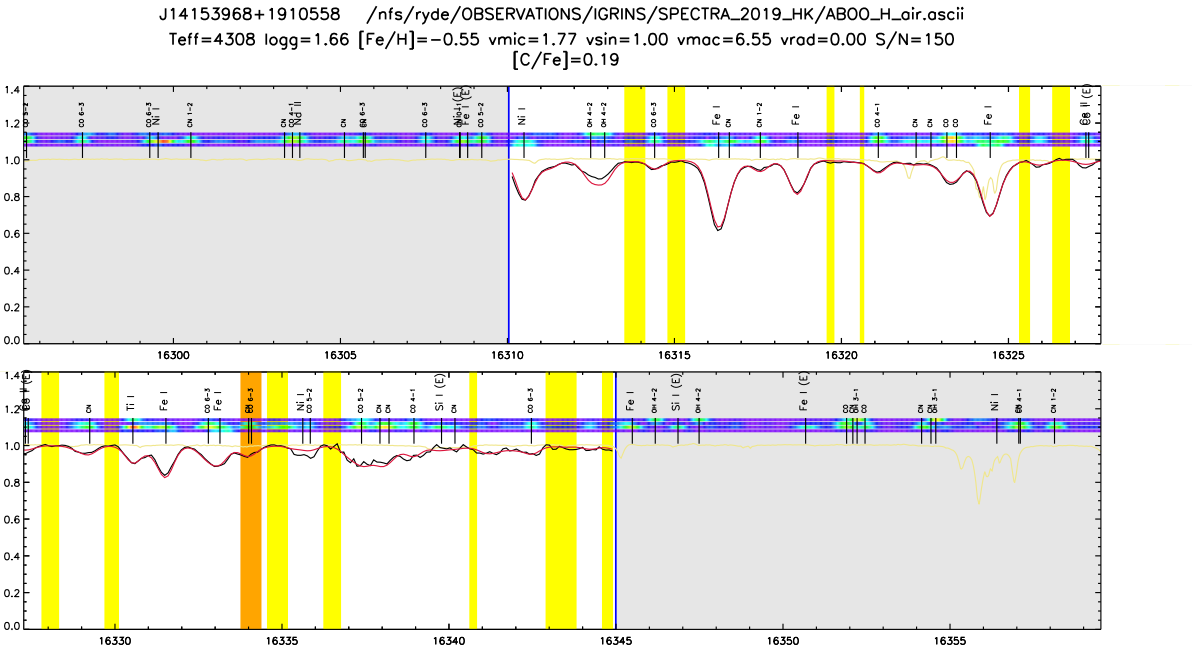
J14153968+1910558 /nfs/ryde/OBSERVATIONS/IGRINS/SPECTRA_2019_HK/AB00_H_air.ascii
Teff=4308 logg=1.66 [Fe/H]=−0.55 vmic=1.77 vsin=1.00 vmac=6.55 vrad=0.00 S/N=150
[C/Fe]=0.19

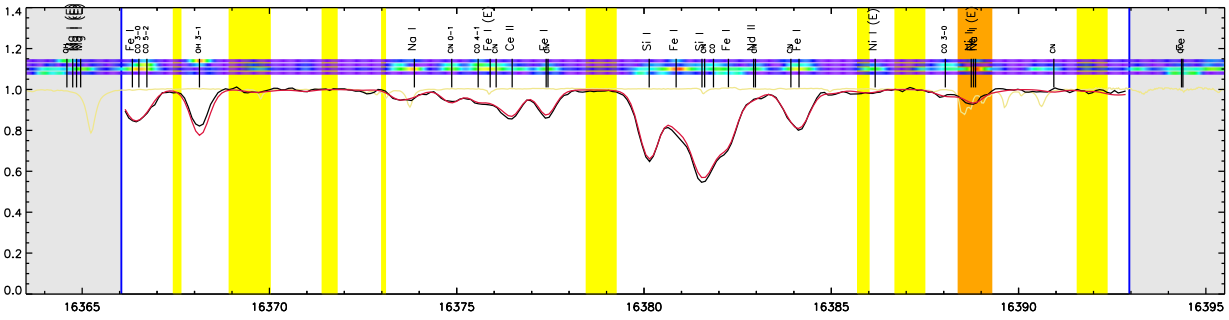
J14153968+1910558 /nfs/ryde/OBSERVATIONS/IGRINS/SPECTRA_2019_HK/AB00_H_air.ascii
Teff=4308 logg=1.66 [Fe/H]=−0.55 vmic=1.77 vsin=1.00 vmac=6.55 vrad=0.00 S/N=150
[Na/Fe]=−0.07

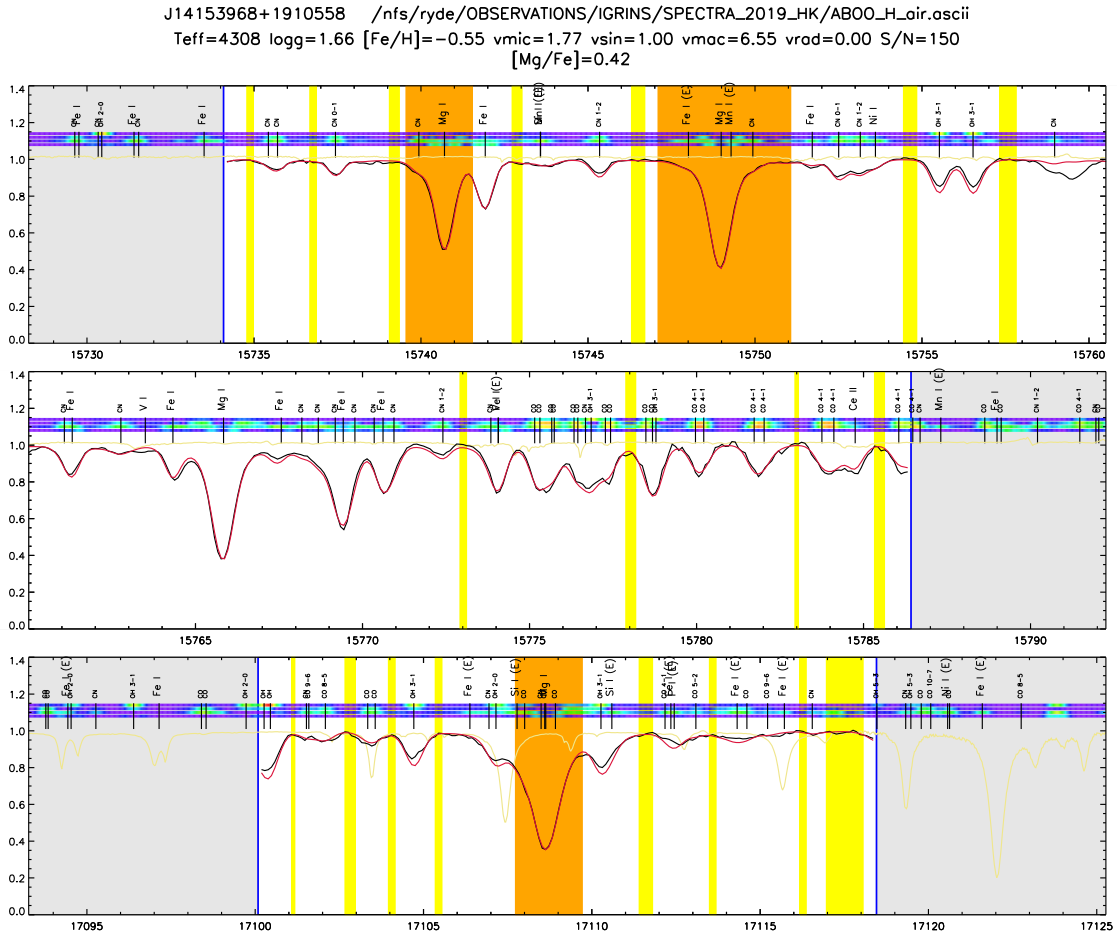
J14153968+1910558 /nfs/ryde/OBSERVATIONS/IGRINS/SPECTRA_2019_HK/A800_H_air.ascii
Teff=4308 logg=1.66 [Fe/H]=−0.55 vmic=1.77 vsin=1.00 vmac=6.55 vrad=0.00 S/N=150
[Mg/Fe]=0.42

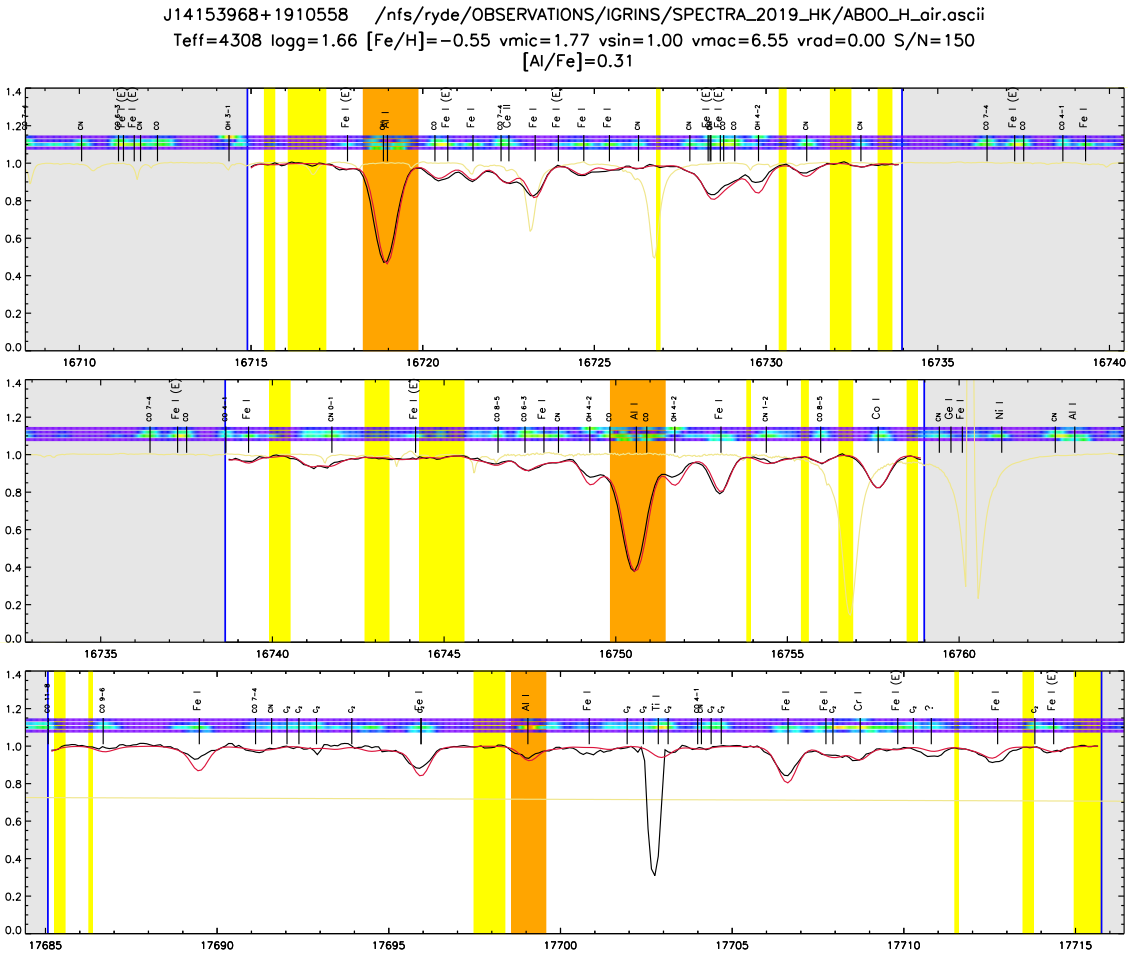
J14153968+1910558 /nfs/ryde/OBSERVATIONS/IGRINS/SPECTRA_2019_HK/ABOO_H_air.ascii
Teff=4308 logg=1.66 [Fe/H]=−0.55 vmic=1.77 vsin=1.00 vmac=6.55 vrad=0.00 S/N=150
[Al/Fe]=0.31

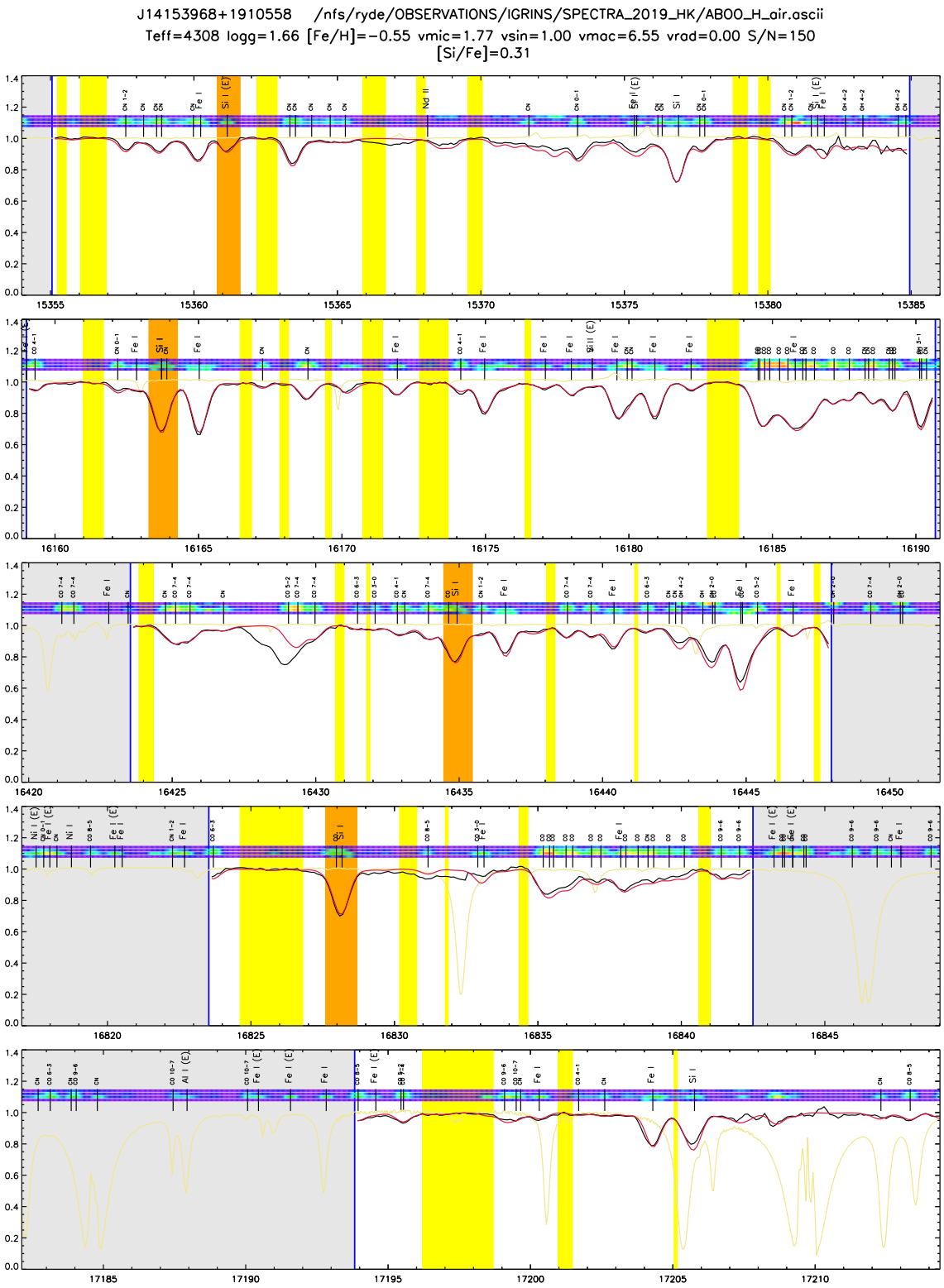
J14153968+1910558 /nfs/ryde/OBSERVATIONS/IGRINS/SPECTRA_2019_HK/ABOO_H_air.ascii
Teff=4308 logg=1.66 [Fe/H]=−0.55 vmic=1.77 vsin=1.00 vmac=6.55 vrad=0.00 S/N=150
[Si/Fe]=0.31

J14153968+1910558 /nfs/ryde/OBSERVATIONS/IGRINS/SPECTRA_2019_HK/ABOO_H_air.ascii
Teff=4308 logg=1.66 [Fe/H]=−0.55 vmic=1.77 vsin=1.00 vmac=6.55 vrad=0.00 S/N=150
[Si/Fe]=0.31

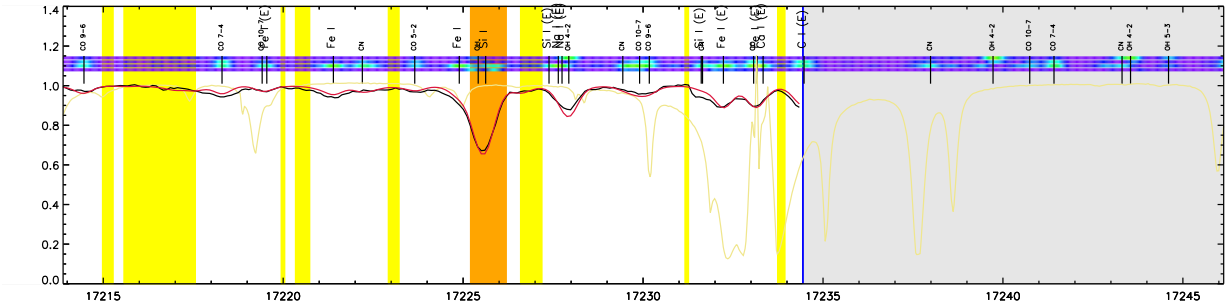

J14153968+1910558 /nfs/ryde/OBSERVATIONS/IGRINS/SPECTRA_2019_HK/ABOO_H_air.ascii
Teff=4308 logg=1.66 [Fe/H]=−0.55 vmic=1.77 vsin=1.00 vmac=6.55 vrad=0.00 S/N=150
[P/Fe]=0.86

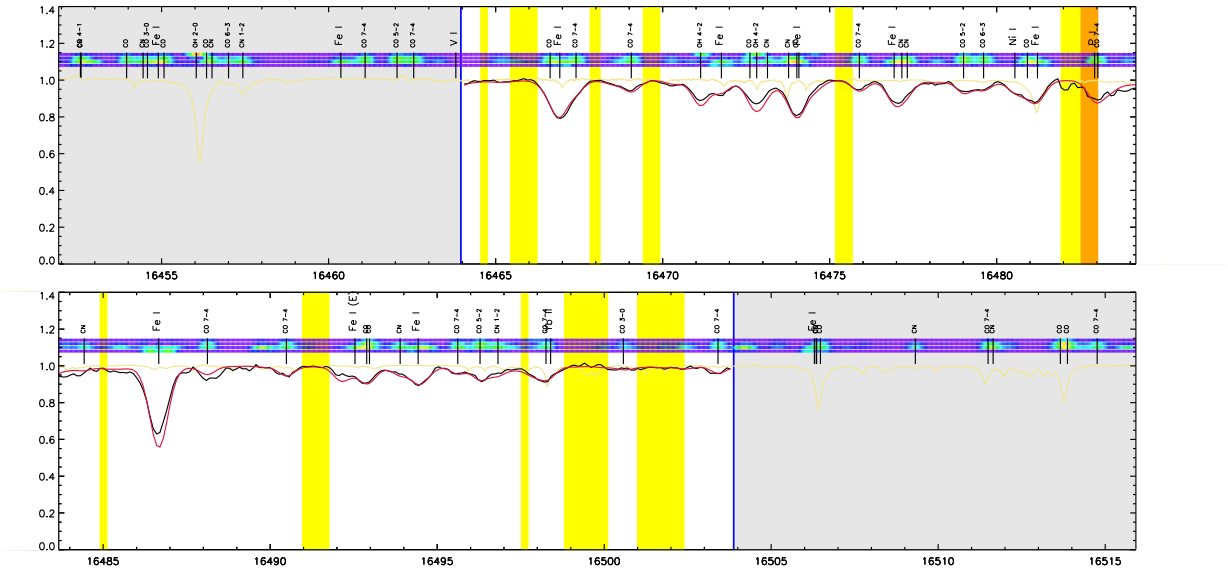

J14153968+1910558 /nfs/ryde/OBSERVATIONS/IGRINS/SPECTRA_2019_HK/ABOO_H_air.ascii
Teff=4308 logg=1.66 [Fe/H]=−0.55 vmic=1.77 vsin=1.00 vmac=6.55 vrad=0.00 S/N=150
[S/Fe]=0.23

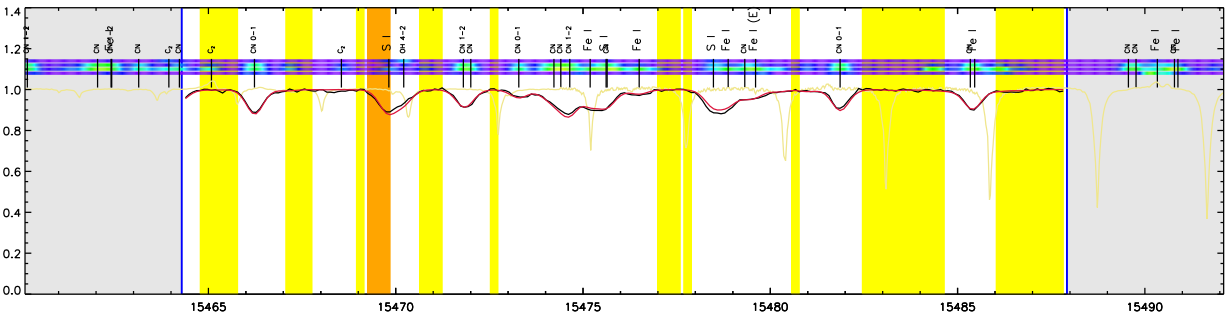

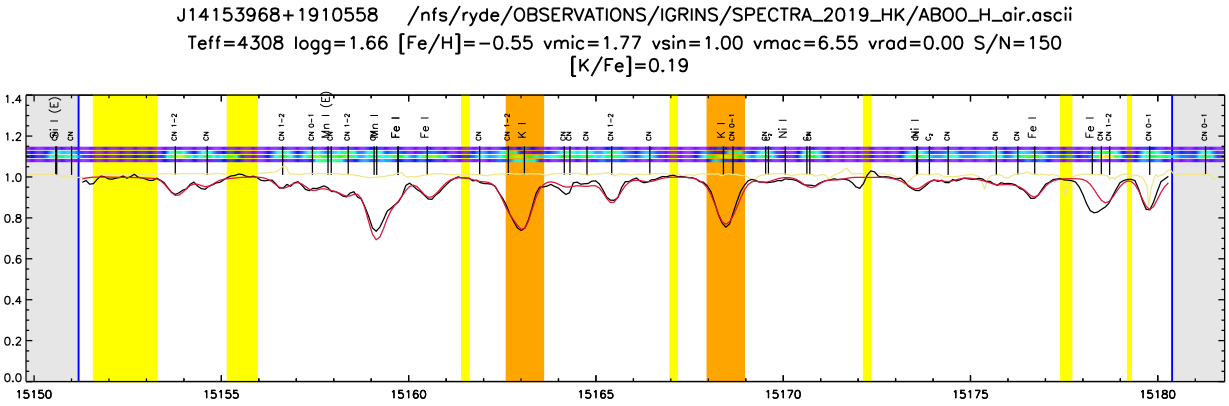
J14153968+1910558 /nfs/ryde/OBSERVATIONS/IGRINS/SPECTRA_2019_HK/ABOO_H_air.ascii
Teff=4308 logg=1.66 [Fe/H]=−0.55 vmic=1.77 vsin=1.00 vmac=6.55 vrad=0.00 S/N=150
[K/Fe]=0.19

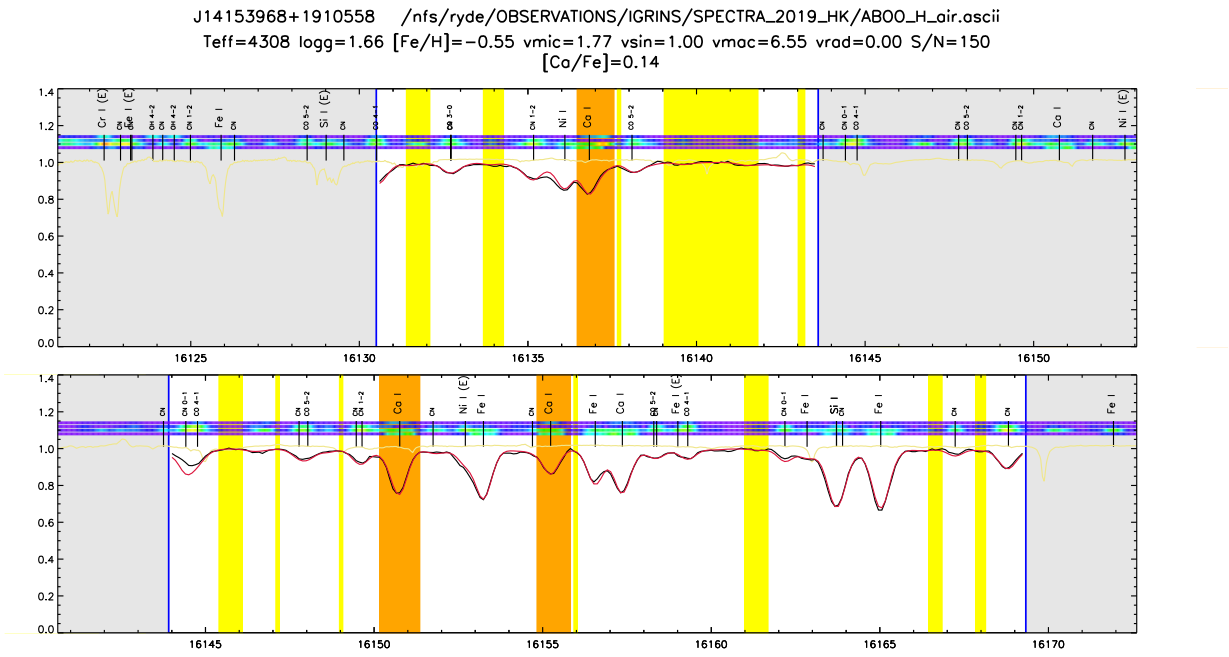
J14153968+1910558 /nfs/ryde/OBSERVATIONS/IGRINS/SPECTRA_2019_HK/ABOO_H_air.ascii
Teff=4308 logg=1.66 [Fe/H]=−0.55 vmic=1.77 vsin=1.00 vmac=6.55 vrad=0.00 S/N=150
[Ca/Fe]=0.14

J14153968+1910558 /nfs/ryde/OBSERVATIONS/IGRINS/SPECTRA_2019_HK/ABOO_H_air.ascii
Teff=4308 logg=1.66 [Fe/H]=−0.55 vmic=1.77 vsin=1.00 vmac=6.55 vrad=0.00 S/N=150
[Ti/Fe]=0.25

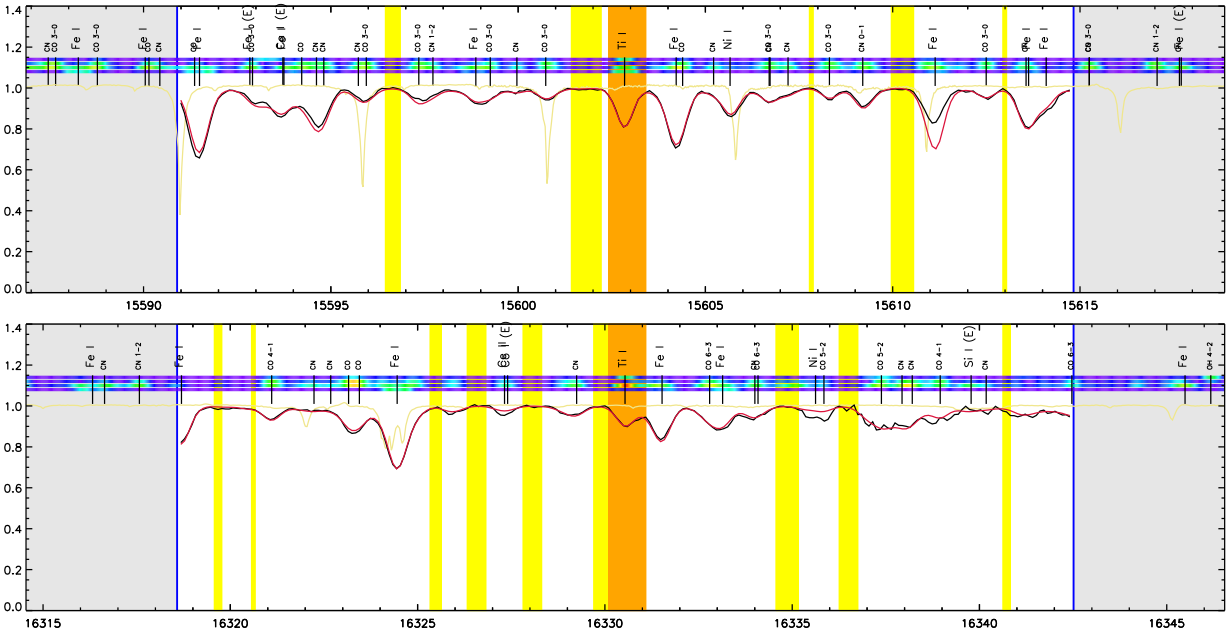

J14153968+1910558 /nfs/ryde/OBSERVATIONS/IGRINS/SPECTRA_2019_HK/ABOO_H_air.ascii
Teff=4308 logg=1.66 [Fe/H]=−0.55 vmic=1.77 vsin=1.00 vmac=6.55 vrad=0.00 S/N=150
[V/Fe]=0.02

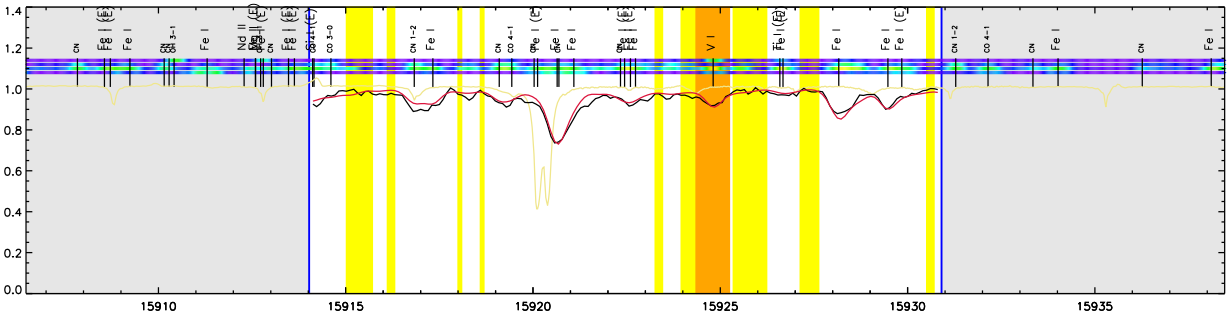

J14153968+1910558 /nfs/ryde/OBSERVATIONS/IGRINS/SPECTRA_2019_HK/ABOO_H_air.ascii
Teff=4308 logg=1.66 [Fe/H]=−0.55 vmic=1.77 vsin=1.00 vmac=6.55 vrad=0.00 S/N=150
[Cr/Fe]=−0.06

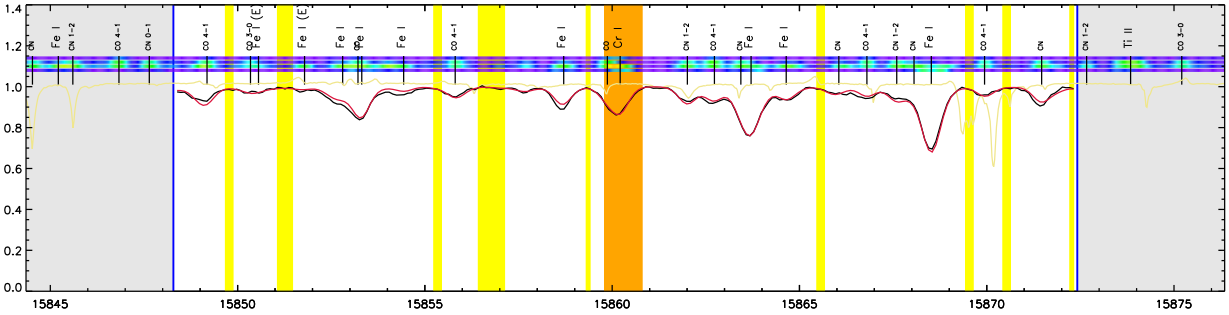

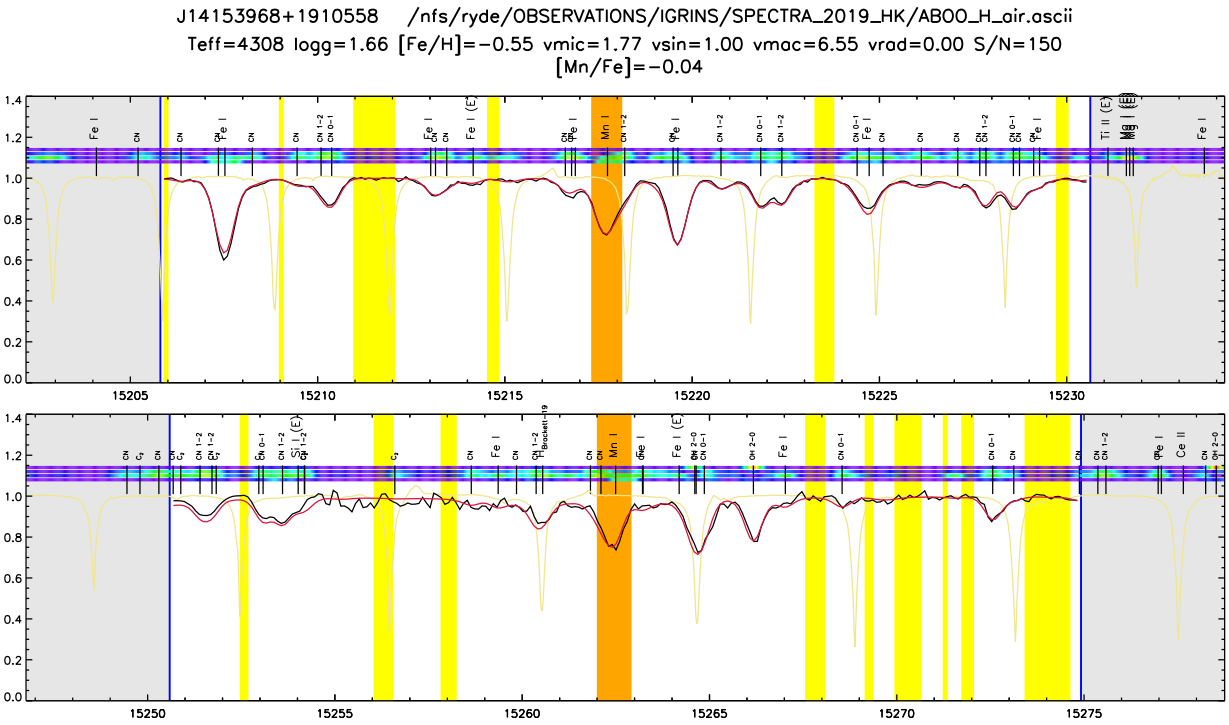
J14153968+1910558 /nfs/ryde/OBSERVATIONS/IGRINS/SPECTRA_2019_HK/ABOO_H_air.ascii
Teff=4308 logg=1.66 [Fe/H]=−0.55 vmic=1.77 vsin=1.00 vmac=6.55 vrad=0.00 S/N=150
[Mn/Fe]=−0.04

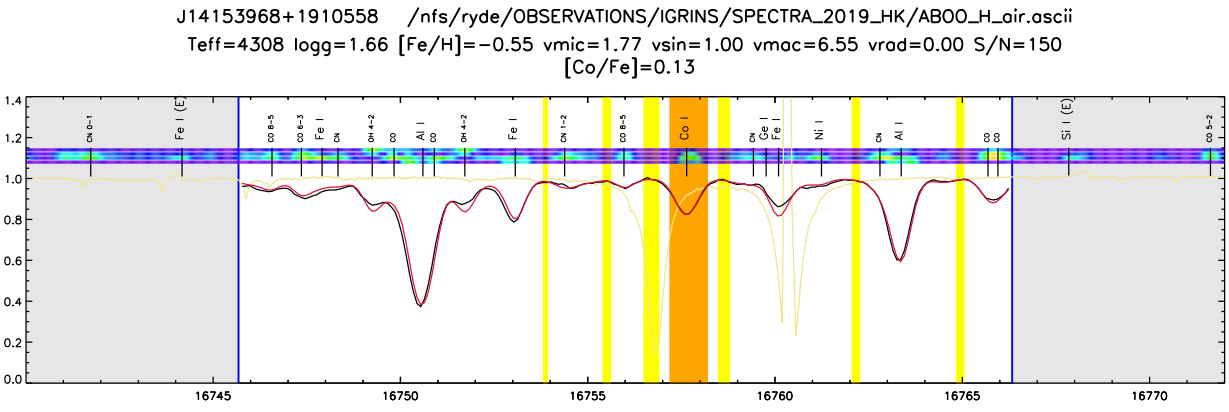
J14153968+1910558 /nfs/ryde/OBSERVATIONS/IGRINS/SPECTRA_2019_HK/ABOO_H_air.ascii
Teff=4308 logg=1.66 [Fe/H]=−0.55 vmic=1.77 vsin=1.00 vmac=6.55 vrad=0.00 S/N=150
[Co/Fe]=0.13

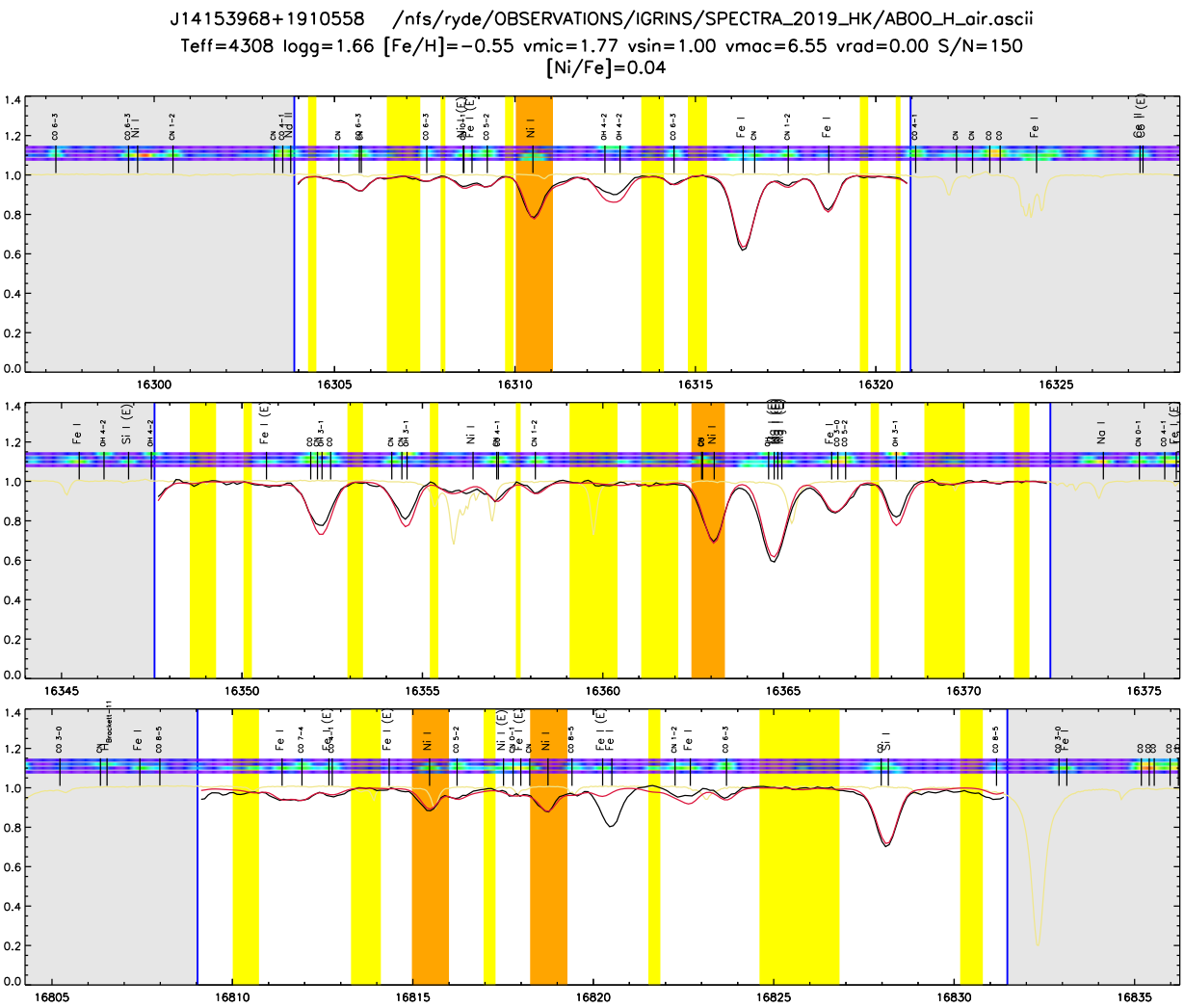
J14153968+1910558 /nfs/ryde/OBSERVATIONS/IGRINS/SPECTRA_2019_HK/ABOO_H_air.ascii
Teff=4308 logg=1.66 [Fe/H]=−0.55 vmic=1.77 vsin=1.00 vmac=6.55 vrad=0.00 S/N=150
[Ni/Fe]=0.04

J14153968+1910558 /nfs/ryde/OBSERVATIONS/IGRINS/SPECTRA_2019_HK/ABOO_H_air.ascii
Teff=4308 logg=1.66 [Fe/H]=−0.55 vmic=1.77 vsin=1.00 vmac=6.55 vrad=0.00 S/N=150
[Cu/Fe]=−0.04

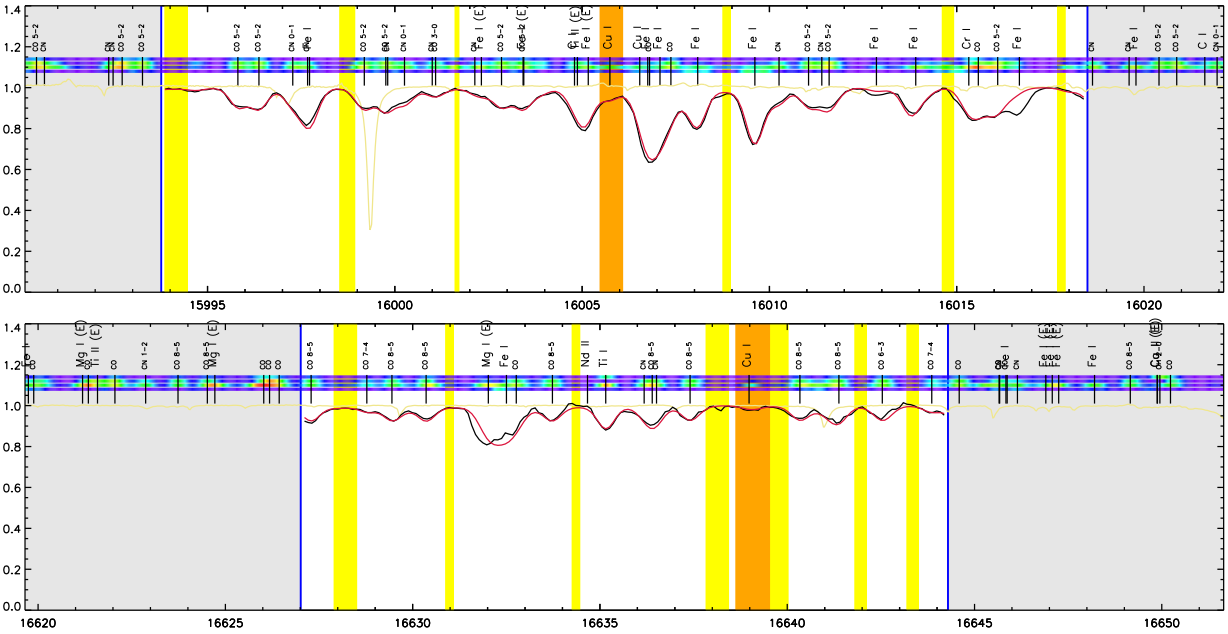

J14153968+1910558 /nfs/ryde/OBSERVATIONS/IGRINS/SPECTRA_2019_HK/ABOO_H_air.ascii
Teff=4308 logg=1.66 [Fe/H]=−0.55 vmic=1.77 vsin=1.00 vmac=6.55 vrad=0.00 S/N=150
[Zn/Fe]=0.66

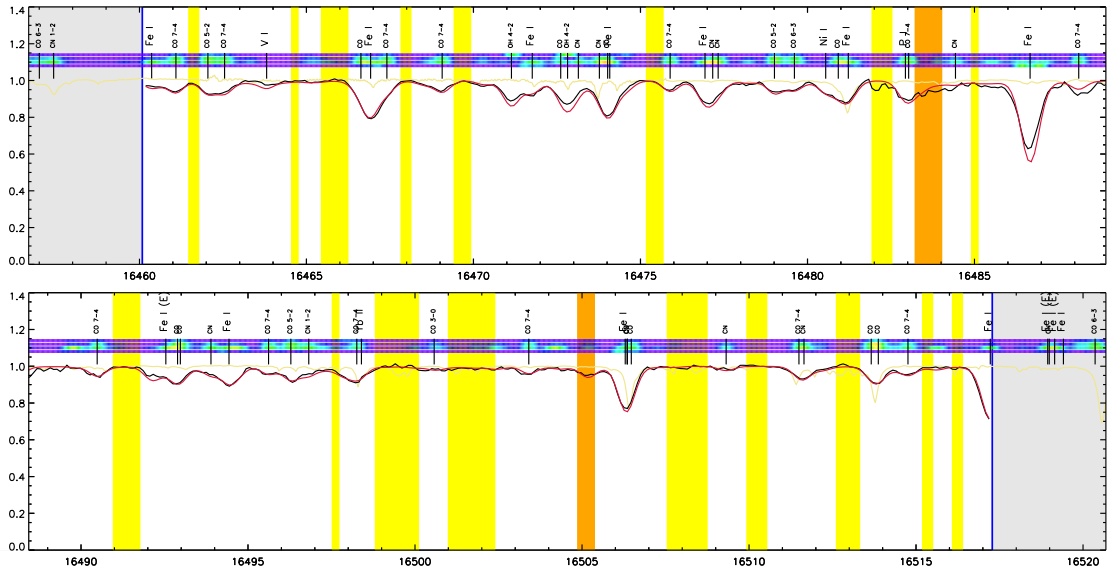

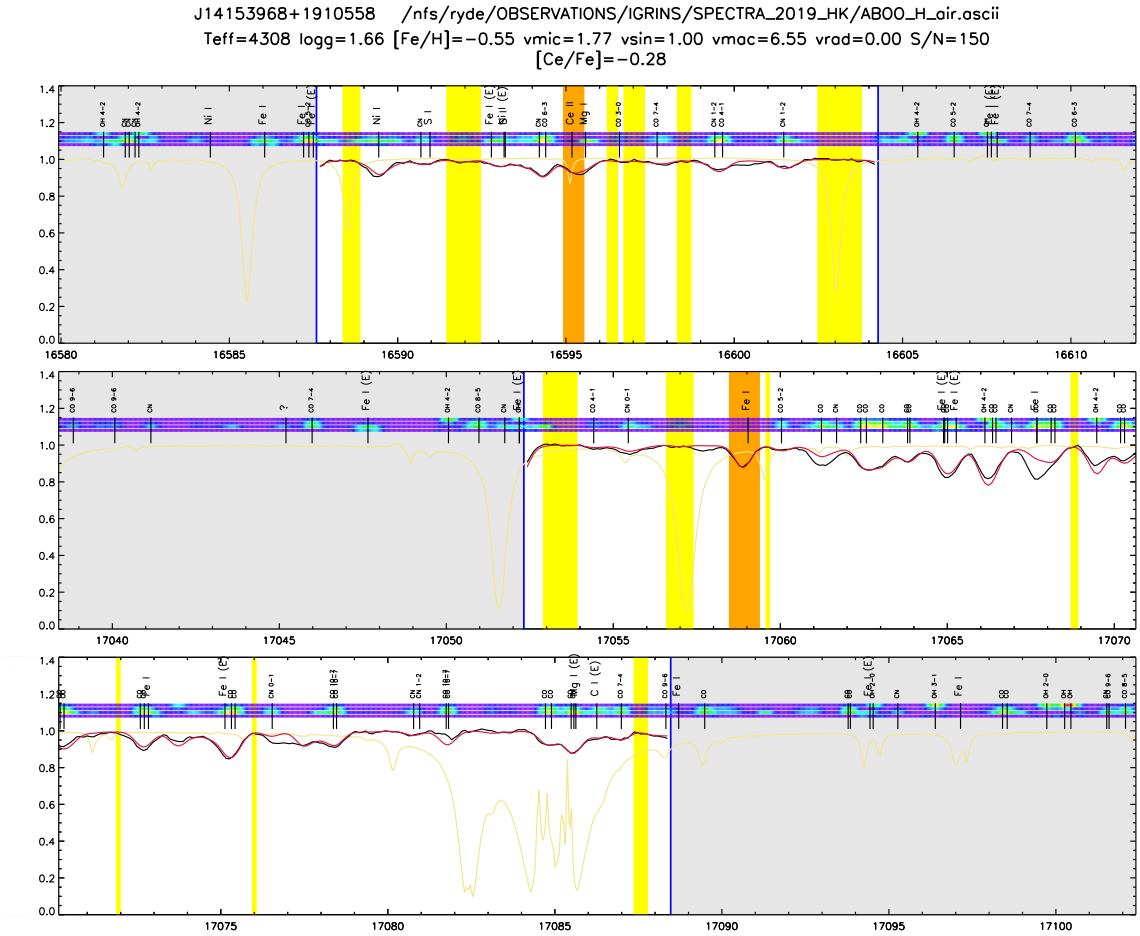
J14153968+1910558 /nfs/ryde/OBSERVATIONS/IGRINS/SPECTRA_2019_HK/ABOO_H_air.ascii
Teff=4308 logg=1.66 [Fe/H]=−0.55 vmic=1.77 vsin=1.00 vmac=6.55 vrad=0.00 S/N=150
[Ce/Fe]=−0.28

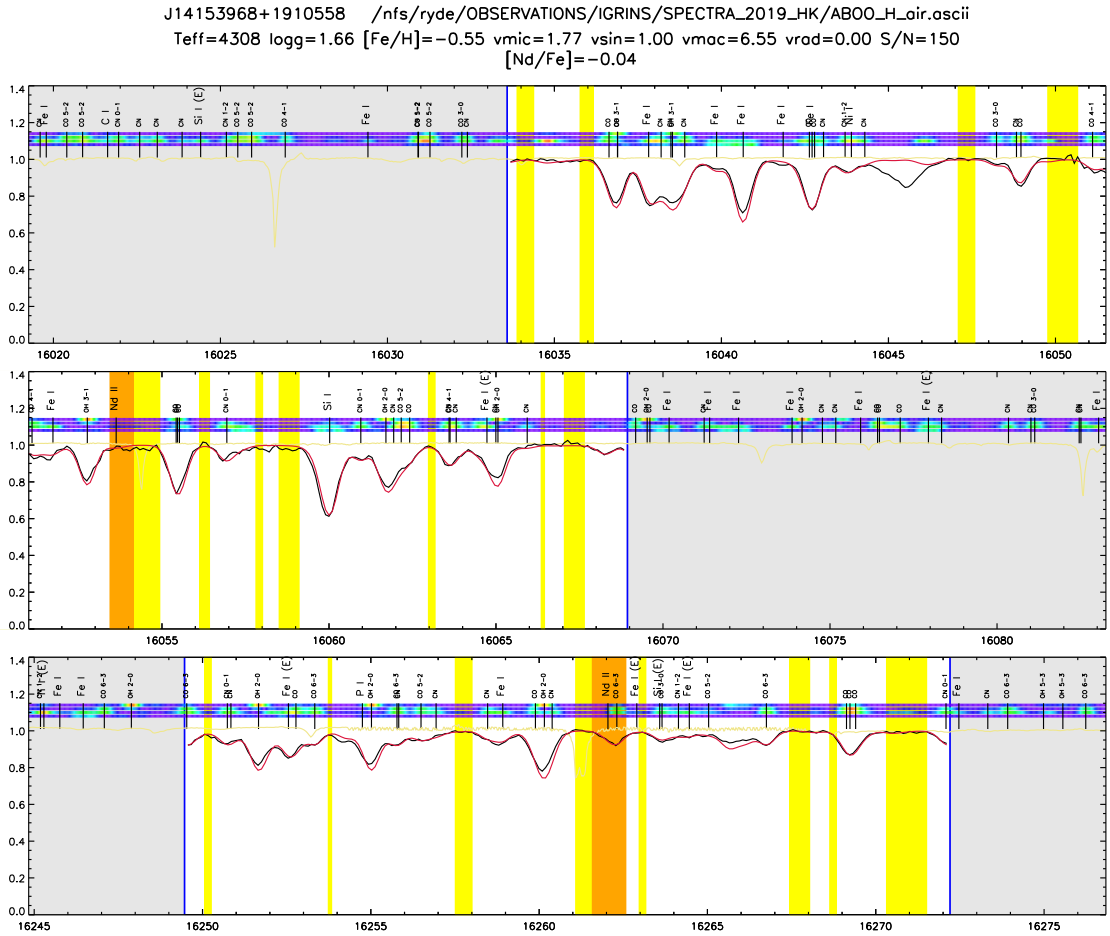
J14153968+1910558 /nfs/ryde/OBSERVATIONS/IGRINS/SPECTRA_2019_HK/AB00_H_air.ascii
Teff=4308 logg=1.66 [Fe/H]=−0.55 vmic=1.77 vsin=1.00 vmac=6.55 vrad=0.00 S/N=150
[Nd/Fe]=−0.04